國立交通大學

材料科學與工程學系

博士論文

幾丁聚醣複合物奈米結構與可控制藥物釋放行為之研究

Study on the nanostructural evolution and controlled drug release behavior of chitosan nanocomposites

研究生：劉昆和

指導教授：陳三元 博士

中華民國 九十八 年 一 月

幾丁聚醣複合物奈米結構與可控制藥物釋放行為之研究

Study on the nanostructural evolution and controlled drug release behavior of chitosan nanocomposites

研 究 生：劉昆和　　Student：Kun-Ho Liu

指導教授：陳三元　　Advisor：San-Yuan Chen

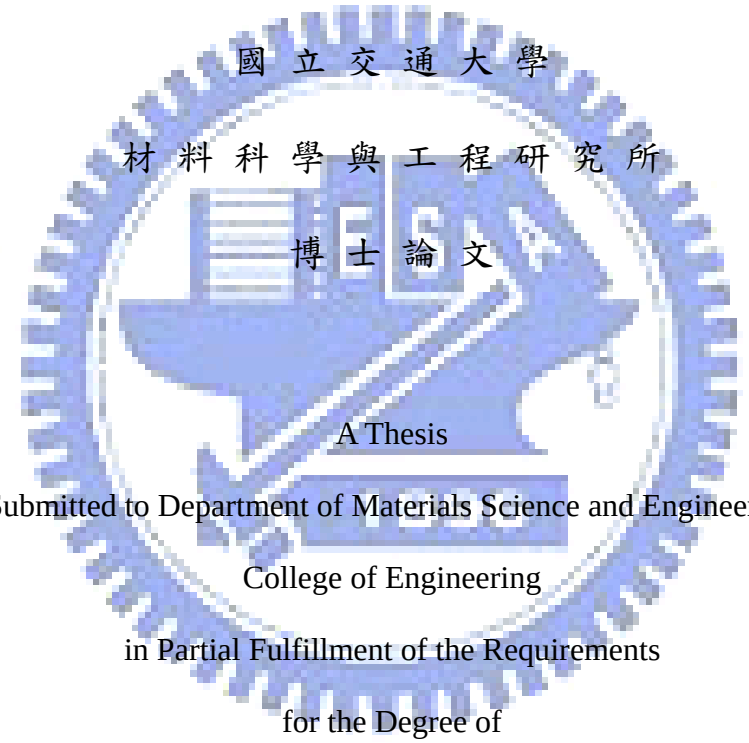

國 立 交 通 大 學

材 料 科 學 與 工 程 研 究 所

博 士 論 文

A Thesis

Submitted to Department of Materials Science and Engineering

College of Engineering

in Partial Fulfillment of the Requirements

for the Degree of

Doctor of Philosophy

in Materials Science and Engineering

January 2009

Hsinchu, Taiwan, Republic of China

中華民國九十八年一月

中文摘要

幾丁聚醣近來在醫藥應用方面受引起很大的注意，因為具有很好的生物相容性使得幾丁聚醣廣泛應用在眼科的局部治療、植入物以及注射藥物領域。而且，由於幾丁聚醣能夠被人體體內酵素(特別是溶解酵素)所代謝，因此也被認為是生物可分解性材料。另外，幾丁聚醣表面帶正電荷的性質使其擁有很好的生物吸附性，在應用上能夠長時間的停留在體內以提升其利用率。幾丁聚醣也擁有能夠幫助傷口癒合以及抗菌等優點。最重要的是，幾丁聚醣大量存在於自然界中讓製作成本變得非常便宜。

幾丁聚醣具有陽離子特性使它能夠形成具有酸鹼敏感與電場敏感特性的聚電解質水膠。本論文的第一部分著重在討論具有電敏感性的幾丁聚醣/奈米黏土複合水膠的合成(第四章)。表面帶負電的黏土顆粒能夠當作幾丁聚醣的交鍊劑來增加複合物的交鍊程度，並且提升其機械強度、膨潤收縮特性和疲勞特性。實驗結果中可以發現，比起純幾丁聚醣來說，複合物在電場不斷開關的循環刺激下能夠擁有較佳的抗疲勞特性。除此之外，我們也利用另一種無機黏土(蒙脫土)來增加幾丁聚醣的抗疲勞特性以及長時效穩定藥物釋放行為(第五章)。脫層後的蒙脫土也能夠當作幾丁聚醣的交鍊劑，結果發現在電場的刺激下，不同的交鍊程度會強烈影響維他命 B12 的釋放行為。當蒙脫土

的含量增加，藥物擴散指數 n 值和複合物的對於電場的反應性將會減低。另外，具有較高蒙脫土含量的複合物在電場不斷開關的循環刺激下電反應性會減弱，但是能夠擁有較佳的抗疲勞特性。除此之外，在第六章中，利用乳化法和溶膠水膠法的製程可以成功製備出顆粒尺寸介於 50-130 奈米的幾丁聚醣-四乙氧基矽複合奈米顆粒。四乙氧基矽經過水解縮合反應，能夠和幾丁聚醣形成網狀結構，進而增加藥物的包覆效率，同時也提供較佳的機械強度，使其在電場關閉時不讓藥物流出載體。

幾丁聚醣因為具有氫氧根和氨根的基團，因此可以很容易被用來做為改質的處理，使其在生藥應用上具有很大的利用價值。雙性幾丁聚醣同時擁有親水性和疏水性的特性使其能夠在水溶液中自組裝形成類似微胞狀的團聚物，這樣的特性主要是由於疏水基團分子或疏水基團分子間的作用力所造成的。在第七章中，我們利用親水性甲基羧基基團與疏水性己醯基團的嫁接物，製備出一種新穎的幾丁聚醣衍生物，能夠在水溶液中自組裝形成空心的奈米膠囊。同時也藉由實驗方法鑑定出此雙性幾丁聚醣衍生物的臨界團聚濃度和表面電性。而此自組裝特性和結構穩定性主要來自於分子間作用力和熱力學的作用。而更有趣的發現指出，改變不同的疏水基團鏈長(變化從 2 個碳到 12 個碳)或嫁接量，可以操控幾丁聚醣奈米團聚物的自組裝行為(第八章)。

從結果中可以發現，嫁接量和碳鏈數的乘積值($X_{DH} \times X_{Cn}$),能夠用來當作一個指標來決定奈米團聚物的結構: 當乘積超過 1.5 時，奈米團聚物會從實心的結構轉變成空心的結構變化。在藥物傳遞應用中，抗癌藥物小紅莓在此奈米結構下被證明可以大大提升吸附性以及包覆率。

關鍵詞: 幾丁聚醣、奈米空心膠囊、電刺激、智慧型釋放、黏土有機混合物

Abstract

Chitosan (CS) is currently receiving a great of interest for medical and pharmaceutical application. Indeed, it is known for being biocompatible allowing it use in various medical applications such as topical ocular applications, implantation or injection. Moreover, chitosan is metabolised by certain human enzymes, especially lysozyme, and is considered as biodegradable. Due to its positive charges at physiological pH, chitosan is also bioadhesive, which increases retention at the site of application. Chitosan also promotes wound-healing and has bacteriostatic effects. Finally, chitosan is very aboundant, and its production of low cost and ecologically interesting.

CS with cationic characteristics is capable to form polyelectrolyte hydrogel that owing pH-sensitivity and electric-sensitivity. The first part in this thesis is focusing on the synthesis of electrostimulus-responsive hybrid composites composed of chitosan (CS) and clay (chapter 4). The addition of negatively charged clay as an ionic cross-linker strongly affect the cross-linking density as well as the mechanical property, swelling–deswelling behavior and fatigue property of the hybrids. Compared with pure CS, a significant improvement in the anti-fatigue property against cyclic electric stimulations of the hybrid was found. In addition, an inorganic phase, MMT, was incorporated in the CS matrix to enhance the anti-fatigue property and corresponding long-term stable release kinetics (chapter 5). The exfoliated silica nanosheets are able to act as cross-linkers to form a network structure between the CS and MMT, and this difference in the cross-linking density strongly affects the release of vitamin B12 under electrostimulation. Further

increasing the MMT content reduced both the diffusion exponent n and the responsiveness of the nanohydrogel to electrostimulation. A consecutively repeated ‘‘on” and ‘‘off” operation shows that the electroresponsiveness of the nanohydrogel with higher MMT concentrations was reduced, but its anti-fatigue behavior was considerably improved. In addition, nanoparticles (NPs) with particle size of 50-130 nm composed of chitosan (CS) and tetraethyl orthosilicate (TEOS) were prepared through emulsion and sol-gel process (chapter 6). TEOS that hydrolyzed and condensed to form network structure with the CS improved the drug loading capacity and also provided the mechanical enhancement of the nano-sphere to restrict drug release when the electric field was switched off.

In addition, CS appears to be more useful in biomedical applications because of its both hydroxyl and amino groups that can be easily modified. Amphiphilic CS consisting of hydrophilic and hydrophobic segments can form micelle-like self-assemblies due to non-covalent association arising from intra- and/or intermolecular interactions among hydrophobic segments in aqueous media. In chapter 7, a new type of amphiphilic chitosan, which was synthesized through the use of both hydrophilic carboxymethyl and hydrophobic hexanoyl substitutions, was employed to self-assemble into a hollow nanocapsule in an aqueous environment. Critical aggregation concentration (cac) and zeta potential were experimentally identified for the amphiphilic chitosan (CHC). The self-assemble mechanism, together with the corresponding nanostructural stability, of this unique CHC nanocapsule was also proposed in terms of intermolecular interaction and thermodynamic reason. Further, a more interesting finding where through the use of acyl chain of varying chain lengths, from C2 to C12, for intramolecular substitution, the

self assembly behavior and the resulting nanostructure of the chitosan nano-aggregate can be well manipulated (chapter 8). It was found that the critical value of (X_{DH} × X_{Cn}), i.e., a product of “degree of acyl substitution” and “carbon number of acyl chain”, can be employed as an indicator for structural variation of the nano-aggregates: when (X_{DH} × X_{Cn}) exceeded 1.5, the architecture of the nano-aggregates underwent a structural transformation from solid nano-particle to hollow nano-capsules. An improved affinity and capacity of doxorubicin drug encapsulation can be technically designed according to the nature of the resulting nanocapsules for controlled delivery.

Keywords: chitosan,, nanocapsule, electric-stimuli, controlled release, clay/organic composites.

Acknowledgments

首先我要感謝我的父母，因為他們無怨無悔的支持以及不求回報的付出，才讓我能夠順利完成博士學位。也感謝我的家人在我求學生活中面臨低潮的時候，願意鼓勵我激勵我。此外，還要感謝我的指導教授陳三元老師以及劉典謨老師，在研究過程中，提供我最大的幫助以及最重要的建議與指導，讓我能夠更深入了解科學的涵意與研究的精神。最後感謝所有實驗室的同學以及學弟妹們，因為有你們，讓我的研究生活變得更多采多姿，也讓我的生命更加豐富，謝謝你們!

Contents

中文摘要..... Ⅰ

Abstract.....Ⅳ

Acknowledgments.....Ⅶ

Contents.....Ⅷ

Figure Captions.....ⅩⅠ

Table Captions.....ⅩⅤ

Chapter 1. Introduction.....**1**

Chapter 2. Literature Review and Theory.....**5**

2.1 Environmental sensitive of chitosan hydrogel.....5

2.2 Inorganic clay-organic (chitosan) hybrid composites.....10

2.3 Self-assembles of modified chitosan derivatives.....12

2.4 Chitosan nanoaggregates for drug delivery system.....14

Chapter 3. Experimental methods.....**17**

3.1 Flowchart of Experiment Process.....17

3.2 Materials.....18

3.3 Characteristics Analysis.....19

Chapter 4. Effect of Clay Content on Electro-stimuli Deformation and Volume Recovery Behavior of Clay-chitosan Hybrid Composite.....**25**

4.1 Introduction.....25

4.2 Preparation of CS-clay films.....28

4.3 Chemical interaction of the CS and clay in the hybrid.....29

4.4 Degree of cross-linking in the hybrid.....31

4.5 Swelling - Deswelling behavior of the hybrid films.....34

4.6 Cyclic deformation and recovery of hybrid films……..…..39

Chapter 5. Drug release behavior of chitosan–montmorillonite nanocomposite hydrogels following electrostimulation…….44

5.1 Introduction……..44

5.2 Preparation of CS-MMT nanohydrogels……..46

5.3 Structural Characterization……48

5.4 Drug release behavior under an applied electric field……51

5.5 Repeating electrical-stimulation on release behavior……55

Chapter 6. Electrical-Sensitive Nanoparticle Composed of Chitosan and TEOS for Controlled Drug Release……...61

6.1 Introduction……..61

6.2 Fabraction of drug-loaded and non-loaded CS/TEOS nanoparticles.64

6.3 Results and Discussion……..…66

Chapter 7. Self-Assembled hollow nanocapsule from amphiphatic carboxymethyl-hexanoyl chitosan as drug carrier……75

7.1 Introduction……..75

7.2 Synthesis of CHC……77

7.3 Preparation of drug-loaded and non-loaded CHC hollow nanocapsules……78

7.4 Formation of CHC Nano-aggregates……80

7.5 Nanostructural development of the CHC Nano-aggregates……...87

7.6 DOX Loading and Release Behavior of CHC Nanocapsules.....……91

Chapter 8. Hydrophobic Effect on the Structural Evolution of Acylated-Carboxymethyl Chitosan and its Self-Assemble Forming of Doxorubicin-loading Nanocapsule……...94

8.1 Introduction……..94

8.2 Synthesis of carboxymethyl chitosan (CC)……96

8.3 Synthesis of acylated carboxymethyl-chitosan (ACC)……..…96

8.4 Preparation of drug-loaded and non-loaded ACC nano-aggregates

……97

8.5 Structural Characteristics of ACC……..101

8.6 Self-assemble behavior of ACC……103

8.7 Molecular configuration of water in ACC…….……..106

8.8 Self-Assembly Map……...111

8.9 Doxorubicin loading……115

Chapter 9. Conclusions.....117

9.1 electric-sensitive of clay/chitosan hybrids……117

9.2 electric-sensitive of TEOS/CS nanoparticles……117

9.3 Acylated-carboxymethyl chitosan nanocapsule……118

Reference.....119

Curriculum Vitae.....127

Publications.....128

Figures Captions

Figure 4-1. Zeta-potential profile of nanoclay (magadiite) in various pH values ……29

Figure 4-2(a) Low-angle powder XRD patterns of hybrid films with various clay loading……31

Figure 4-2(b) FTIR spectra of hybrid films with various clay loading……31

Figure 4-3 Mechanical properties of hybrid film. Initial cross-sectional area (10 mm2) was used for calculating the modulus and strength……...32

Figure 4-4 Clay content dependencies of the number of cross-linked chain (N*) ……34

Figure 4-5(a) Swelling kinetics of hybrid film with different Cclay at pH 7.4….35

Figure 4-5(b) Plots of ln(W0/Wt) against time of hybrid film with different Cclay at pH 7.4……..36

Figure 4-5(c) Equilibrium swelling ratio of hybrid film with different Cclay at pH 7.4……..37

Figure 4-6(a) Deswelling behavior in 1.5h of hybrid film with different Cclay under applied voltage of 1, 5, and 10V……38

Figure 4-6(b) Deswelling water ratio in 1.5h of hybrid film with different Cclay under applied voltage of 1, 5, and 10V……39

Figure 4-7(a) Relative ratio of swelling after cyclic on-off switching of electric-stimuli of 5V in a 20-minute interval of hybrid films with different Cclay……40

Figure 4-7(b). Relative ratio of deswelling after cyclic on-off switching of electric-stimuli of 5V in a 20-minute interval of hybrid films with different Cclay……41

Figure 4-8. Weight changes of pure chitosan and hybrid film with 1 wt % clay addition under cyclic on-off switching of electric-stimuli of 5V…….43

Figure 5-1 Low-angle powder XRD patterns of (a) neat MMT and the CS/MMT nanocomposites with the CS and MMT ratios of (b) 0.5:1 (c) 2:1 and (d) ball milling for 24 h……48

Figure 5-2 Time dependence of optical absorbance A (relative to its initial value, A0) of the (a) exfoliated MMT (b) original MMT and (c) monolayer or bilayer intercalated-MMT suspensions……50

Figure 5-3 Side-angle powder XRD patterns of pure CS, CS-MMT1 and CS-MMT4……51

Figure 5-4 (a) Time-dependent cumulative release curves of vitamin B12 from the nanohydrogels upon an applied electric voltage, showing the different release profiles with different CMMT. (b) Dependences of the loaded MMT contents on the diffusion exponent n and voltage-induced swelling ratios of the nanohydrogels. (The filled boxes indicated the diffusion exponent n and the empty circles indicated the V-induced swelling ratio)……53

Figure 5-5 Real (…) and the ideal (—) pulsatile drug release profiles of pure CS hydrogels as an electric field was switched “on” and “off”…….56

Figure 5-6 (a) Standard release rates of drug from the nanohydrogels (CS, CS-MMT1, CS-MMT2, and CS-MMT4) after cyclic on-off switching operations. (b) Dependences of the loaded MMT contents on the drug standard release rate in the first on-off cycle (filled boxes) and anti-fatigue coefficient of the nanohydrogels (empty circles)……...58

Figure 5-7 Standard release rates of drug from pure CS and CS-MMT2 under cyclic on-off switching of electric-stimuli……59

Figure 6-1. The illustrations of the formation of CS and TEOS NPs. (a) the formation of TEOS network structure, (b) the original CS polymer entwined into the network, (c) the formation of NPs by ionic gelation of TPP……..67

Figure 6-2 (a) SEM image of pure CS NPs. The (b) lower- magnification and higher-magnification TEM image of the CS and TEOS NPs (23%). ……68

Figure 6-3 AE and LC of the CS and TEOS NPs with different TEOS contents. ……69

Figure 6-4 In vitro release of myoglobin from the CS and TEOS NPs with different TEOS contents……70

Figure 6-5 The pulsatile myoglobin release profiles with different TEOS contents when applied DC electric field was switched “on” and “off”. ……73

Figure 6-6 Illustration of the proposed electric-sensitive drug release mechanism of CS/TEOS NPs……..74

Figure 7-1 Molecular structure of carboxymethyl-hexanoyl chitosan (CHC)...80

Figure 7-2 Change of the intensity ratio (I372/I385) from excitation spectra of pyrene (1.0×10-6 mol/L) with various concentrations of CC and CHC-4……..82

Figure 7-3 Zeta potential of carboxymethyl-hexanoyl chitosan (CHC) with different DH……84

Figure 7-4 TEM images of self-aggregates prepared, respectively, from (a) CC and (b) CHC-4 by ultrasonication in water……..86

Figure 7-5 Fraction of mean size 1 and 2 of CC and CHC nano-aggregates..87

Figure 7-6 Schematic illustration of formation process of CHC hollow

nanocapsules……..88
Figure 7-7 SEM images of CHC-4 nanocapsules……91
Figure 7-8 (a) DOX encapsulation efficiency and (b) DOX release profiles of CHC hollow nanocapsules……...92
Scheme 8-1 Acylation Reaction of carboxymethyl chitosan……101
Figure 8-1 FTIR spectra of CC, C2-0.5, and C12-0.5……102
Figure 8-2 Dependence between the DH of ACC as Cn=2, 6 and 12 and (a) the critical aggregation concentration, CAC and (b) ln(CAC), respectively……105
Figure 8-3 DSC curves of CC and ACC derivates (Cn-0.5) measured at water content=200%. Dash lines represent the curve fitting by Lorentzian curve-fitting procedure……107
Figure 8-4 Dependence between the content of bound water, Wnf, max, and the hydrophobic side chain with different Cn of ACC in DH=0.25 and 0.5……109
Figure 8-5 Plot of CAC (◯) and Wnf, max (■) of ACC derivates with different values of (X_{DH} × X_{Cn})……112
Figure 8-6 TEM images of (a) C2-0.5, (b) C6-0.5, and C6-0.5 after dehydration; and (d) SEM image of the ACC nano-aggregates after electron-induced rupturing……...113
Figure 8-7 Schematic illustration of formation process of ACC nano-aggregates……...114
Figure 8-8 DOX encapsulation efficiency of ACC nano-aggregates with various values of (X_{DH} × X_{Cn})……...116

Table Captions

Table 6-1. Kinetics contants (K), and release exponents (n) following linear regression of release of myoglobin from CS and TEOS NPs....72

Table 7-1 Sample Name and Corresponding Estimation of Substitution Degree by 1H-NMR.....80

Table 7-2 Characterization of CC and CHC self-assembled hollow nanocapsules.....84

Table 8-1 The preparation conditions and the characteristics of ACC nano-aggregates.....99

Chapter 1

Introduction

Research on site-specific and temporal control of drug delivery systems is receiving a major impetus towards the development of new and/or improved drug therapies. “Intelligent” drug carriers which released the right amount of drug at the right time and/or at the right place may enable us to precisely control the delivery of drugs. These “smart” drug delivery vehicles would also enable the tailoring of medical treatment to individual patients. However, the precise control of drug levels in the body can only be achieved if the drug carrier responds in a reproducible and predictable fashion to an internal or external chemical, physical or biological stimulus. In addition, the carrier should be non-toxic, non-irritant biodegradable, biocompatible, easy to administer and should not need to be removed when drug-depleted.

Hydrogels have been used extensively in the development of the smart drug delivery systems, since hydrogels containing such ‘sensor’ properties can undergo reversible volume phase transitions or gel–sol phase transitions upon only minute changes in the environmental condition. Many physical and chemical stimuli have been applied to induce various responses of the smart hydrogel systems. Therefore, environment-sensitive hydrogels are ideal candidates for developing self-regulated drug delivery systems. However, the most significant weakness of all these external stimuli-sensitive hydrogels is that their response time is too slow. Thus, fast-acting hydrogels are necessary, and the easiest way of achieving that goal is to make thinner and smaller hydrogels, which indicates that nanotechnology is becoming more important

for such high sensitive drug- delivery structure.

Recently, nanotechnology has become a popular term representing the main efforts of the current science and technology. One of the important areas of nanotechnology is “nanomedicine,” which, according to the National Institute of Health (NIH) Nanomedicine Roadmap Initiative, refers to highly specific medical intervention at the molecular scale for diagnosis, prevention and treatment of diseases [1]. The importance of nanotechnology in drug delivery is in the concept and ability to manipulate molecules and supramolecular structures for producing devices with programmed functions. The approach which may come closest to the original intention may probably be found in the application of dispersed nanoparticles loaded with an active ingredient [2]. Within the solid matrix of the particles, the active ingredient can be dissolved, entrapped or encapsulated.

In addition, a significant drawback of most environmentally stimulus-sensitive hydrogels is that the responsivity and reversibility often decrease with both time and number of on–off operation cycles as the gel fatigues considerably. It is necessary to obtain a most suitable composition and viscoelasticity at a certain cross-linking density for optimal responsiveness that the deformation and relaxation properties of hydrogel with cyclic on–off operations. Herein, considerable attention was paid to inorganic–organic hybrid materials because their solid-state properties could be tailored in relation to the nature and relative content of their constitutive components. The strong chemical bonds (covalent or ionic) or interactions such as van der Waals forces, hydrogen bonding, or electrostatic forces, often exist between the organic and inorganic components that usually leads to some novel nanocomposites with improved performance properties.

Chitosan (CS), poly- β (1,4)-2-amino-2-deoxy-$_D$-glucose, is the deacetylated product of chitin, poly(N-acetyl-$_D$-glucosamine), a natural polymer found in the exoskeletons of crustaceans and insects and in the cell wall of fungi and microorganisms. The chemically active groups in the chitosan structure are the free amine groups, located in the C2 position of the glucose residue in the polysaccharide chain, and the hydroxyl groups, with both being susceptible to modification [3]. CS, a cationic biopolymer with very low toxicity, has been evaluated extensively as an excipient for drug delivery systems. Hence, in this study, a new class of “electrically-charged” hybrid composite based on chitosan (CS) and clay will be first investigated and developed by taking the advantage of the electrochemical properties, i.e., surface charge, and nanostructural properties, i.e., layer of the clay particles, as illustrated in Chapter 4. Moreover, the effects of various cross-linking degrees caused by different clay content of the hybrid composite on the electrically-stimulated swelling-deswelling behavior, mechanical deformation were elucidated. In Chapter 5, the release kinetics and mechanism of the vitamin B12 in terms of MMT contents were investigated under a given electric-field stimulus. Furthermore, the anti-fatigue behavior with respect to the repeated field stimuli of the resulting nanohydrogel in terms of MMT addition was also elucidated. In chapter 6, nanoparticles (NPs) with particle size of 50-130 nm composed of CS and TEOS were obtained through emulsion and sol-gel process. Therefore, the mechanism of the drug release from the CS/TEOS NPs effectively controlled by electric-stimuli operations was demonstrated in this work.

In Chapter 7, a new type of chitosan hollow structure, i.e., carboxymethyl-hexanoyl chitosan (CHC), which was modified first by hydrophilic carboxymethylation, followed by hydrophobic modification with

hexanoyl groups to add amphiphilic character, was employed to study its self-aggregation behavior to form nanocapsule in aqueous solution and nanostructural evolution. The stability of nancapsules and formation mechanism of the CHC macromolecules were explored through the use of critical aggregation concentration (CAC), zeta-potential, electron microscopy, and dynamic light scatter (DLS). By taking the advantage of self-aggregation nature, the CHC was employed to encapsulate doxorubicin (DOX), an anticancer agent of broad spectrum with reasonable therapeutic index and intriguing biological and physicochemical actions, to further understand its loading efficiency and release behavior. Then, in Chapter 8, the structural evolution of the chitosan-based nano-aggregates was systematically investigated in terms of different degrees of acyl substitution (DH) and number of carbon of the acyl ligand (C_n). In addition, the doxorubicin (DOX)-encapsulated capacity of the nano-aggregates of varying degrees of hydrophobicity, in terms of DH and C_n, was also studied.

Chapter 2

Literature Review and Theory

2.1 Environmental sensitive of chitosan hydrogel

Controlled drug delivery systems, which are intended to deliver drugs at predetermined rates for predefined periods of time, have been used to overcome the shortcoming of conventional drug formulations. In fact, it would be most desirable if the drugs could be administered in a manner that precisely matches physiological needs at proper times (temporal modulation) and/or at the proper site (site-specific targeting). In addition, it would be highly beneficial if the active agents were delivered by a system that sensed the signal, and then acted to release the right amount of drug in response. Hydrogels have been used extensively in the development of the smart drug delivery systems. A hydrogel is a network of hydrophilic polymers that can swell in water and hold a large amount of water while maintaining the structure. The drugs can be protected in hydrogel from hostile environments, e.g., the presence of enzymes and low pH in the stomach, and controlled-released by changing the gel structure in response to environmental stimuli. The types of environment-sensitive hydrogels are also called “Intelligent” or “smart” hydrogels. Many physical and chemical stimuli have been applied to induce various responses of the smart hydrogel systems, where the physical stimuli include temperature, electric fields, solvent composition, light, pressure, sound and magnetic fields; while the chemical or biochemical stimuli include pH, ions and specific molecular recognition events [4]. Smart hydrogels have been used in diverse applications, such as in marking artificial muscles [5], chemical

valves, immobilization of enzymes and cells [6], and concentrating dilute solutions in bioseparation.

All the pH-sensitive polymers contains pendant acidic (e.g. carboxylic and sulfonic acids) or basic (e.g. ammonium salts) groups that either accept or release protons in response to change in environmental pH. The polymers with a large number of ionizable groups are known as polyelectrolytes. Chitosan is an N-deacetylated product of chitin mainly composed of D-glucosamine (GlcN) residue. Chitosan, a cationic polyelectrolyte, is capable of forming hydrogels useful for drug delivery. Hypothetically, chitosan is positively charged in solution due to its protonated amine groups. The residual amino groups of chitosan will be ionized in acidic buffers, which contributes to the electrostatic repulsion between adjacent ionized residual $-NH_2$ groups of chitosan leading to chain expansion and eventually increases the water uptake of the gel. Since the swelling of polyelectrolyte hydrogels is mainly due to the electrostatic repulsion among charges present on the polymer chain, the extent of swelling is influenced by any condition that reduce electrostatic repulsion, such as pH, ionic strength, and type of counterions [7]. Albertsson et al. [8] had reported that physically crosslinked chitosan hydrogels with pH-sensitive were synthesized by grafting D,L-lactic acid (LA) and/or glycolic acid (GA). The hydrophobic side chains caused stronger effect on the water state and swelling behavior of chitosan hydrogels. In addition, semi-interpenetrating networks (semi-IPN) have also attracted a lot of attentions. The IPNs, by their original definition, are composed two or more chemically distinct components held together ideally and solely by their permanent mutual entanglements. Agnely groups [9] had synthesized a chitosan-poly(ethylene oxide) (PEO) semi-IPN of its swelling properties at pH 1.2 and pH7.2. Comparison with a chitosan

reference network, it was concluded that the semi-IPN had a promising potential because of its higher pH-dependent swelling properties. Kim et al. [10] had prepared the IPN hydrogels composed of poly (vinyl alcohol) (PVA) and chitosan by UV irradiation and found that the swelling ratio increased with increasing the molar ratio of hydrophilic groups of chitosan in IPNS. In addition, γ-irradiation copolymerization of chitosan and polyvinyl pyrrolidone (PVP) exhibited pH-sensitive behavior in aqueous solution were synthesized by Mun et al. [11]. It was shown that increasing of PVP concentration in feed composition also as radiation dose accompanied of increase of yield of gel fraction and decrease of swelling degree.

Most polymers increase their water-solubility as the temperature increases. Polymers with LCST (lower critical solution temperature), however, decrease their water-solubility as the temperature increases. Hydrogels made of LCST polymers shrink as the temperature increases above the LCST. This type of swelling behavior is known as inverse (or negative) temperature-dependence. The inverse temperature-dependent hydrogels are made of polymer chains that either possess moderately hydrophobic groups or contain a mixture of hydrophilic and hydrophobic segments. At lower temperatures, hydrogen bonding between hydrophilic segments of the polymer chain and water molecules are dominates, leading to enhanced dissolution in water. As the temperature increases, however, hydrophobic interactions among hydrophobic segments become strengthened, while hydrogen bonding becomes weaker. The net result is shrinking of the hydrogels due to inter-polymer chain association through hydrophobic interactions. In additionm, as the polymer chain contains more hydrophobic constituent, LCST becomes lower [12]. The LCST can be changed by adjusting the ratio of hydrophilic and

hydrophobic segment of the polymer. In addition, hydrogels that are responsive to both temperature and pH can be made by simply incorporation ionizable and hydrophobic (inverse thermo-sensitive) functional groups the same hydrogels. Wang et al. [13] reported the preparation and characterization of PNIPAM/CS hydrogels with semi-interpenetrating and full-interpenetrating polymeric networks. Leung et al. [14] prepared PNIPAM/CS core-shell microgel via a new method; both thermo-sensitivity and pH-sensitivity were characterized. Lin et al. [15] reported the synthesis of multi-responsive core-shell copolymer latex with the crosslinked copolymer of NIPAM and CS as the core and the copolymer of methacrylic acid and methyl methacylate as the shell. Chu et al. [16] reported that chitosan-based hydrogel having both temperature and pH sensitivity were prepared by blending chitosan with temperature sensitive PNIPAM and polyethylene glycol (PEG). Khurma et al. [17] prepared the chitosan-based semi-IPN hydrogels containing different amounts of PEG and found that the equilibrium water content and the amount of freezing water in the swollen hydrogels increased with the increase in PEG concentration in the gels. In addition, Gao et al. [18] developed a novel copolymer p(CS-Ma-DMAEMA) with chitosan, maleic anhydride (Ma) and 2-(dimethylamino)ethyl methacrylate (DMAEMA) by grafting and copolymerization.

Hydrogels sensitive to electric current are usually made of polyelectrolytes, as are pH-sensitive hydrogels. Electro-sensitive hydrogels undergo shrinking or swelling in the presence of an applied electric field. An electric field as an external stimulus has advantages such as the availability of equipment which allows precise control with regards to the magnitude of current, duration of electric pulses, intervals between pulses, etc. Under the

influence of an electric field, electro-responsive hydrogels generally deswell or bend, depending on the shape of the gel and its position relative to the electrodes. Bending occurs when the main axis of the gel lies paralled to (but dose not touch) the electrodes whereas deswelling occurs when the hydrogel lies perpendicular to the electrodes [19]. Upon the application of an electric field above a threshold value, polyelectrolyte gels generally deswell as water is synthesized from the gel. Anionic gels shrink at the anode [20] while cationic gels shrink at the cathode [21]. Since volume changes of responsive hydrogels are usually diffusion-controlled [22], the deswelling equilibrium is reached slowly, i.e., gel response to an electric stimulus is slow. The extent of the gel deswelling increases with the magnitude of the electric field, but is not linearly proportional to it. Gong et al. [23] and Budtova et al. [24] have shown that the extent of deswelling depends on the amount of charge transported through the gel, rather than on the voltage applied. When the electric field is removed, the gel absorbs fluid and swells. Thus, upon sequential switching “on” and “off” of the electric field, the gel deswells and swells, following the electric field protocol. The magnitude of the gel response, as well as the degree of reversibility often decreases with time and with increasing number of on-off cycles as the gel fatigues. Three main mechanisms of electro-induced gel deswelling, namely: (1) the establishment of a stress gradient in the gel, (2) changes in local pH around the electrodes and (3) electroosmosis of water coupled to electrophoresis, have been suggested. The mechanical response of polyelectrolyte hydrogels to an applied electric field can be used to control drug release from these gels. The effects of electrical stimulation on drug release depends to a large extent on the mechanisms by which the gel responds to the stimulus, the mechanisms via which drug is released from the

gel and any interactions between the drug and the gel network [21]. The main mechanisms of drug release are forced convection of drug out of the gel along with syneresed water, diffusion, electrophoresis of charged drugs, and liberation of drugs upon erosion of electro-erodible gels. Block et al. [21] first use chitosan as matrices for electrically-modulated drug delivery. It was found that gel syneresis was pronounced, particularly at higher milliamperage (mA) and for chitosan gels with lower degrees of acetylation. In addition, the release of the model drugs from the gel matrix was in the order benzoic acid (anionic)>hydrocortisone (neutral)>lidocaine (cationic), which is consistent with the electrokinetically competing forces that are involved in these gels. In addition, the IPN system could be a promising candidate to meet many requirements because it can induce quite strong mechanical properties. Therefore, Chitosan/Polyallylamine IPN [25], Poly(vinyl alcohol)/Chitosan IPN [26], Chitosan/Poly(diallyldimethylammonium chloride) semi-IPN [27], and Chitosan/Hyaluronic acid complex [28] were synthesized and characterized for their electrical sensitivity.

2.2 inorganic clay-organic (chitosan) hybrid composites

Over the last decade, the utility of inorganic nanoparticles as additives to enhance polymer performance has been established and now provides numerous commercial opportunities, ranging from advanced aerospace systems to commodity plastics. Low-volume additions (1-5 wt.-%) of highly anisotropic nanoparticles, such as layered silicates or carbon nanotubes, provide property enhancements with respect to the neat polymer that are comparable to those achieved by conventional loadings (1-40 wt.-%) of traditional fillers. In addition, unique value-added properties not normally

possible with traditional fillers are also observed, such as reduced permeability, tailored biodegradability, optical clarity, self-passivation, electrical conductivity, electrostatic discharge, remote-actuated shape recovery, and flammability, oxidation, and ablation resistance. Although much attention gas been paid to polymer/clay nanocomposites, relatively little attention has been paid to biopolymer/clay nanocomposites. These are the cases of polylactide/clay nanocomposites [29], cotton/clay nanocomposites [30], poly(butylenes succinate)/clay nanocomposites [31] and plant oils/clay nanocomposites [32].

Chitosan has been extensively investigated for several decades for molecular separation, food packaging film, artificial skin, bone substitutes, water engineering and so on owing to its good biocompatibility, biodegradability, as well as multiple functional groups. However, its properties, such as thermal stability, hardness and gas barrier properties are frequently not good enough to meet those wide ranges of applications. Up to now, there is only a limited number of reports about the enhancement of properties of chitosan using polymer-layer silicate nanocomposite (PLSN) technology [33]. Asira had a preliminary study about chitosan-clay nanocomposites and reported a markedly improved tensile property but inferior thermal property of composites to that of pure chitosan [34]. Ruiz-Hitzky and his coworkers synthesized functional chitosan/mintmorillonite nanocomposites, which can effectively act as active phase for an electrochemical sensor in the detection of different anions [33]. Wang et al. [35] successfully synthesized chitosan/montmorillonite nanocomposites and reported that nanodispersed clay improved the thermal stability and enhanced the hardness and elastic modulus of the matrix systematically with increased clay loading, up to a loading of 10 wt.%. Because of the polycationic nature of chitosan in acidic

media, this biopolymer also appears as an excellent candidate for intercalation in Na^+-montmorillonite by mwans of cationic exchange processes [36]. On the other hand, an acidic pH value is necessary to provide $–NH_3^+$ groups in the chitosan structure. In such conditions, the adsorption process is mainly controlled by a cationic exchange mechanism due to the Coulombic interactions between the positive $–NH_3^+$ groups of the chitosan and the negative sites in the clay structure.

2.3 Self-assembles of modified chitosan derivatives

Chitosan usually has high molecular weight and strong network of intermolecular or intramolecular hydrogen bonds. Its poor solubility in water and common organic solvents has so far limited its widespread utilization. As a result, there have been many publications about the methods to enhance the solubility of chitosan, one of which was derivatization. For example, its solubility can be dramatically enhanced by introducing the carboxymethyl (CM) groups to the chitosan. The structure of CM-chitosan is similar to amino acids with amino group and carboxyl group in the molecule, and the difference from chitosan is the carboxymethyl group linked to the nitrogen or oxygen atom. Its good water-solubility, non-cytotoxicity and good bioactivity as functional biomaterial made CM-chitosan an important derivative [37]. Several biological properties of CM-chitosan [38] as well as its synthesis [39] have already been reported. Further, the aggregation behavior of CM-chitosan in neutral aqueous solution was investigated by Zhu et al. [40]. It was proposed that the driving force for the aggregation of CM-chitosan in the dilute solution is a combination of the effects of intermolecular H-bonding of CM-chitosan, electrostatic repulsions between COO^- groups on the CM-chitosan chains and hydrophobic

interaction among the hydrophobic moieties in CM-chitosan such as acetyl groups and glucosidic rings. Thus, CM-chitosan nanoparticle as carrier for the anticancer drug, doxorubicin (DOX), was evaluated by Du et al. [41]. It was found that the DOX release rate can be hindered by CM-chitosan nanoparticle with high molecular weight (MW) and degree of substitution (DS).

Polymeric amphiphiles consisting of hydrophilic and hydrophobic segments can form micelle or micelle-like self-assemblies with a hydrophobic core and a hydrophilic shell due to the intra- and/or intermolecular interactions of hydrophobic segments in aqueous media [42]. Hydrophobically modified chitosan derivatives such as alkylated chitosan [43] and deoxycholic-modified chitosan [44] have been focusing on recently due to their amphiphilic nature. This novel kind of polymeric amphiphiles can form monodisperse self-aggregated nanoparticles in aqueous media, and their morphology can be controlled by the chemical structures of hydrophobically modified chitosan such as the molecular weight of chitosan, the types and the DS of hydrophobic groups [45]. Zhang et al. [46] reported the synthesis of Cholesterol-modified chitosan conjugate with succinyl linkages (CHCS). CHCS formed monodisperse nanoparticles in aqueous media and showed a potential as a sustained-release carrier of epirubicin in vitro. Delair et al. [47] reported the synthesis of biocompatible nanoparticles from the pH-induced self-complexation of the amphoteric polysaccharide N-sulfated chitosan. These particles were assembled by electrostatic interactions between the protonated amino residues and the sulfate functions and stabilized by an excess of surface sulfate groups. Chung et al. [48] prepared the polymeric nanoparticles from amphiphilic chitosan derivatives fluorescenin isothiocyanate (FITC)-conjugated glycol chitosans that provided a novel and

simple method for size control of self-assembled nanoparticles. Park et al. [49] had prepared hydrophobically modified chitosan using linolenic acid as hydrophobic group. The hydrogel nanoparticles formed with hydrophobized chitosan was used as water soluble proteins such as BSA carriers. Fang et al. [50] prepared the amphiphilic graft copolymer using chitosan as hydrophilic segment and poly (L-lactic acid) (PLLA) as hydrophobic segment through a protection-graft-deprotection route. The results indicated both hollow and solid spherical micelles were present in aqueous solutions.

However, due to the rigidity of the molecular chains in water, it is difficult for hydrophobically modified chitosan derivatives to form perfect spherical-shaped self-aggregated nanoparticles [51]. Hence, chitosan was hydrophilically modified by O-carboxymethylation to increase the flexibility of chitosan molecular chains in water, then followed by the hydrophobic modification with cholesterol to yield novel polymeric amphiphiles, cholesterol-modified O-carboxymethyl chitosan conjugates, which were used to prepare self-aggregated nanoparticles in water by probe sonication [52]. The results showed that the negatively charged carboxymethyl groups are advantageous for the formation of well-shaped and stable self-aggregated nanoparticles.

2.4 Chitosan nanoaggregates for drug delivery system

A general and widely accepted classification of nanoparticles has been given that the nanoparticles are solid colloidal particles with a diameter between 10 and 1000 nm. Among these colloidal particles, those formed by a shell-like wall with a liquid content may be considered as nanocapsules, while their solid counterparts are often referred to as nanospheres. Among the

nanosized polymer materials, hollow polymeric nanospheres (nanocapsules) obtained particular interest because of their great potential in biomedical utilization, for instance, to encapsulate large quantities of therapeutic and diagnostic agents in their hollow cavities and release them at later stage. Such encapsulation can greatly increase drug bioavailability, protect agent from destructive factors upon parenteral administration, and modify their pharmacokinetics and biodistribution in body. Various methods, such as the self-assembly of block copolymers in selective solvent [53], layer-by-layer deposition of polyelectrolytes on temporary core [54] (which will be removed permanently at later stage), and microemulsion as well as microemulsion polymerization [55], has been developed to fabricate hollow polymeric spheres. Jiang et al. [56] demonstrated a simple and direct method for fabricating hollow polymeric nanospheres with biocompatible and biodegrafable macromolecules. In the approach, hollow polymeric nanospheres were formed in a completely aqueous system without the aid of surfactants, organic solvents, precursors of block and graft copolymers, template cores, or emulsion phase, and decreasing their potential toxicity. This hollow CS/poly(acrylic acid) (PAA) nanospheres as the drug carrier and their drug release pattern in vitro and in vivo with DOX as a model drug was further investigated [57]. The nanospheres showed a continuous release of the entrapped DOX up to 10 days in vitro and showed comparable in-vitro cytotoxicity against HepG2 cells compared to the free DOX.

Upon entrapment of therapeutic agents or drugs, oral administration is the most convenient and comfortable means of administering protein drugs and eliminates pain caused by an injection, the stress associated with multiple daily injections, and possible infections [58]. However, peptide drugs are

poorly absorbed after oral administration because of their susceptibility to enzymatic degradation and their low permeability across the intestinal epithelium. Mucoadhesive polymers represent one class of biomaterials with an interesting potential for the design of trans-mucosal nanoparticulate carriers. These polymers offer the possibility to facilitate the interaction of the nanocarrier with the intestinal mucosa and, hence, its access to the underlying epithelium. Indeed, this mechanistic principle has been adopted to explain the efficacy of particles made of acrylic polymers [59], polyanhydrides [60], and chitosan [61] as carriers for the trans-mucosal delivery of peptides. Alonso et al. [] had shown that high molecular weight (MW>100kDa) chitosan nanocapsules are efficient vehicles for improving the oral absorption of salmon calcitonin. Sung et al. [62] reported a simple ionic-gelation method to prepare nanoparticles composed of chitosan and poly(γ-glutamic acid) (γ-PGA) for oral insulin delivery. The in vivo results indicated that the insulin-loaded nanoparticles could effectively reduce the blood glucose level in a diabetic rat model. However, outside the range of pH 2.5-6.6, the nanoparticles became unstable and disintegrated. To overcome this problem, chitosan was conjugated with trimethyl groups for the synthesis of N-trimethyl chitosan (TMC) [63]. Nanoparticle self-assembled by the synthesized TMC and (γ-PGA) for oral delivery of insulin was successfully prepared and showed that TMC/γ-PGA nanoparticles were able to open the tight junctions between Caco-2 cells, and their effect on the tight junction's integrity appeared to be reversible.

Chapter 3

Experiment Methods

3.1 Flowchart of Experiment Process

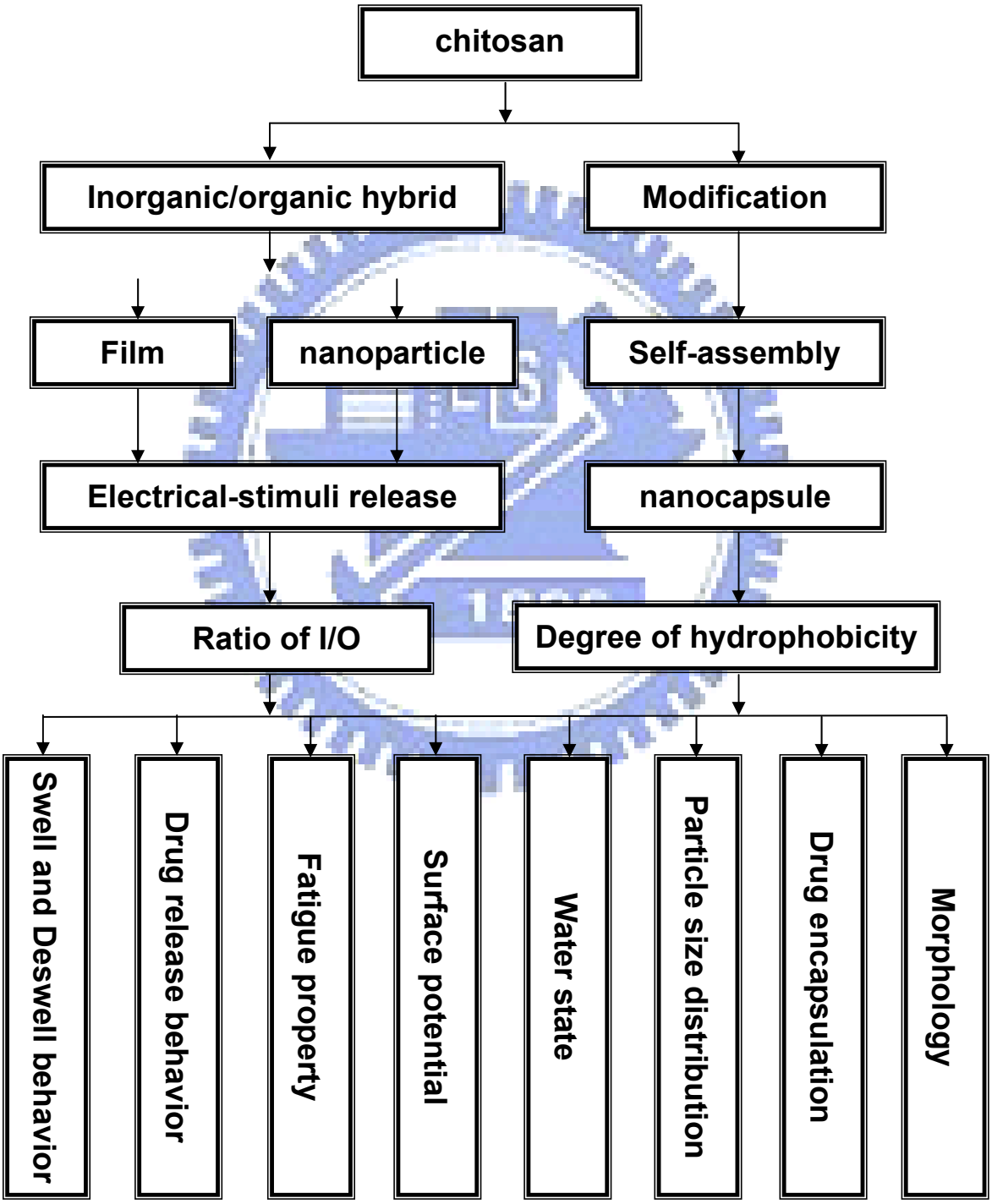

3.2 Materials

The chitosan used in this study was supplied by Aldrich-Sigma and used without purification. The same type of chitosan had been used by Darder et al. who pointed out that the chitosan has an average molecular weight of 342500 g $mole^{-1}$ and a deacetylation degree (DD) of ca. 75% [33].

As inorganic clay, Na-magadiite was purchased from Chang-Chun Petrochemical Co. (Hsinchu, Taiwan). The mean particle size and size distribution of the clay were measured by UPA (Ultrafine Particle Size Analyzer), Honeywell. The mean particle size of the clay (Na-magadiite) is estimated about 3 μm and a narrow particle size distribution of 2-4 μm can be observed.

Na^+-Montmorillonite, supplied by Nanocor Co., is a Na^+ form of layered smectite clay with a cationic exchange capacity (CEC) of 120 mequiv (100 g)–1. The MMT platelet shows a surface dimension of about 200-500nm in length and several ten nm in width.

Sodium phosphate for the preparation of buffers and acetic acid were purchased from Aldrich Chemicals. 2-propanol, sodium hydroxide, chloroacetic acid, acetic anhydride, hexanol anhydride, decanoic anhydride, and dodecanoic anhydride purchased from Sigma Co, USA, were reagent grade.

3.3 Characteristics Analysis

The crystallographical structures of CS-clay hydrogel were determined using XRD diffractometer (XRD, M18XHF, Mac Science, Tokyo, Japan) equipped with a Cu Kα radiation source (λ=0.154 nm). The diffraction data were collected from 2θ= 1~30^{o} at a scanning rate of 2^{o} per minutes.

FTIR spectra were recorded with KBr pellets on a Bomem DA8.3 spectrometer (Canada) for tablet analysis in the spectral region (4000-400 cm^{-1}) with 64 scans recorded at a resolution of 4 cm^{-1}.

Malvern Zreasizer HS3000 photon correlation spectrometer with an applied voltage of 100V and a 5-cm quartz cell was used to determine the zeta potential values of clay (Na-magadiite) in the phosphate buffer solution (PBS) with different pH value (pH= 4, 6, 7, and 10). The concentration of clay in aqueous suspension was fixed at 0.1 wt%.

The tensile mechanical properties of the hybrid composites were measured using a complete system of MTS Tytron 250 and TestStar IIs system in the following conditions: crosshead speed, 10 mm min^{-1}; test temperature, 25°C. The initial cross section (10 mm^2) was used to calculate the tensile strengths and the tensile modulus. All results reflect the average of three measurements. The difference between each measurement is <5%.

The stability of the CS-MMT suspensions were characterized using the optical absorbance of a UV-VIS spectrometer (SP-8001, Metertech Inc.), at a wavelength of 550 nm. Square glass cuvettes with a path length of 1 cm were used as sample holder. All the data shown in the work is an average value of three measurements and the measurement error is well below 5%.

The mean size and size distribution of the nanocapsules were measured by dynamic light scattering (DLS) Nanoparticle Size Analyzer (LB-550,

HORIBA, Japan). All measurements were done with a wavelength of 633.0 nm at 25^{o}C with an angle detection of 90^{o}. Each sample was repeatedly measured three times.

For elemental analyses, samples were extensively dried (80^{o}C, 24h) prior to submission of samples. Elemental analyses were performed with a Heraeus Vario III-NCH elemental analyzer (Germany).

Morphological evaluation was performed by Transmission Electron Microscopy (TEM) (JEOL2100, Japan) and Scanning Electron Microscopy (SEM) (S6500, JEOL, Japan). Sample solutions were dropped onto the carbon-coated 300 mesh copper grids and dried at 50^{o}C, then examined without being stained for TEM analysis. For SEM observation, sample was suspended into anhydrous ethanol, then dip-coated on the silicon substrate. After evaporation at 50^{o}C for 24 h, dried samples were coated with gold (~ 20 nm thickness) for analysis.

Proton nuclear magnetic resonance spectroscopy (^{1}H-NMR) spectra were acquired to confirm the sites and degrees of substitution recorded by NMR spectrometer (Varian unityinova 500) at 270 MHz. The samples were dissolved at a concentration of 10 mg/ml in D_2O and the spectra were performed at 353 K.

Differential scanning calorimeter (DSC, Perkin-Elmer instrument) was employed to identify the content and structural configuration of water molecules. The ACC solutions of 1.3% (w/v) were prepared by dissolving the obtained derivates in DI water. These suspensions were then cast onto petri dishes and dried at room temperature for 24 h, to form final dried samples. Those dried samples were later subjecting to swelling in DI water with various time duration of 1, 2, 3, 4, and 5 min of swelling, respectively, corresponding to

various amount of water content. Samples were quenched from room temperature to 213K and conditioned at 213 K for 10 min prior to the DSC test. DSC curves were then obtained by heating the sample to 300 K at a scanning rate of 10 K min^{-1}. The maximum content of non-freezable bound water ($W_{nf,max}$) can be determined by detecting the endothermic peak assigned to the first-order phase transformation of water in the samples with various contents of water. The endothermic peak of freezable bound water is not detected until a critical amount of water is added to the sample. The critical amount of water is correlated with the number of tight water binding sites.

Measurement of swelling behavior of CS-clay films

The film was first cut into round-shaped plate (its radius about 1 cm). The average thickness and the average weight of the obtained dried films were measured about 0.20 mm and 0.12 g, respectively. In order to measure the swelling ratio, each sample was weighed before and after immersion in phosphate buffer solution. After the excessive surface water had been removed with filter paper, the weight of swollen samples was measured at various time intervals. The procedure was repeated five times, until no further weight gain was detected. The swelling ratio was determined according to the following equation:

Swelling Ratio (%) = $[(W_s-W_d)/W_d] \times 100$

where W_s and W_d represent the weight of swollen and dried samples, respectively. All results reflect the average of five measurements. The difference between each measurement is <5%.

Electric-stimuli response behavior of CS-clay films

The film, pre-equilibrated and swollen in PBS, was cut into round-shaped plate (its radius about 1 cm) and weighed. Two platinum electrodes (its radius about 1.5 cm) were kept in contact with opposite surface of the film. The released water from hybrid films was continually removed using filter paper and the weight change of swollen hybrid films was checked periodically under electric field. The deswelling water ratio was evaluated as W_t/W_{t0} where W_{t0} and W_t were the initial weight of fully swollen films and the weight of films at deswelling time t, respectively. All results reflect the average of five measurements. The difference between each measurement is <5%.

Swelling under an applied voltage

The dry nanohydrogel, pre-equilibrated and swollen in 20 ml PBS (phosphate-buffered solution, pH7.4) for equilibrium, was cut into round-shaped plate (1 cm radius) and weighed. Two ring-shaped platinum electrodes (outer radius is 1.5 cm and inner radius is 0.5 cm) were kept in contact with opposite surface of the swollen nanohydrogel in the PBS. The electric voltage of 5V was applied from a dc power source for one hour. After the excessive surface water had been removed with filter paper, the weight of swollen samples was measured. The procedure was repeated three times, until no further weight gain was detected. All the data shown is an average of three measurements, where the measurement error is well below 5%.

Drug Release under an applied voltage

2% vitamin B12 (relative to the total weight of the final suspensions) was added into those final suspension (prepared for forming nanohydrogel in the second stage.) prior to drying. The drug-loading nanohydrogel, pre-equilibrated and swollen in 20 ml PBS for five minutes, was cut into round-shaped plate (radius of 1 cm) and weighed. Two ring-shaped platinum electrodes (outer radius is 1.5 cm and inner radius is 0.5 cm) were kept in contact with opposite surface of the swollen nanohydrogel in the PBS. The electric voltage of 5V was applied from a dc power source [64]. At appropriate time intervals, 3 ml solution was extracted from the container and analyzed using a UV spectrophotometer (Agilent 8453) at a specific wavelength λ=361 nm.

For on-off switching operation, the drug-loading nanohydrogel swollen in 20 ml PBS was then kept in contact with two platinum electrodes for electric-stimulation. A repeated operation between switching on and switching off of the electric-stimuli of 5V were carried out for ten cycles and the time durations of switching between “on” and “off” are both five minutes. The amount of drug release was measured spectroscopically at various time intervals. Since there has a risk of measurement error of drug release rate between different batches of drug loads in the nanohydrogels upon repeated on-off operation, where the difference in drug concentration between each operation for different samples will cause a variation, mostly reduction, of the release rate for later stage of the on-off electric-stimuli release, we then defined a standard release rate (R_{sd}) by normalization of the release rate upon each cycle of test.

$$R_{sd} = \left[\left(M_{i-1} - M_i\right)/M_{i-1}\right]/t \qquad i \geqq 1$$

Here, M_i is the residual drug amount in the nanohydrogel for the ith electric-stimulation and t is the time of applied voltage of 5V (five min). The obtained values are an average of three measurements and the difference between each measurement is <5%.

Measurement of self-aggregation behavior

The pyrene solution (1.0×10^{-4} M) in methanol was added into the test tubes, and evaporated under a stream of nitrogen gas to remove the solvents. Then, solutions of CHC self-aggregates in distilled water were, respectively, added into the above test tubes, brought the final concentration of pyrene to 1.0×10^{-6} M, which was nearly equal to the solubility of pyrene in water at 22°C [65]. The mixtures were sonicated for 30 min in an ultrasonic bath and shaken in a shaking air bath for 1 h at room temperature. Pyrene emission spectra were obtained using a fluorescence spectrophotometer (Hitachi FL-4500, Japan). The probe was excited at 343 nm, and the emission spectra were recorded in the range of 350-500 nm at an integration time of 1.0 s. The excitation and emission slit opening were 10 and 2.5 nm, respectively.

Chapter 4

Effect of Clay Content on Electro-stimuli Deformation and Volume Recovery Be-havior of Clay-chitosan Hybrid Composite

4.1 Introduction

"Intelligent" or "smart" hydrogels which can control drug release by changing the gel structure in response to environmental stimuli have been used in diverse applications, such as artificial muscles [66], bio-separation [67], and drug delivery system [68]. The environmental stimuli such as pH, pressure, temperature, light, magnetic fields and electric fields cause smart hydrogels to undergo macroscopic deformation and produce contractile force. In those stimuli, electric field is one of the most frequently employed stimulus methods to trigger desirable mechanical deformation of those "smart" hydrogels for specific engineering purposes. A typical example is "artificial" muscle which can be applied directly as a medical device with simple mechanical movement or employed as an electrically-controllable matrix or "switch" for drug delivery in vitro and in vivo [69]. An electric field as an external stimulus provides advantages with the enhanced feasibility of equipment currently available in the market that allows precise control of a number of parameters included the magnitude of current, duration of pluses, intervals between pulses, etc, which can be directly translated as a precise of the deformation behavior of the hydrogels.

Significant drawback of most environmentally stimuli-sensitive hydrogels

is that the responsivity and reversibility often decrease with both time and number of on-off operation cycles as the gel fatigues considerably. Generally, the deformation under a stimulus is increased with a larger molecular mobility in a gel of smaller cross-linking density. It is well known that the extent of gel deswelling increases with the magnitude of the electric voltage, but is not linearly proportional to it. Gong et al. [23] reported that the extent of deswelling depended on the amount of charge transported through the gel, rather than on the voltage applied. Furthermore, after removal of the stimulation, volume recovery occurs because the gel absorbs fluid and swells, which is also increased with the low cross-linking density. Sutani et al. [70] reported that the differences, including cross-linking density, the mobility and flexibility of the network and the viscosity properties of the gel, might affect the deformation and relaxation properties of gel with cyclic on-off operations. At the same time, it was also proved that there is a most suitable composition and viscoelasticity at a certain cross-linking density for the optimal electro-responsiveness. Shiga et al. found that an acrylacid-acrylamide gel swelled or deswelled under electric-stimulation, depending on the concentration of ions in the gel [71]. In order to further understand the dynamics of ion species in ionic gels, Doi et al. [72] proposed a semi-quantitative theory to explain the swelling and shrinking (deswelling) behaviors of electric-response gels. However, the actual mechanism to result in the fatigue of gel under stimulation is still not clear. Moreover, the fatigue problem of those hydrogels has to be circumvented for a reliable performance in medicine.

During the last decade, it was well-known that a considerable attention has been paid to inorganic-organic hybrid materials because it is possible to tailor their solid-state properties in relation to the nature and relative content of

constitutive components. Low-volume additions (1-5 wt.-%) of highly anisotropic nanoparticles, such as layered silicates, provide property enhancement with respect to the neat polymer that are comparable to those achieved by conventional loadings (15-40 wt %) of traditional fillers. Besides, unique value-added properties not normally possible with traditional fillers are also observed, such as enhanced strength, electrical conductivity, electrostatic discharge, remote-actuated shape recovery, and ablation resistance [73, 74]. Wang et al. [35] successfully synthesized chitosan/montmorillonite nanocomposites and reported that the nano-dispersed clay improved the thermal stability and enhanced the hardness and elastic modulus of the matrix systematically with the increase of clay loading, up to loading of 10 wt%. However, higher clay loading in the matrix perhaps enhances the possibility of inhomogeneous distribution of clay. In this case, this increase in both hardness and elastic modulus of the chitosan/clay nanocomposite imparts sufficient rigidity to the nanocomposite. This will then deteriorate desirable flexibility of the composite upon controlled contractile-expansion deformation under environmental stimuli. Therefore, it is more technically interesting to prepare such a nanocomposite system which is flexible and mechanically strong enough to be operated reliably under cyclic environmental stimuli, such as electrical stimulation.

By taking the advantage of the electrochemical properties, i.e., surface charge, and nanostructural properties, i.e., layer of the clay particles, a new class of “electrically-charged” hybrid composite based on chitosan (CS) and clay was studied. The inorganic material, clay, used in this investigation is poly-silicate magadiite ($Na_2Si_{14}O_{29} \cdot nH_2O$), which is composed of one or multiple negatively charged sheets of SiO_4 tetrahedra with abundant

silanol-terminated surface compensated by either Na^+ or H^+ in the interlayer spacing. The cationic biopolymer chitosan composed mainly of β-(1, 4)-linked 2-deoxy-2-amino-d-glucopyranose units is a deacetylated product of chitin. In the present study, with the incorporation into CS matrix, it is expected to enhance the thermal stability and mechanical properties of the resulting hybrid composite compared to neat CS polymer. Moreover, electrically-stimulated swelling-deswelling behavior, mechanical deformation, and clay content of the hybrid composite will be elucidated.

4.2 Preparation of CS-clay films

To prepare the CS-clay films, 1g CS was first dissolved in 40ml 1% acetic acid solution and then followed by centrifuging to remove the insoluble material. This ensures that the chitosan used to prepare the hybrid films can be completely dissolved without detectable insoluble fractions. Then, a small amount of clay (0.005g, 0.01g, 0.015g, 0.02g, and 0.03g) was added into 10ml distilled water to form suspension. Next, the mixed suspension added into the prepared CS solution with clay content of 0.5 wt %, 1 wt %, 1.5 wt %, 2 wt %, and 3 wt %, followed by stirring at 60°C until a uniformly-distributed CS-clay suspension was obtained. This solution was then cast onto petri-dishes (the radius is ca. 1.5 cm), and dried at 30°C for 24 h. The dried films were then immersed into an aqueous solution of 1M NaOH to remove residual acetic acid. The obtained products were washed with distilled water and dried for a week at 40°C in vacuum.

4.3 Chemical interaction of the CS and clay in the hybrid

Magadiite has a layered structure with negatively charged silicate layers compensated by interlayer sodium ions. Zeta-potential profile in Fig. 4-1 shows the change of the electrical charge of the clay in buffer solution with different pH values. The isoelectric point of the clay is determined to be about 5.3, which indicates that above pH 5.3 the net charge of the clay is negative. The poly-cationic nature of CS makes it an excellent candidate for interaction with the negatively-charged Na-magadiite clay by means of electrostatic attraction [75]. Thus, the clay in CS matrix can be acted as an effective multi-functional cross-linker [76]. For this purpose, aqueous medium with a low pH value is employed to generate ionized $-NH_3^+$ groups in the CS structure. An electrostatic attraction is expected to take place as a result of the Coulombic interactions between the positively-charged $-NH_3^+$ groups of the CS and the negatively-charged sites in the clay structure, which mainly controls the adsorption process.

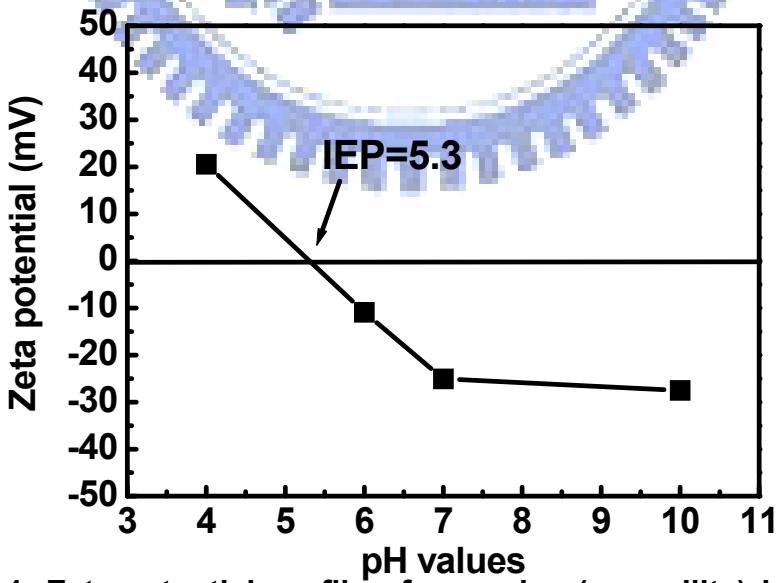

Figure 4-1. Zeta-potential profile of nanoclay (magadiite) in various pH values.

Figure 4-2(a) shows the low-angle XRD patterns of the Na-magadiite, neat CS and CS-clay hybrid films. The d_{001} spacing is obtained using the first rational orders corresponding to the (001) reflection. From the XRD pattern of Na-magadiite, three reflection peaks at about $2\theta=5.63^{o}$, 11.3^{o}, and 17.4, corresponding to the reflection plane of (001), (002), and (003), can be observed. Herein, the peak at 5.63^{o} is corresponding to a basal spacing of 1.55 nm. After incorporating small amount of the clay (1 and 2 wt %), the basal plane of clay at $2\theta=5.63^{o}$ disappeared, substituted by a new weakened broad peak at around $2\theta=8.1^{o}$. The movement of the basal reflection of clay from $2\theta=5.63^{o}$ to 8.1^{o} (the basal spacing =1.1 nm) is believed to be a result of replacement of Na^{+} by H^{+}. When the clay placed in contact with acids, even weak and diluted acids, an exchange reaction of the interlayer sodium ions by protons will take place, it is believed that during the preparation of chitosan-based film, due to the presence of acetic acid, sodium ions are exchanged by protons, yielding the layered silicic acid called H-magadiite [77]. On the other hand, it is found that the intensity of the peak at $2\theta\sim20^{o}$ which was identified as semi-crystalline CS decreased with the incorporation of the clay. From above results, it is believed that the dispersion of layer-type H-magadiite in the CS matrix may slightly deteriorate the crystallinity of CS. A further examination using IR spectroscopy reveals a strong absorption peak at $\lambda=1560\ cm^{-1}$, which corresponds to the vibration of the protonated amine group (δ_{NH3}) in CS and is broadened with the increase of clay addition (2 wt %), as shown in Figure 4-2(b). This correlation strongly suggests that the $-NH_3^{+}$ groups in the CS were interacted electro-statically with the negatively-charged sites of clay surface. This electrostatic interaction between the CS and the clay particles ensures the formation of bonding in between, which further generates

a strong cross-linking structure in the final hybrid.

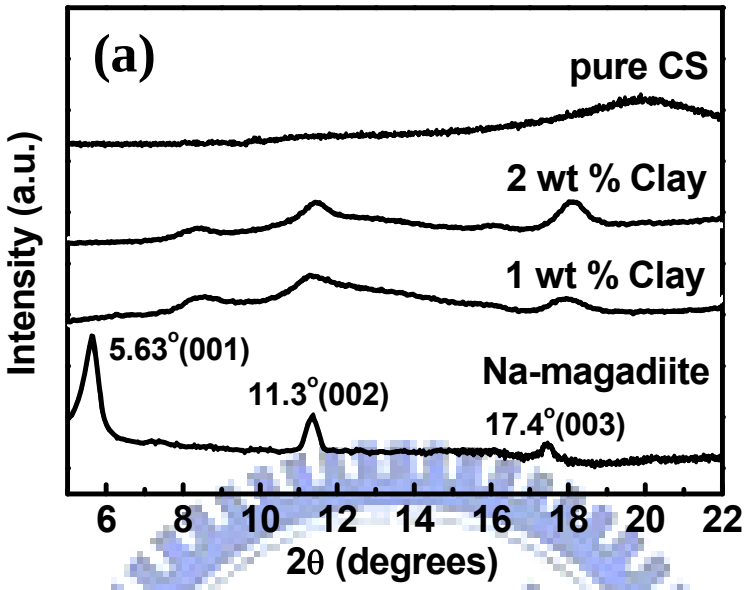

Figure 4-2(a) Low-angle powder XRD patterns of hybrid films with various clay loading.

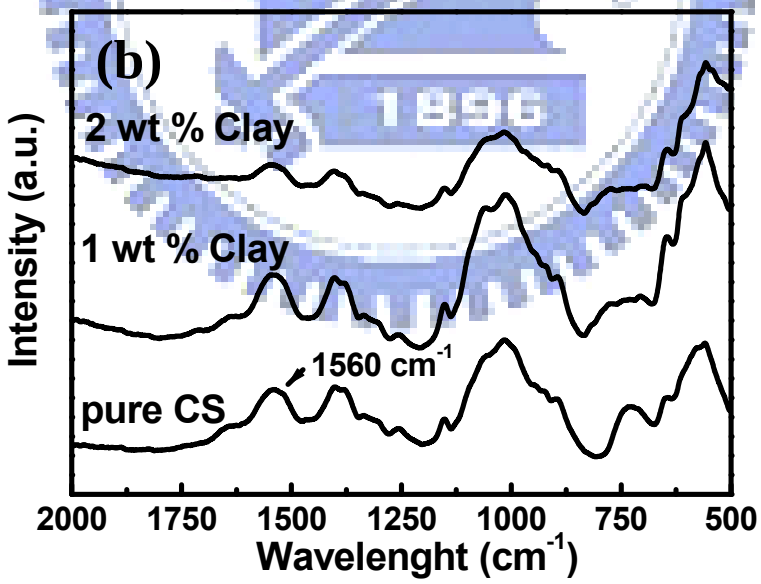

Figure 4-2(b) FTIR spectra of hybrid films with various clay loading.

4.4 Degree of cross-linking in the hybrid

As negatively-charged clay, acting as an ionic cross-linker, the addition of

the clay will strongly affect the cross-linking density as well as the mechanical property of the hybrids. From mechanical properties, Figure 4-3 shows the both breaking tensile strength and tensile modulus slightly decreased as 0.5 wt % clay was added. However, the breaking tensile strength and tensile modulus of the hybrid were improved with a further increase of clay concentration. This improvement of the mechanical properties was believed to be attributed to the formation of higher population of CS-clay bonds in the hybrid and more effective reduction in the molecular relaxation of CS matrix.

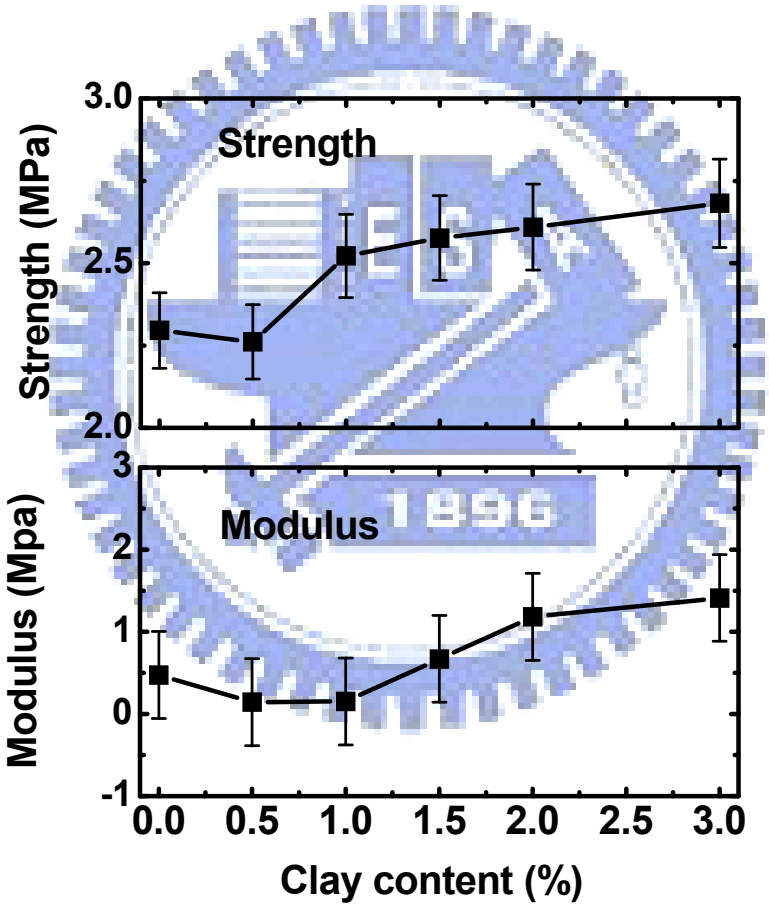

Figure 4-3 Mechanical properties of hybrid film. Initial cross-sectional area (10 mm^2) was used for calculating the modulus and strength.

Therefore, it is reasonably to believe from the mechanical behavior of the

hybrid composites that the incorporation of the negatively-charged clay is able to form a physically strong network structure associated with the positively-charged CS matrix. Furthermore, the cross-linking density which is equivalent to the number of cross-linked chain per unit volume is mainly determined by the concentration of CS polymer and the initiator at a fixed amount of the clay. The number of cross-linked polymer chains per unit volume of the hybrid, N^*, can be estimated according to equation (4-1) [78] by using the stress at 100% elongation (α=2).

$$F = \Phi N^* kT\left\{\alpha - \left(\frac{1}{\alpha}\right)^2\right\} \quad (4\text{-}1)$$

here, F is the force per unit original cross-sectional area of the swollen network, Φ is a front factor (=1), α is the elongation ratio, and k and T are Boltzmann's constant and the absolute temperature. The data, N^*, measured from Eq. (4-1) with different concentrations of clay (C_{clay}) were illustrated in Fig. 4-4. At lower clay content (e.g., 0.5-1 wt %), it was observed that the value of N* of the hybrids was less than that of the pure CS. This lower cross-linking density of the hybrids is most probably due to its lower crystallinity. As evidenced from the results of XRD (Figure 2(a)), it was demonstrated that the incorporation of clay would slightly deteriorate the crystallinity of CS. But at the same time, increase of the clay in the CS matrix will also provide chemically cross-linking bonds between the CS and clay, resulting in a more pronounced effect on improved mechanical properties. As clay was incorporated, a competition between the deterioration of CS crystallinity and increasing cross-linking density, that dominates the performance of resulting hybrid composites. While further increasing clay concentration, the increasing cross-linked bonds reinforce the hybrid over the adverse effect with only small addition of the clay.

Thus, the number of cross-linked polymer chains per unit volume (N^*) is then increased with increasing C_{clay}, wherein an improved physical properties can then be expected.

Accordingly, it is more interesting to explore the swelling and de-swelling behavior of this new class of hybrids and is particularly expecting to exhibit improved anti-fatigue property under cyclic electro-stimulus operations.

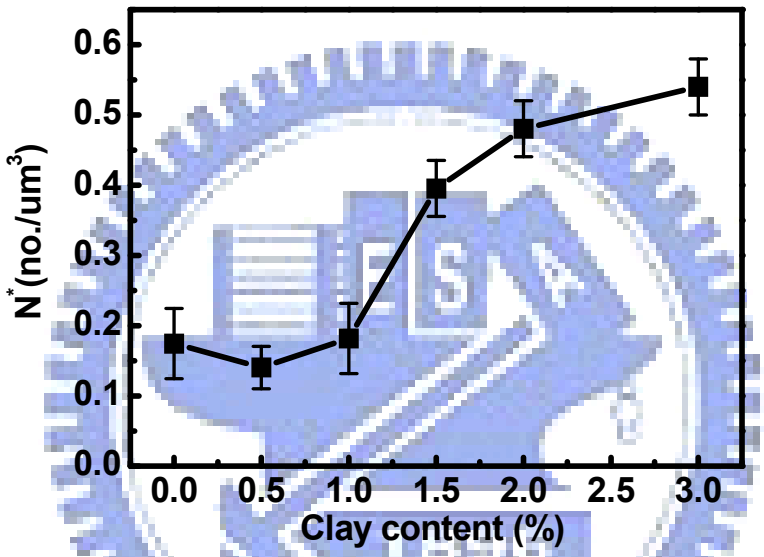

Figure 4-4 Clay content dependencies of the number of cross-linked chain (N*)

4.5 Swelling - Deswelling behavior of the hybrid films

It is well-known that positively charged CS at low pH exhibits a high swelling ratio due to the repulsive force between the same positively-charged molecules, which would result in longer intermolecular distance and more hydrophilic property. In other words, increasing the pH of the solution will reduce the repulsion force, thus further limiting the hydration of the CS. The swelling kinetics at PBS (pH=7.4) of pure CS and hybrid film with different C_{clay}

are displayed in Figure 4-5(a). It should be noticed that the swelling equilibrium was reached rapidly at pH 7.4 within 20 minutes. The gained equilibrium state in a short time period was helpful for further cyclic swelling and de-swelling test.

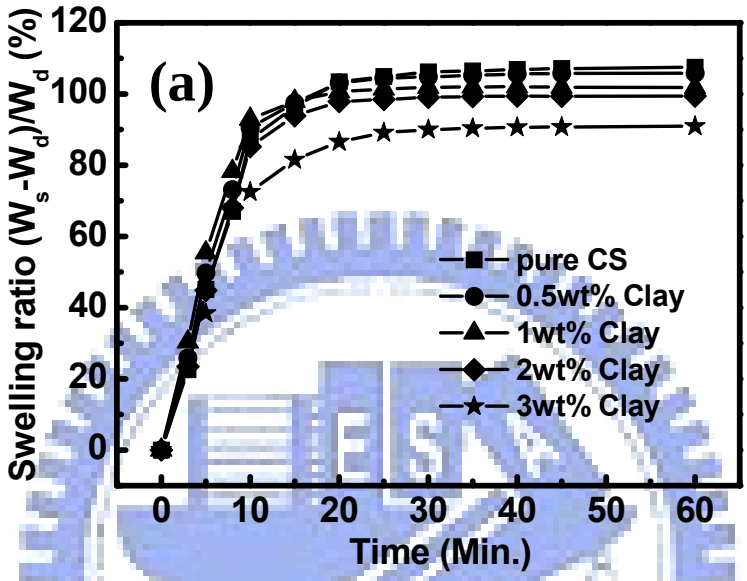

Figure 4-5(a) Swelling kinetics of hybrid film with different C_{clay} at pH 7.4.

In order to gain better understanding of the effect of clay on the swelling behavior of the composites, the plots of $\ln(W_0/W_t)$ against time at initial ten minutes was illustrated in Figure 4-5(b). All plots show straight-like lines, indicating that the process of the swelling may be illustrated with apparent first-order kinetics as described by the pseudo-first-order kinetic equation [79]:

$$\ln\left(\frac{W_0}{W_t}\right) = nt + k \qquad (4\text{-}2)$$

where W_0 and W_t are the weight of the hybrid composites at t = 0 and any time t, respectively, n is the first-order rate constant (1/s), and k is a constant. Evidently, the linear fitting showed a reasonably good correlation (with a correlation coefficient, r^2=0.9862). It can be found that the value of the first-order rate constant n showed a small increase, compared to the pure

chitosan, from 0.063 to 0.066 as a small amount of clay was added (0.5-1 wt %). However, when the amount of the clay increased above 3 wt%, high cross-linking degree decreased the swelling rate, resulting in a greater decrease in n value (n=0.054) was observed. In addition, the equilibrium swelling ratios of the composites are also affected by the incorporation of the clay.

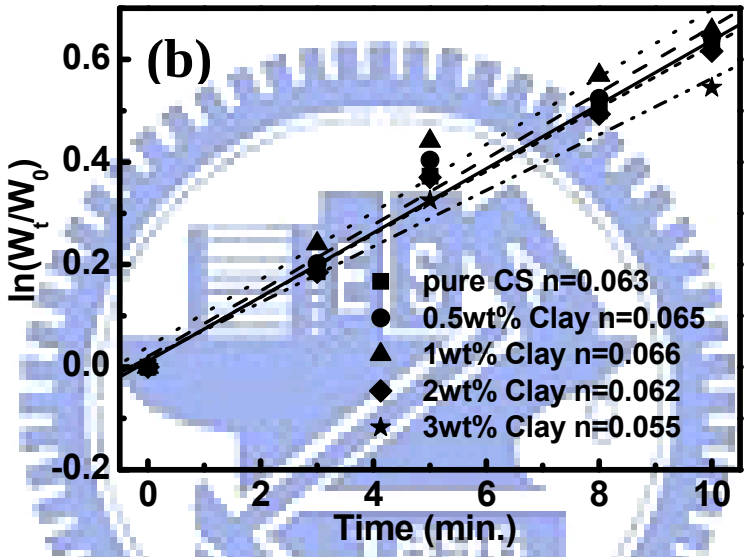

Figure 4-5(b) Plots of $\ln(W_0/W_t)$ against time of hybrid film with different C_{clay} at pH 7.4.

As seen from Figure 4-5(c), the equilibrium swelling ratio of the composites reduced from 106% to 91.0% with the increase of clay from 0 to 3 wt %. The decrease in the equilibrium swelling ratio with increasing C_{clay} was also observed at pH 4 and 10 (not showed here). This can be attributed as a result of either a reduced amount of functional groups or a proportional reduction in ionizable functional groups in the CS as a result of extensive cross-linking bonding formed between the positively-charged CS and the negatively-charged clay. From the results above, the swelling behavior of chitosan film does not differ substantially from that of the hybrid films with 0-2

wt % clay contents. For example, when a small amounts of clay was added (0.5-2 wt %), the value of n and equilibrium swelling ratio was calculated to lying between 0.063~0.062 and 106%-102%, respectively. However, the hybrid film with 3 wt% addition of clay does show a larger difference in the swelling kinetics and equilibrium swelling ratio, compared to other samples, i.e., n= 0.054 and 91.0%, respectively. This suggests that as the clay concentration exceeds a critical concentration, an effective cross-linked interaction between the surface of clay particles and chitosan molecular chain can be efficiently developed. Hence, high cross-linking density caused by higher addition of the C_{clay} (3 wt %) decreased both the swelling rate and the equilibrium swelling ratio as well.

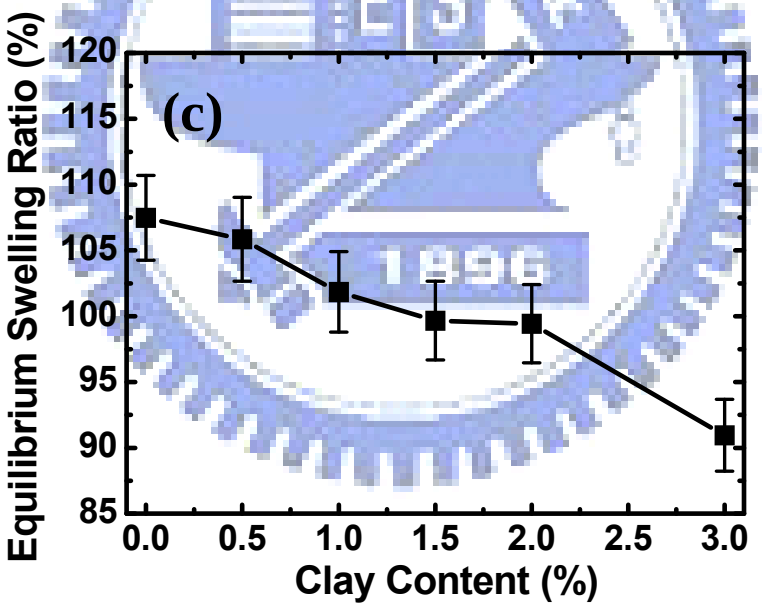

Figure 4-5(c) Equilibrium swelling ratio of hybrid film with different C_{clay} at pH 7.4.

Since CS is a cationic biopolymer and has been proposed for electrically-modulated drug delivery [21], therefore, the deswelling behavior is becoming so critical for a reliable performance for a number of biomedical

applications, such as drug delivery, wherein a release rate can be externally or internally controlled from slow to pulsatile release profiles according to practical needs. The mechanism of deswelling behavior is generally thought to be a macroscopic contractile deformation of a polymer hydrogel under an electric field. This is due to a voltage-induced movement of ions across the entire polymeric matrix and the concomitant expansion on one side and contraction on the other side of the polymer [8]. Figure 4-6(a) exhibits the deswelling ratio as a function of time with different applied voltages and clay concentrations.

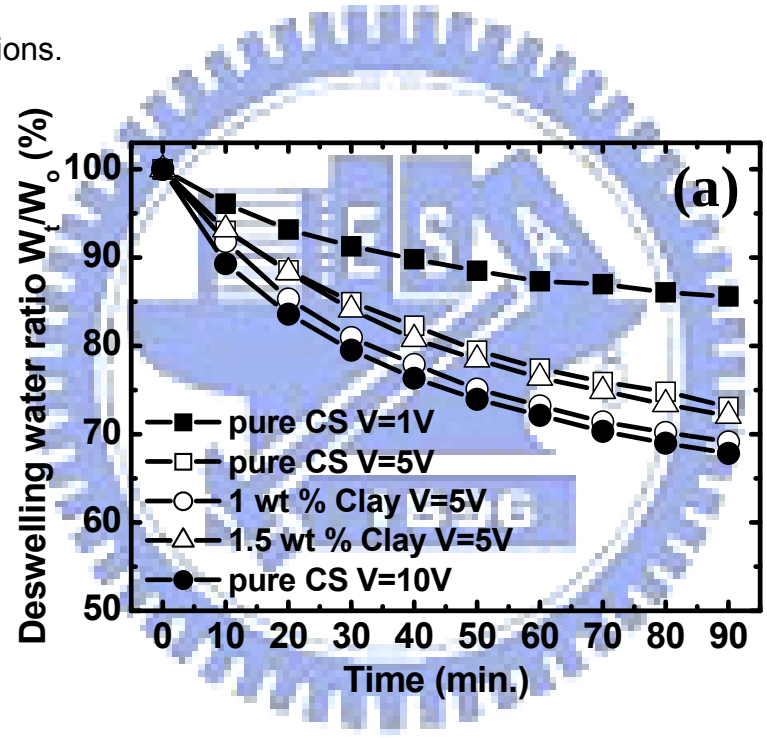

Figure 4-6(a) Deswelling behavior in 1.5h of hybrid film with different C_{clay} under applied voltage of 1, 5, and 10V.

The deswelling rate of the composites was enhanced in proportion to the applied voltage, which suggests that the increased potential gradient in electric field caused an increase in the rate of movement of those counter ions to different electrolytes.

At the same time, the incorporation of the clay was found to influence strongly the deformation of the hybrid films under an electrical field. As a

consequence, the electro-stimuli deformation reached equilibrium after 1.5h of operation. Concerning the deswelling ratio at the time of 1.5h, as shown in Figure 4-6(b), the hybrids with lower C_{clay} are subjected to smaller restriction of molecule relaxation than that of pure CS. In other words, with increasing C_{clay}, the mobility of the hybrid composites was gradually restricted by the formation of increasing amount of the cross-linking bonds.

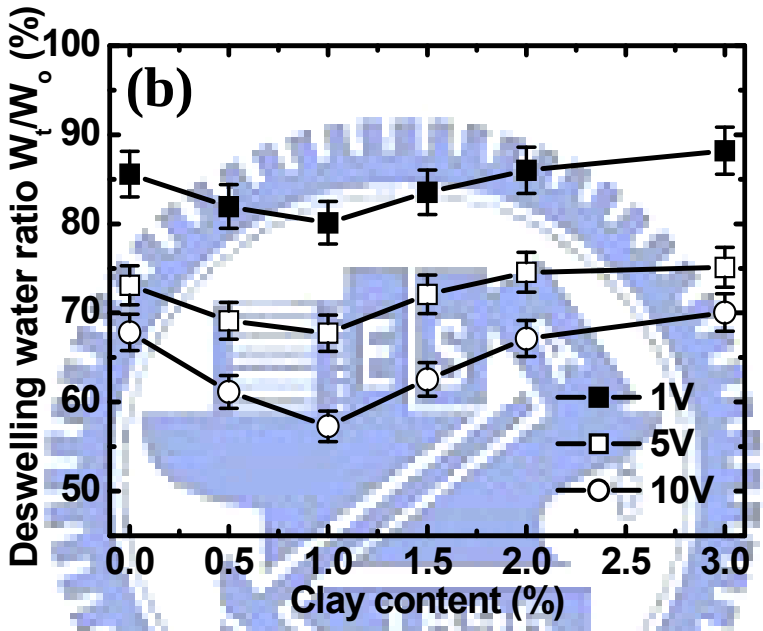

Figure 4-6(b) Deswelling water ratio in 1.5h of hybrid film with different C_{clay} under applied voltage of 1, 5, and 10V.

Therefore, the deswelling ratio of the resulting hybrid is decreased with increase of C_{clay}. As shown in Fig. 4-6(b), the hybrid composites containing the lower clay concentration (0.5-1 wt %) exhibited more rapid responsivity and larger deformation to a given electrical voltage. However, the rate and extent of the deswelling kinetics are both decreased as C_{clay} is increased.

4.5 Cyclic deformation and recovery of hybrid films

Above a threshold value of a given electrical field, the hybrid film showed

a deswelling behavior wherein the water is gradually expelled from the hybrid. When the electric field was removed, the matrix swelled by absorbing surrounding water. A repeated on-off operation of the electrical field stimulates the hybrid films with a cyclic swelling-deswelling mechanical deformation. Figure 4-7(a) shows that the relative swelling ratio of the CS film after cyclic on-off operation of the electrical field in a 20-minute interval to that of original equilibrium swelling ratio of the hybrid film with different clay concentrations under applied voltage of 10V.

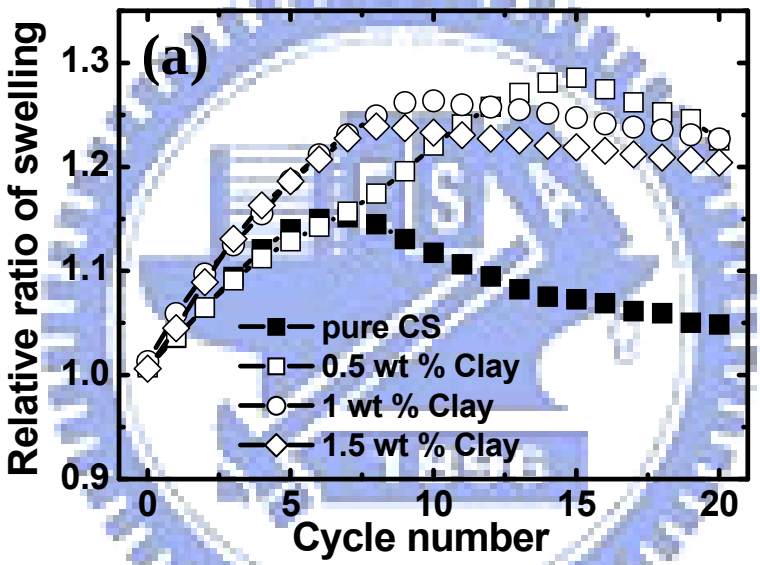

Figure 4-7(a) Relative ratio of swelling after cyclic on-off switching of electric-stimuli of 5V in a 20-minute interval of hybrid films with different C_{clay}.

Initially, the equilibrium swelling of pure CS film was slightly increased at first several times of the on-off operation. It may be due to a collapse of the CS structure under applied voltage and then produce more and more porous structure on the CS film as was visually observed. The enhanced porosity will improve the degree of swelling to about 1.15 times after six cycles. After then, the degree of swelling started to reduce, indicating a fatigue behavior of the CS

film. This observation suggests that the CS film should lose its structural integrity after 6 cyclic operations and this deteriorates the CS film by losing its capability of absorbing water. On the contrary, the hybrid composite with lower clay content (0.5 wt %) showed much better structural integrity allowing the hybrid to be operated by as high as 15 times of the cyclic operation and a higher relative ratio of swelling achievable at about 1.3.

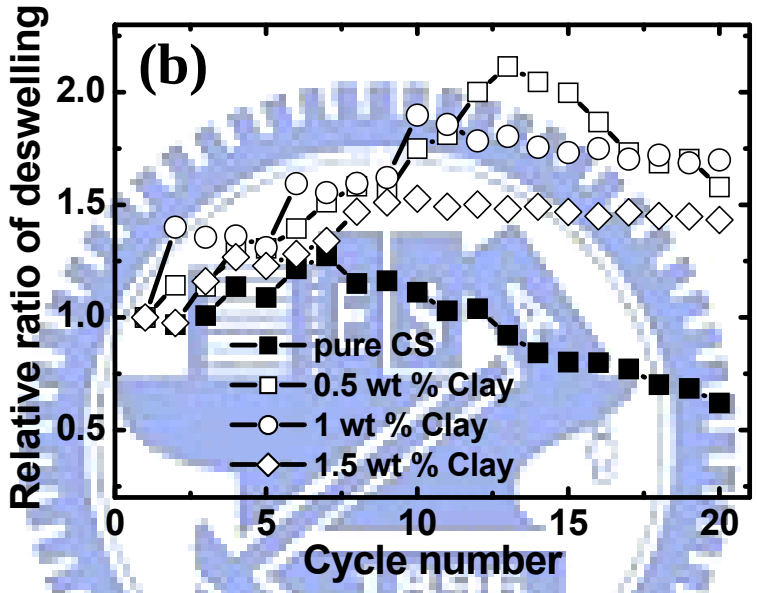

Figure 4-7(b). Relative ratio of deswelling after cyclic on-off switching of electric-stimuli of 5V in a 20-minute interval of hybrid films with different C_{clay}.

The increase of swelling degree may be associated with the decrease of cross-linking degree caused by lower C_{clay}. However, as the higher concentration of the clay was loaded (>0.5 wt %), the swelling ratio remained the same when the number of cyclic stimulation exceeded six times. Actually, the swelling ratio would also not decrease enormously with increased cyclic stimulation like the case of pure CS and hybrid of 0.5 wt % clay. It is believed that greater cross-linking density of the hybrid composites is capable of

bearing larger applied voltage and more on-off switching operations. Similarly, the higher C_{clay} (>0.5 wt %) of the hybrid composites can maintain the same degree of deswelling after over 10 times of cyclic operation, compared to the pure CS film and hybrid composites with lower clay content , as shown in Figure 4-7(b). Hence, the incorporation of the clay particles can structurally adjust the cross-linking density of the hybrid with improved anti-fatigue property of the hybrids under cyclic electric-stimuli operation.

Figure 4-8 shows the weight changes of the pure CS film and the hybrid film (1 wt % clay) under an applied voltage of 10V in PBS and consecutive on-off operation in a 20-minute interval. For pure CS, the degree of reversibility (i.e., the ability for the hybrid to structurally return back to initial swelling state as first prepared) is decreased apparently with the on-off operation more than 7 cycles. Furthermore, the deswelling ratio of the pure CS film could not restore to original level after several cyclic operations. The decrease of the swelling and deswelling ratio of the hybrid film can be translated directly as an indication of fatigue behavior of the hybrid. In this study, the films with a composition of 1 wt % clay showed the best anti-fatigue property where the swelling and deswelling behavior remained identical even after 20 cycles of on-off operation. Since the contractile deformation under stimulus and volume recovery of a given polyelectrolyte hydrogel is associated with the optimal viscoelasticity at a certain cross-linking density, it is suggested that the incorporation of the negatively-charged clay as cross-linkers provides more effective anti-fatigue property for pure positively-charged chitosan under cyclic electro-stimuli operation. On this base, it is believed that this hybrid is considered in biomedical applications with improved and reliable performance, especially used as drug delivery system which is currently under investigation

and will be reported shortly.

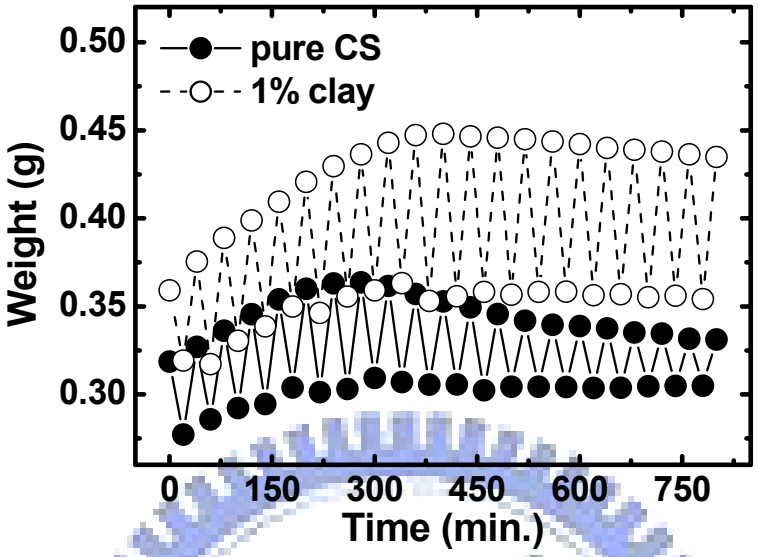

Figure 4-8. Weight changes of pure chitosan and hybrid film with 1 wt % clay addition under cyclic on-off switching of electric-stimuli of 5V.

Chapter 5

Drug release behavior of chitosan–montmorillonite nanocomposite hydrogels following electrostimulation

5.1 Introduction

Smart polymer hydrogels have been studied with a particular emphasis on their reversible volume changes in response to external stimuli, such as pH, solvent composition, temperature, ionic concentration, and electric field [80-82]. These hydrogels have been developed and studied with regard to the application to several biomedical fields; for example, separation techniques, soft-actuators, and controlled drug delivery systems [83, 84]. Among them, electrically controlled drug delivery may particularly offer unique advantages for providing on-demand release of drug molecules from implantable reservoirs. In addition, electrical control is advantageous for coupling to sensors and microelectronics in feedback controlled systems [85].

For electro-sensitive hydrogels as controlled drug delivery systems, the drug release rate can be easily controlled simply by modulating the electric field. Generally, the extent of drug release increases with the magnitude of electric field and time, but is not linearly proportional to them [86]. Hence, it becomes more difficult to precisely control the release of drug by electric-stimulation. In particular, an important goal of drug delivery is to obtain a constant release rate for a prolonged time. However, as common problems of all hydrogels, the responsivity and reversibility will be decreased after several switching on-off operations. For commercial application, this fatigue property has to be improved to reach stable pulsatile release under repeatedly

operations. Unfortunately, as we have learned so far, little study had addressed this important issue and this is then one of the research objectives of this investigation. Hence, in order to overcome the fatigue problem to a certain extent of the conventional hydrogels, incorporation of inorganic nanophase becomes an attractive alternative, i.e., inorganic-organic nanocomposite hydrogel (hereinafter, we named it as nanohydrogel), where the properties of polymer matrix would be improved with a large effect on the electric-deformation and relaxation behaviors [70]. For example, Gong et al. [87] had reported that organically modified clay can enhance temperature response of clay-poly(N-isopropylacrylamide) (PNIPAAm) nanocomposites. Based on hydration theory, the organically modified clay introduces a hydrophobic environment at the interface that would enhance the efficiency of the thermal transition, narrow the transition range, and increase the transition rate. However, to the best of our knowledge, little research work had been reported on the electric-stimuli drug release behavior of polymer-(nano)clay nanohydrogel.

Polymer-clay nanohydrogels are expected to have novel properties because of the nanometric scale on which the nanoclay particles (i.e., plate-like shape) would alter the physical and chemical properties of the polymeric materials and improved their mechanical properties and thermal stability [35]. Chitosan (CS) used as polymeric matrix in this work is a cationic biopolymer and has been proposed for electrically-modulated drug delivery [21]. In chapter 4, it was demonstrated that the addition of clay in the CS matrix could strongly affect the cross-linking density as well as the mechanical property, swelling–deswelling behavior and fatigue property of the nanohybrids. Hence, the incorporation of negatively-charged delaminated (exfoliated)

montmorillonite (MMT) is expected to electrostatically interact with the positively-charged $-NH_3^+$ group of CS, which generates a strong cross-linking structure in the nanohydrogel [76] and then, strongly affects the macroscopic property of the nanohydrogel and the drug diffusion through the bulk entity. In present work, the release kinetics and mechanism of the vitamin B12 in terms of MMT contents were investigated under a given electric-field stimulus. Furthermore, the anti-fatigue behavior with respect to the repeated field stimuli of the resulting nanohydrogel in terms of MMT addition was also elucidated.

5.2 Preparation of CS-MMT nanohydrogels

To prepare the CS-MMT nanohydrogels, the preparation procedure is separated into two stages, the first stage is first to prepare a suspension containing MMT and CS with a weight ratio of 1:2 (where the CS solution was prepared by dissolving the pre-determined amounts of CS in 1 wt % acetic acid solution and stirring for about 4h till the CS completely dissolved). The CS-MMT suspensions were obtained by adding CS, to an aqueous solution containing 2 wt % MMT (i.e., 0.5 g of Na^+-MMT dispersed in 25 ml of double-distilled water), stirred at 50°C for 24h. To enhance the formation of exfoliation of the MMT in the final nanohydrogel, the suspension with CS to MMT ratio of 2:1 was then subject to ball-milling for 24h, after then, the as-prepared final CS-MMT suspension was used to form nanohydrogel.

In the second stage of the CS-MMT nanohydrogel preparation, 2 wt % CS solution was obtained by dissolving CS into 1 wt % acetic acid solution. Then, a small amount of the ball-milled CS-MMT suspension was added into the prepared CS solution to form CS-rich suspension with the MMT content controlled in the range of 1 wt %, 2 wt %, 3 wt %, and 4 wt %, relative to the

total weight of CS in the suspensions, under continuous stirring at 60^{o}C for 1h. This final suspension was then cast onto petri-dishes and dried at 30^{o}C for 24 h, to form a final dried nanohydrogels. The dried nanohydrogels were then rinsed with an aqueous solution of 1M NaOH to remove residual acetic acid, followed by washing with distilled water and dried for a week at 40^{o}C in vacuum till use. The compositions of the nanohydrogels are expressed using the value of n to define the content of MMT (1-4 wt %) in the CS-MMTn, where n=C_{MMT}, the content of the incorporated MMT, for the nanohydrogels, ranging from 1 to 4 %.

5.3 Structural Characterization

The hydrophilic and polycationic nature of CS in acidic media permit a good miscibility with MMT and can easily intercalate into the interlayers of the MMT by means of cationic exchange processes [33]. For this purpose, an acidic pH value is used to ionize the formation of $-NH_3^+$ groups in the CS structure. Given that the pKa of the primary amine groups in the CS structure is 6.3, 95% of the amine groups will be protonated at pH 5 of the CS-MMT suspensions. Figure 5-1 illustrates the XRD patterns of neat MMT and CS-MMT suspensions with different ratios of CS-to-MMT. The XRD pattern of the neat MMT (Figure 5-1a) shows a reflection peak at about $2\theta=6.5^o$, corresponding to a basal spacing of 1.35 nm.

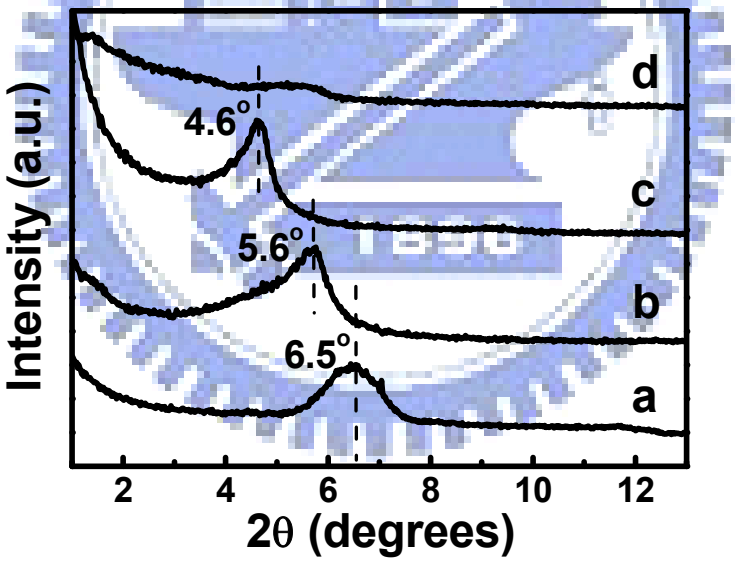

Figure 5-1 Low-angle powder XRD patterns of (a) neat MMT and the CS/MMT nanocomposites with the CS and MMT ratios of (b) 0.5:1 (c) 2:1 and (d) ball milling for 24 h.

The MMT in the suspension with lower CS-to-MMT ratio (0.5:1) shows a decrease of 2θ value to about 5.6^o suggesting the intercalation of CS in a monolayer disposition (Figure 5-1b). The lower 2θ value obtained for the MMT

in the suspension with the highest ratio of CS-to-MMT (2:1) is related to the intercalation of the CS as a bi-layer (Figure 5-1c). After ball-milling for 24h, the XRD pattern of the MMT in the suspension shows a faint, broad peak at around $2\theta=5\text{-}6^{o}$ (Figure 5-1d). The broad peak with decreased intensity most likely indicated a disordered, exfoliated and little intercalated structures of the MMT. In addition, it is hard to give a definitive conclusion regarding the nanostructural evolution without more convincing information but through XRD analysis only. Recording the optical absorbance with time gives a suitable indication of the aggregation and sedimentation of the MMT in the suspensions. This method allows us to distinguish accurately the difference in surface structures acquired by particle aggregates.

Figure 5-2 shows the time dependence of the optical absorbance A (relative to its initial value, A_0) of the exfoliated MMT, original MMT and monolayer or bilayer intercalated-MMT suspensions. In theory [88], sedimentation velocity U of interacting colloidal particles depends both on the hydrodynamic interactions mediated by the suspending solvent, and on the microstructure of the suspension. In equilibrium, the latter is determined by direct potential forces arising, for example, from the steric repulsion between the particles and from the electrostatic repulsion of overlapping double layers. On the other hand, the long-ranged electrostatic repulsion occurring in suspensions of charged particles can give rise to a reduction in U, as compared to hard spheres dispersion at the same volume fraction. Watzlawek and Nägele [18] proposed a model that the reduced sedimentation velocity of dilute deionized suspensions of weakly charged particles scaled like $U/U_0=1\text{-}p\psi 1/2$ where ψ is the particle volume fraction and U_0 is the sedimentation velocity at finite dilution, with a parameter p depending on the

macroion charge Z ($p \sim |Z|^3$). Hence, it is believed from the time dependence of optical absorbance A, Fig. 5-2a, that the exfoliated MMT keeps a greater value of A/A_0 (~1) for a period of 180 minutes which is due to that it carried more negatively-charged sites on the surface layer resulting in stronger electrical repulsion than that of non-exfoliated MMT.

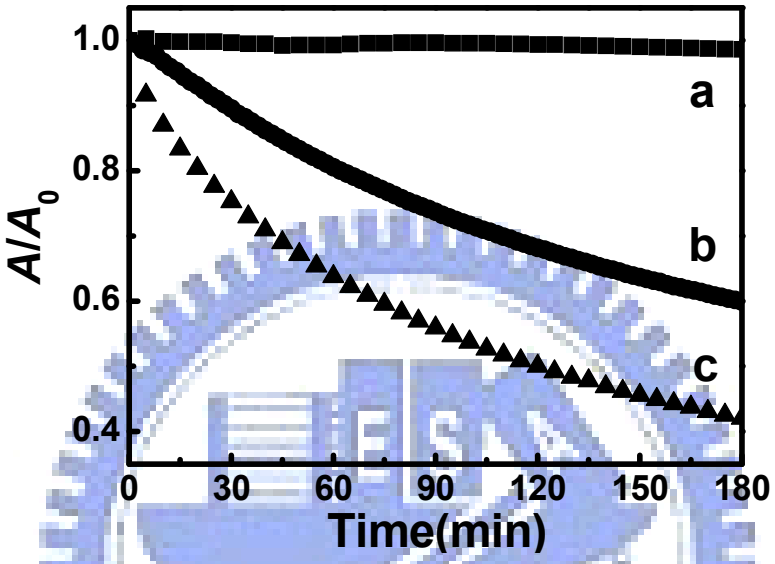

Figure 5-2 Time dependence of optical absorbance *A* (relative to its initial value, A_0) of the (a) exfoliated MMT (b) original MMT and (c) monolayer or bilayer intercalated-MMT suspensions.

Nevertheless, the electrostatic attraction between ionized $-NH_3^+$ groups in the CS structure and negatively charged silicate layers neutralizes this repulsion force, it is then expected that monolayer or bilayer intercalated-MMT (Figure 5-2c) exhibited faster sedimentation (lower values of A/A_0 after 180 minutes) than non-exfoliated MMT (Figure 5-2b).

As shown in Figure 5-3, it was found that the intensity of the diffraction peaks at $2\theta \sim 20^o$ which was identified as semi-crystalline CS decreased with the incorporation of MMT. Furthermore, the XRD patterns do not show any diffraction peak at $2\theta = 2\text{-}10^o$ as opposed to the diffraction peak at $2\theta = 6.5^o$ (d spacing = 1.35 nm) for original MMT, indicating development of exfoliated

silicate layers of MMT in CS matrix. It can be expected that the interaction between CS and exfoliated sheets ensures the formation of bonding in between, which further generates a strong cross-linking structure in the final nanohydrogels.

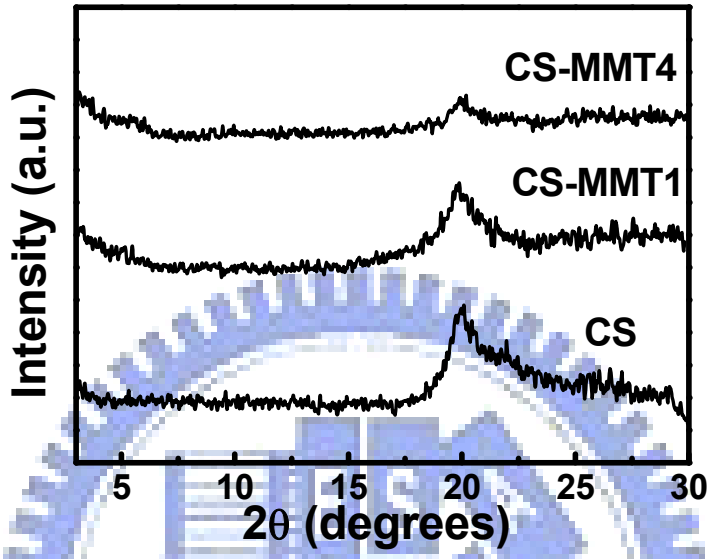

Figure 5-3 Side-angle powder XRD patterns of pure CS, CS-MMT1 and CS-MMT4.

5.4 Drug release behavior under an applied electric field

Vitamin B12 is water soluble and has low molecular weight (1355Da). Its small molecular size and neutral charged state allows the molecule to be a suitable model drug for controlled release study in this nanohydrogels. Under constant driving voltage (at 5V), the time-dependent cumulative release of the drug from the nanohydrogels with different MMT concentrations revealed that both the release rate and cumulative drug amount from pure CS hydrogel or the nanohydrogels upon electric-stimulation are higher than that of pure CS without applying electric field (Fig. 5-4(a)). This may be due to an action of ejection of drug from the electro-sensitive hydrogels as a result of deswelling and syneresis [70]. In addition, it has to be mentioned that without

electric-stimulation, the release rate of vitamin B12 from pure CS hydrogel is much closer to that of the nanohydrogels (the release profiles of vitamin B12 from the nanohydrogels are not shown). It suggests that nano-scale dispersion of MMT may not strongly influence the swelling of the CS matrix and then hinder the molecules from diffusion. In particular, this result is in good agreement with the fact that the MMT nanoplates were well-dispersed in the CS matrix.

In order to further understand the electric-stimuli drug release behavior of this nanohydrogel, diffusion exponent n was determined by the use of Power Law [89].

$$\left(M_t / M_0\right) = kt^n \qquad (5\text{-}1)$$

where M_t is the amount of drug released at time t, M_0 is the loading amount of drug during preparation of nanohydrogel, k is rate constant and n is diffusion exponent related to the diffusion mechanism. The changes of calculated values of n of the nanohydrogels with different CMMT were shown in Fig. 5-4(b). It is clear that the electrically-controlled drug release behaviors of the nanohydrogels were changed with different amounts of MMT. It can be observed that the diffusion exponent n increased when 1 wt % MMT was added to the pure CS. A small addition of MMT (1 wt %) brings the n to a value close to 1, which indicates a change in drug release mechanism from diffusion-controlled to swelling-controlled mode.

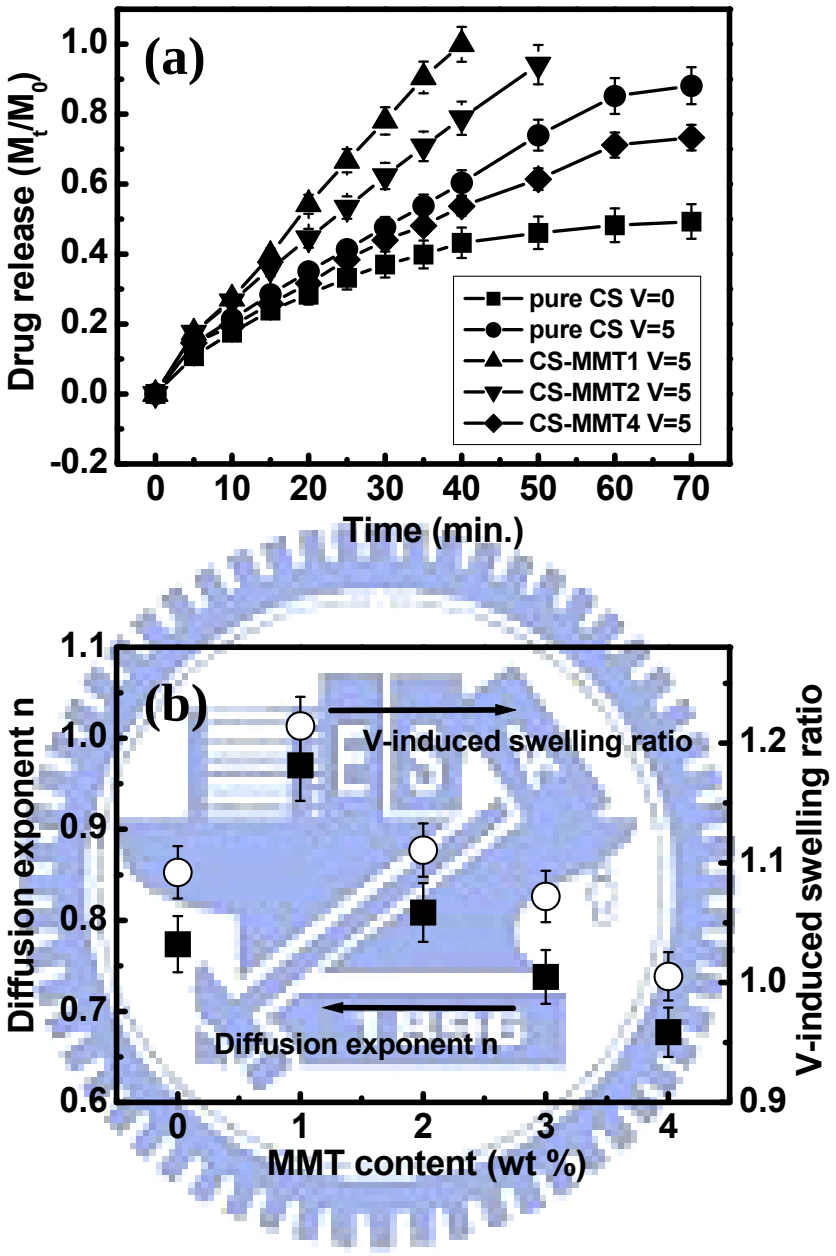

Figure 5-4 (a) Time-dependent cumulative release curves of vitamin B_{12} from the nanohydrogels upon an applied electric voltage, showing the different release profiles with different C_{MMT}. (b) Dependences of the loaded MMT contents on the diffusion exponent n and voltage-induced swelling ratios of the nanohydrogels. (The filled boxes indicated the diffusion exponent n and the empty circles indicated the V-induced swelling ratio)

However, when MMT was continuously increased to 4 wt %, the diffusion exponent n then decreased. This decrease of n means a change in drug release mechanism from swelling-controlled to diffusion-controlled. The plausible explanation can be deduced from chapter 4, where the incorporation of clay would slightly deteriorate the crystallinity of CS, in contrast, increase of the clay concentrations in the CS matrix will provide cross-linking bond between the CS and clay. The influence of increasing clay concentration is likely to be more pronounced in adding mechanical reinforcement to the nanohydrogel by increasing cross-linked density, than those with a smaller clay addition, causing a decreased swelling ability. Moreover, the different degree of cross-linking will sharply change the mesh size of the CS matrix, resulting in various transport paths and diffusion velocity for the solute molecules.

It was evidenced that the resulting equilibrium swelling ratios of the nanohydrogels with various MMT contents were increased after applying electric-stimulation and hereinafter, defined as voltage-induced swelling ratio. Here, voltage (V)-induced swelling ratio can be appropriately estimated by Equation (5-2):

$$\text{V-induced swelling ratio} = W_t/W_s \qquad (5\text{-}2)$$

where W_t is the weight of the nanohydrogel swelling in PBS under an applied voltage of 5V for 1h and Ws is the equilibrium weight of the nanohydrogel swelling in PBS before electric-stimulation. As shown in Fig. 5-4(b), it was found that the ratio increases with small MMT addition (e.g., C_{MMT}=1 wt %), and then decreases with increase of C_{MMT}. It is then suggested that such a small MMT addition deteriorates the crystallinity of the nanohydrogel and enlarges the pore sizes in the CS matrix after electric-stimulation. This

nanostructural enlargement will increase the passage of ionic species and accelerate the drug release (and the rate) from the nanohydrogel, resulting in a pseudo-zero-order release under electric-stimulation. On the contrary, higher cross-linking density as a result of higher MMT addition retards the diffusion of the drug molecules across the nanohydrogel.

An interesting finding revealed that the effect of MMT increment on the diffusion exponent n is very similar to that on the voltage-induced swelling ratio. As observed in Figure 5-4(b), both parameters show exactly the same dependence of the MMT concentration. Under applied voltage of 5V, the diffusion exponent n exhibits a linear correlation with the voltage-induced swelling ratio with a R_2 as high as 0.99, indicating that the degree of cross-linking in the nanohydrogels due to the incorporation of MMT profoundly affects the drug diffusion behavior. This provides powerful evidence that electric-stimuli release of drug is strongly determined by the free volume in the matrix as the diffusion passage of molecules.

5.5 Repeating electrical-stimulation on release behavior

A change in the electrical field has been realized to cause a change in drug release profile. It is therefore to use a switch of the electrical field from “on” to “off” or vise versa to create pulsatile patterns of drug release. Figure 5-5 shows the resulting variation in the release profile of pure CS where a pulsatile release appeared immediately right after an electric field was applied and followed by little or negligible release of drug when the applying electric field was removed, i.e., switch “off”. After several on-off switching operations, pure CS (solid curve) exhibited a decrease of responsiveness to the stimulation and cumulative release amount, compared to the ideal case (which is able to

maintain identical release rate as first-time release behavior after repeated electric-stimulation, i.e., dotted curve) which is believed due to fast swelling of the polymeric matrix to the stimulus.

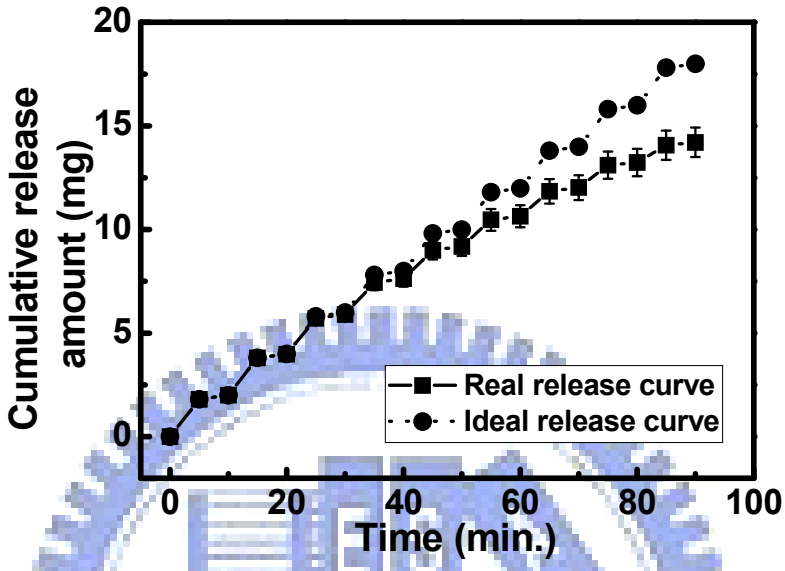

Figure 5-5 Real (…) and the ideal (—) pulsatile drug release profiles of pure CS hydrogels as an electric field was switched "on" and "off".

In order to understand the mechanism that led to the decrease of electric-stimuli responsivity after several on-off switching operations, the standard release rates (R_{sd}) as defined in previous section of the nanohydrogels with different CMMT upon stimulations is plotted against the numbers of on-off switching cycles, which is shown in Figure 5-6(a). Under an applied voltage, a noticeable shrinkage of CS at the cathode occurred, presumably due to bulk solvent flow towards the anode. The H^+ ions formed by the electrolysis of water are subjected to intra- and intermolecular electro-repulsive forces arising from their interactions with adjacent H^+ ions and the positively-charged CS network. These electro-repulsive interactions will lead to an osmotic pressure gradient, which facilitates CS syneresis and

ultimately results in gel shrinkage. Water together with the dissolved drug was expelled out of the hydrogel due to this contractile deformation. Moreover, the voltage-induced collapse after on-off switching operations leads to a decrease of ionizable groups (i.e., lower charged density) on pure CS, resulting in a decrease of the amount of the ions transported through the gel. As a result, for pure CS, it exhibited a substantial decrease of release rate with increasing number of switching operations. In order to improve the anti-fatigue property of pure CS, the incorporation of MMT into the CS matrix, i.e., the nanohydrogel, effectively maintained the same capability of deswelling-swelling behavior after several cyclic switching operations, compared the pure CS hydrogel [12].

For the nanohydrogels with 1 wt % MMT addition, it was observed that it has greater pulsatile release rate in the beginning stage (i.e., first two cycles) of operation but after several on-off cycles (until ten cycles), its release rate becomes smaller than that of pure CS. As mentioned above, the nanohydrogels with lower MMT addition (1 wt %) would deteriorate the crystallinity of CS and increase the passage of charge, which enhanced the release rate of model drug. Also, this deterioration of crystallinity weakened the strength of the nanohydrogels, which reduced the electric-stimuli responsiveness (release rate) after cyclic on-off operations as well. However, with higher MMT concentrations (exceed 1 wt % addition), stronger cross-linking in the nanohydrogels effectively improved the on-off cyclic electric-stimuli responsiveness, as shown in Fig. 5-6(a). The release rate under electric stimulation is reduced because of the decrease of the molecular mobility in the nanohydrogels with addition of MMT. Hence, it also suggested that loose structure of the nanohydrogels (i.e., pure CS and the nanohydrogels with 1 wt % MMT concentration) can hardly control the release upon

electric-stimulation protocol in an effective manner.

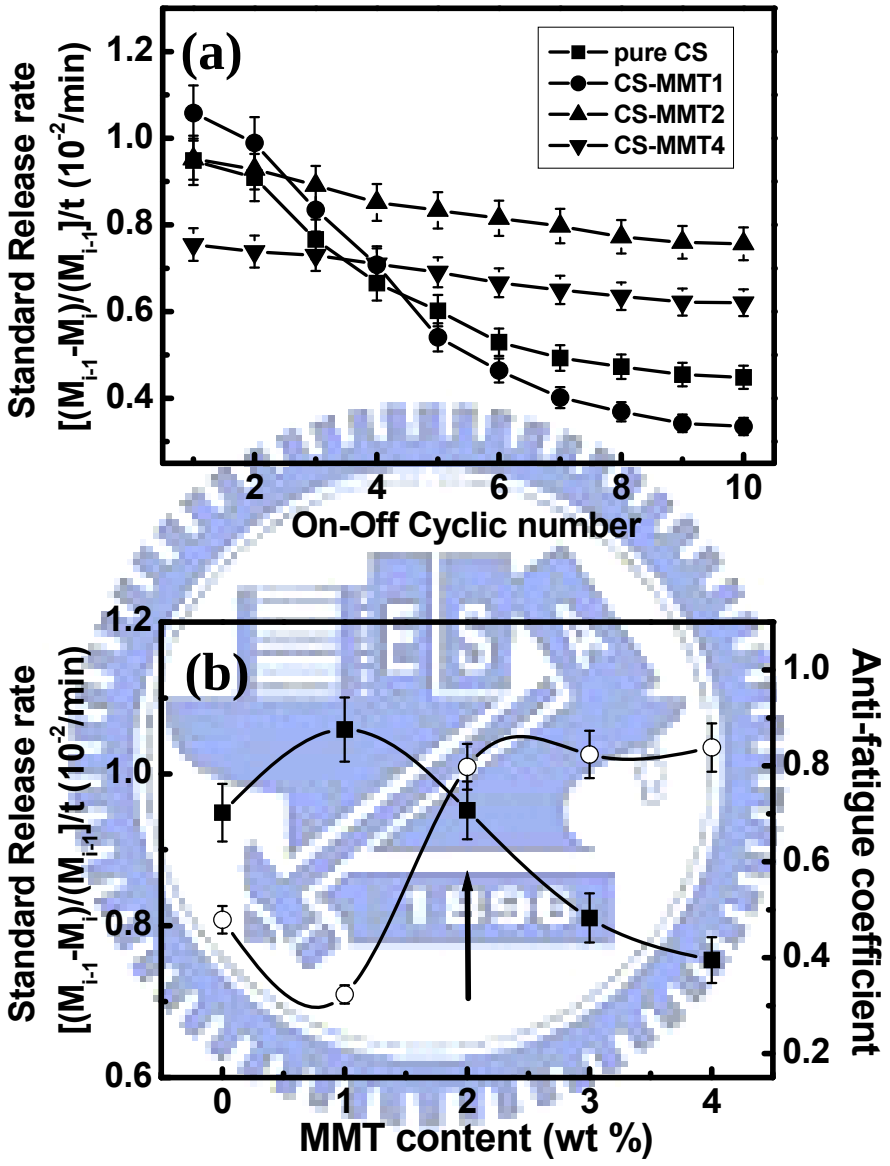

Figure 5-6 (a) Standard release rates of drug from the nanohydrogels (CS, CS-MMT1, CS-MMT2, and CS-MMT4) after cyclic on-off switching operations. (b) Dependences of the loaded MMT contents on the drug standard release rate in the first on-off cycle (filled boxes) and anti-fatigue coefficient of the nanohydrogels (empty circles).

However, this electrically-stimuli control can be effectively improved in the nanohydrogels with higher density of crosslink, i.e., higher MMT concentrations. Both initial release rate (R_1) and relative anti-fatigue dependence of MMT addition can be further plotted in Figure 5-6(b) in which anti-fatigue coefficient was expressed with R_{10}/R_1; R_1 and R_{10} indicate the standard release rate under on-off cycle number of 1 and 10, respectively. A higher R_{10}/R_1 ratio means that the nanohydrogels displays a better anti-fatigue property. Therefore, the optimal range of MMT contents, typically around 2 wt %, in the nanohydrogels is expected where the resulting nanostructure of the nanohydrogels can be well manipulated with optimal cross-linking density to keep the pulsatile release profile relatively constant even after numerous on-off switching operations. Figure 5-7 shows a typical comparison of repeated on-off operation for pure CS and CS-MMT2 compositions, the anti-fatigue property of the CS can be largely improved with the incorporation of the MMT nanoplates.

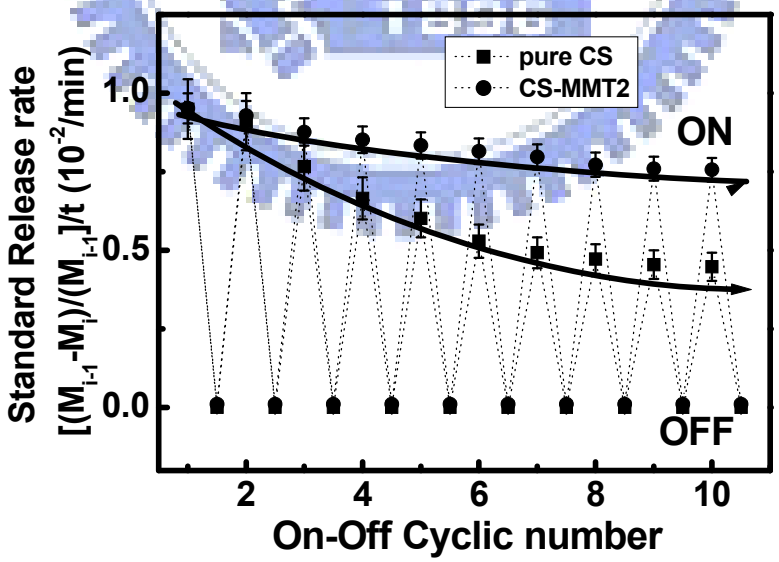

Figure 5-7 Standard release rates of drug from pure CS and CS-MMT2 under cyclic on-off switching of electric-stimuli

Such an improvement in the anti-fatigue behavior can be explicitly observable from a reversible mechanical action of the nanohydrogels upon cyclic switching operation under a given electrical stimulation. This constantly reversible action of the nanohydrogels also ensures a constant rate of pulsatile release of the drug, as experimentally evidenced, and this allows a more reliable performance of a consecutive pulsatile-type drug release profile to be achieved from such nanohydrogels.

Chapter 6

Electrical-Sensitive Nanoparticle Composed of Chitosan and TEOS for Controlled Drug Release

6.1 Introduction

It is one of the most challenging works to develop new multi-functional materials that possess smart functionality capable of monitoring the changes of environment, followed by a corresponding actuation according to the stimuli. A number of different polymer hydrogels that are able to mechanically respond to stimuli, which has been named as smart hydrogel and has been used as drug delivery vehicles. Environmental stimuli such as pH, pressure, temperature, light, magnetic fields and electric fields, would cause those smart polymer gels to undergo macroscopic deformation and produce contractile force. Numerous smart or responsive hydrogels have been studied with regard to their applications in biomedical fields, e.g. controlled drug delivery systems [68], muscle-like actuators [66], and bio-separation [67]. One most significant drawback of such smart hydrogels is their slow stimuli-to-response activity. Thus, hydorgels with fast responsivity to its environmental stimuli are practically desirable, and a simple and straightforward method to enhance its responsivity is to make such responsive hydrogels with thinner and smaller dimensions.

In recent years, chitosan (CS) nanoparticles (NPs) have been widely studied for the controlled release of drugs included antibiotics, catalysts, proteins, and peptides [69, 90, 91]. Chitosan is a biodegradable, biocompatible, and non-toxic polycationic polymer with low immunogenicity. It has been

extensively investigated for formulating carrier and delivery systems for therapeutic macrosolutes, particularly genes and protein molecules because positively charged chitosan can be easily combined with negatively charged DNAs and proteins [92, 93]. To date, there have been a variety of reports in the preparation of CS NPs by ionic cross-linking. Alonso et al. [94] reported the use of an ionic gelation method to prepare CS NPs. In this method, positively charged CS NPs were formed through the inter- and intra-cross-linking of the amino groups of CS with the negatively charged phosphate groups of tripolyposphate (TPP). They demonstrated the encapsulation of bovine serum albumin (BSA) by the CS NPs with maximum loading capacity (LC) of 51 wt %. Zhang et al. [95] reported the preparation of CS NPs in the size range of 90-200 nm achieved by combining post-deacetylation and fractionation of commercially available CS. They showed that the BSA could be loaded into the CS NPs at protein-to-material weight ratios of up to 40%. In addition, the CS NPs were found to provide sustained release of this protein in simulated intestinal fluid (pH=7.5) over 6-day period. Physical crosslinking by electrostatic interaction is simple and mild. However, CS NPs crosslinked by TPP have poor mechanical strength thus, limiting their applications in drug delivery.

During the last decade, considerable attention has been paid to inorganic-organic hybrid materials and interpenetrating polymer hybrid networks because it is possible to tailor their solid-state properties in relation to the nature and relative content of constitutive components [96]. Sol-gel process is known as a very straightforward way to prepare hybrid materials that effectively combine inorganic oxides and organic polymers. Seong-Bae et al. [97] developed a novel organic-inorganic composite membrane via a sol-gel

process, using tetraethyl orthosilicate (TEOS) as an inorganic material and CS as an organic compound. In the study, TEOS was hydrolyzed and condensed to form network structure and CS was incorporated into TEOS network structure to prepare pH-sensitive membrane. Some metal oxides are highly biocompatible because of their surfaces decorated with hydroxyl groups that render them intrinsically hydrophilic, as demonstrated by their numerous applications as implants or coatings. Most specifically, amorphous silica particles in contrast to crystalline silica are not toxic and are regularly used as food additives and components of vitamin supplements. It was also found that the shelf life of bioactive molecular encapsulated in silica could be prolonged [98, 99]. Even though all of these intrinsic advantages, metal oxide particles largely remain an untapped resource for the drug delivery system. It is due to the high processing temperature in traditional technique (>1000^{o}C) and the difficulty of manipulating the internal microstructure of particles. However, sol-gel technology can easily overcome both problems above. Furthermore, the addition of organic molecules during the formation of the oxide backbone facilitates their encapsulation within the evolving oxide matrix and then forms a composite gel with homogeneously distributing throughout the resulting gel.

In this study, the NPs with particle size of 50-130 nm composed of CS and TEOS were obtained through emulsion and sol-gel process. Here, TEOS that hydrolyzed and condensed to form network structure with the CS improved the drug loading capacity (LC) and encapsulation efficiency (AE) of the process, compared to the pure CS NPs. Besides, the drug release mechanism was changed with increase of TEOS contents. Interpenetration network of CS/TEOS was expected to provide the mechanical enhancement of the nano sphere to restrict drug release before each electric-stimuli application

of cyclic operations. Therefore, the drug release from the CS/TEOS NPs effectively controlled by electric-stimuli operations was demonstrated in this work.

6.2 Fabraction of drug-loaded and non-loaded CS/TEOS nanoparticles

The NPs composed of CS and TEOS were prepared by hydrolysis of TEOS in reverse microemulsion and ionic gelation between CS and sodium tripolyposphate (TPP). Typically, a mixture of 12g Triton X-100, 9.6 ml hexanol, and 20.4 ml H_2O was ultrasonicated for 30 minutes to generate the microemulsion. After a pre-calculated amounts of TEOS were added to the mixture and mixed for six hours, 0.03 ml HCl solution was introduced to initiate TEOS hydrolysis. Next, 0.06g CS was dissolved in 10 ml 0.1 wt % acetic acid solutions which was then added to the TEOS solutions until the homogeneous solution was obtained. These two components were mixed to yield CS-TEOS with weight ratios of 10:1, 5:1, 10:3, and 2:1. After 24 h, 4mL TPP solution (10 wt %) was added to the mixed solution and then vibrated for additional 30 minutes by ultrasonic processor. Ethanol was used to wash the NPs to remove the surfactant and un-reacted chemicals. Finally, the CS/TEOS NPs were dispersed in the water solution.

Myoglobin protein was added to the mixture of TEOS and CS solution prior to the addition of TPP solution. The encapsulation efficiency and loading capacity of NPs with the different TEOS contents were determined by ultra-centrifugation of samples at 20,000g and 15^{o}C for 30 min. The amount of free myoglobin protein was determined in clear supernatant by UV-visible spectrophotometer at 410 nm. The loading capacity (LC) of NPs and the encapsulation efficiency (AE) of the process were calculated from Eqs (6-1)

and (6-2) indicated below:

$LC=(A-B)/C\times 100$ (6-1)

$AE=(A-B)/A\times 100$ (6-2)

where A is the total amount of myoglobin added during preparation, B is the amount of myoglobin remaining in the supernatant and C is the weight of the NPs.

The in vitro release of myoglobin from the NPs was evaluated over a 10-day period in pH=7.4 phosphate buffer solution (PBS). A total of 5 ml of release buffer was added to each of a series of 5mg of protein-loaded NPs. The vials were incubated at 37^{o}C without stirring. At specific time points, the NPs were isolated from buffer by ultracentrifugation. The concentration of myoglobin in the supernatant was measured by UV-visible spectrophotometer (Shimatzu, Model UV-2101PC) at a wavelength of 410 nm. Each batch was analyzed in triplicate. The drug release percent was determined using Eq (6-3) [100]:

Drug release (%) = $R_t/L \times 100\%$ (6-3)

where L and R_t represent the initial amount of drug loaded and the cumulative amount of drug released at time t.

For electrical-induced drug release, drug-loaded NPs were placed in the middle of two platinum electrodes in phosphate buffer solution (PBS) (7.4). Then, the amount of myoglobin protein released into medium was monitored and analyzed periodically by a UV spectrophotometer (Shimatzu, Model UV-2101PC). The UV absorbance of myoglobin protein was measured at λ_{max}= 410 nm.

6.3 Results and Discussion

The CS-TEOS hybrid NPs were prepared using ionic gelation between CS and TEOS by TTP. In this sol-gel synthesis, polymer CS was encapsulated within the TEOS matrix resulting in a composite with homogeneous microstructure (or nanostructure). At first, TEOS was hydrolyzed and condensed to form meshed matrix or network structure wherein the silica nanophase and porous phase formed a dual continuous network throughout the materials (Fig. 6-1(a)). Then, CS was incorporated into the TEOS IPN structure homogeneously (Fig. 6-1(b)). When it was completely ionically crosslinked by $P_3O_{10}^{3-}$ ions in an acidic TPP solution, CS could almost consume most of the binding sites and interact with the negatively charged phosphate groups of TPP (Fig 6-1(c)). In acidic condition, only TPP ions exist in the medium and then, CS NPs gelled in the TPP solution are completely ionically-crosslinked.

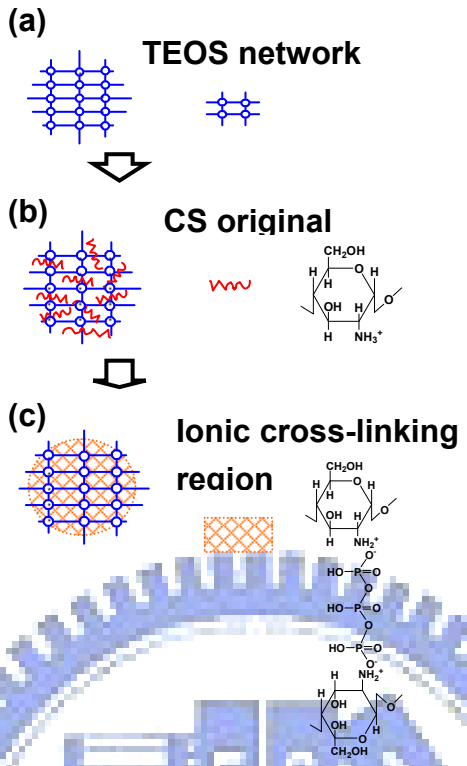

Figure 6-1. The illustrations of the formation of CS and TEOS NPs. (a) the formation of TEOS network structure, (b) the original CS polymer entwined into the network, (c) the formation of NPs by ionic gelation of TPP.

The SEM image (Fig. 6-2(a)) of pure CS NPs ionically crosslinked by TPP shows the nanoparticle having a size of 20-50 nm. However, with the TEOS content of 23%, as shown in Fig 6-2(b), hybrid NPs shows large aggregates. The CS and TEOS-IPN NPs reveal that the NP has a size range between 50 and 130 nm and shows an oval-like morphology. After swelling in the solution, the NP has a size about 150-230 nm.

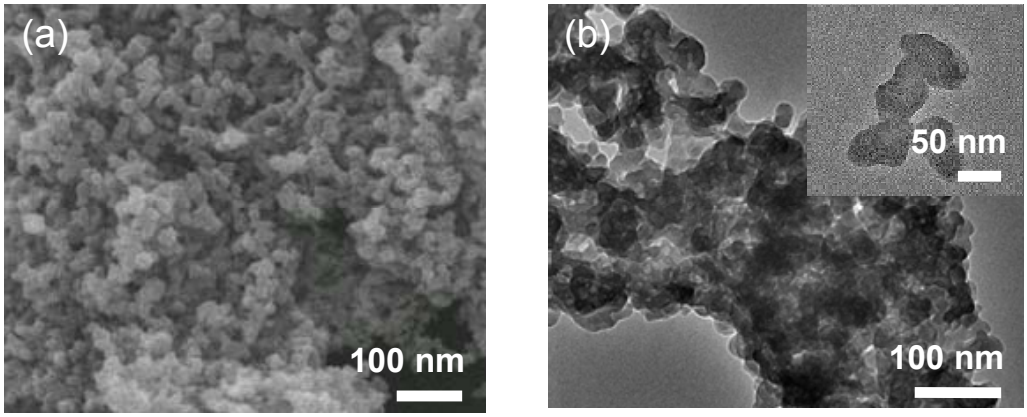

Figure 6-2 (a) SEM image of pure CS NPs. The (b) lower- magnification and higher-magnification TEM image of the CS and TEOS NPs (23%).

The model protein, myoglobin, was encapsulated into the hybrid NPs to evaluate their suitability as a delivery system It was found that the AE (the encapsulation efficiency of the process) of the CS NPs was improved from 62.38 to 91.53% with the increase of TEOS content up to 33%.The LC (the loading capacity of NPs) of CS NPs was enhanced greatly from 32.18 to 70.24%, as shown in Fig. 6-3. The LC and AE of the hybrid NPs for myoglobin were relatively high and comparable to that obtained from pure CS NPs. Furthermore, the LC and AE can be improved by increasing the TEOS content. The improvement of TEOS interaction with CS can be explainable that a higher TEOS concentration enhances the entwining degree of the interpenetration network and reduced the mesh sizes between the network structures. Hence, it is reasonable to believe that the encapsulation efficiency of myoglobin can be improved by increasing TEOS.

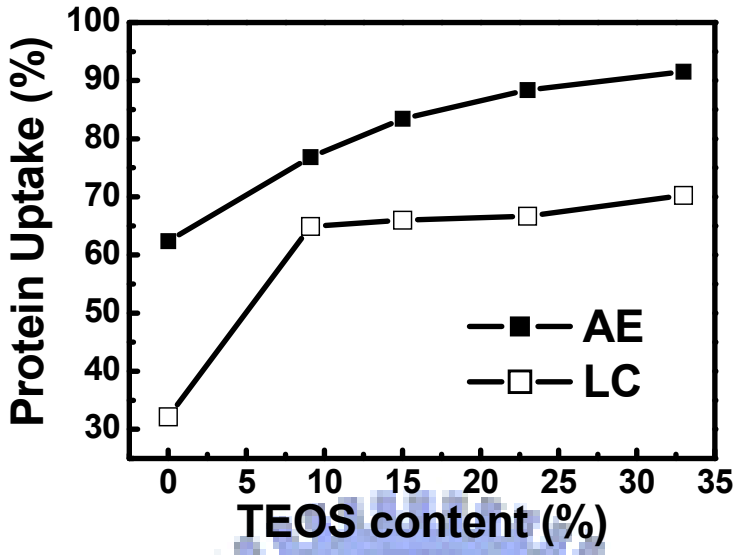

Figure 6-3 AE and LC of the CS and TEOS NPs with different TEOS contents.

Christophe et al. [101] pointed out that the physical characteristics of the oxides produced by the sol-gel processing can be tailored by controlling the sol-gel reaction kinetics, and in particular, the relative rates of hydrolysis and condensation. Hence, the ability of manipulating the gel microstructure has a very important consequence for design of a drug controlled release system. For example, in sol-gel silica chemistry, introduction of acids or bases during the sol-gel process results in significantly different polymeric structures. In our work, acid catalysis promoted hydrolysis and end-of-chain condensation, leading to the production of small linear polymeric entities. A further crosslink between these linear polymers leads to the formation of microporous gels during gelation. As expected, the diffusion of molecules inside a microporous solid is much slower than that inside a mesoporous gel if a basic-catalyzed synthesis is carried out. This leads to significantly lower release rate for the gels synthesized using acid catalysis. As shown in Fig 6-4, the in vitro release of myoglobin from the NPs was measured over a 10-day period in PBS

(pH=7.4). It was found that the release of myoglobin from the pure CS NPs is much faster than that from the hybrid nanoparticles. In fact, 80% of the total myoglobin loaded in the pure CS NPs was released in the first 5 days.

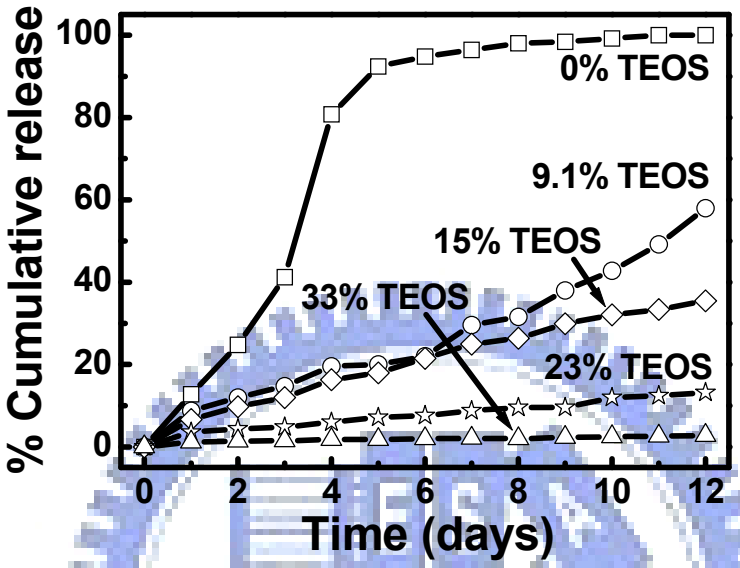

Figure 6-4 In vitro release of myoglobin from the CS and TEOS NPs with different TEOS contents.

However, what is more than surprising is that the loaded myoglobin can still stay in the hybrid NPs even over 12 days. The released amount of myglobin from the hybrid NPs was less than 60% for 12 days. As mentioned above, the TEOS network structure could effectively stop the model protein myoglobin from diffusing outward from the hybrid NPs. In order to investigate the diffusion mechanism in the NPs, the data were further characterized with Eq (6-4):

$$\frac{M_t}{M} = Kt^n \qquad (6\text{-}4)$$

where M_t is the amount of drug released at time t, M is the amount of drug released at equilibrium state, K is a constant and n is diffusion exponent related to the diffusion mechanism. Lee et al. [102] distinguished three classes

of diffusion according to the relative rates of diffusion and polymer relaxation. The first is Fickian diffusion (n=0.5), in which the rate of diffusion is much smaller than the rate of relaxation. When the exponent n takes a value of 1.0, the drug release rate is independent of time (zero-order release kinetics). It indicates a swelling controlled mechanism (Case Ⅱ transport). For most polymeric drug delivery system (DDS), the values of n in Eq (6-4) are lying between 0.5-1. It was reported that both the diffusion and relaxation rates are comparable in those drug delivery systems.

From the plot of ln (M_t/M) versus ln (t), kinetic parameters, n and K, were calculated, as listed in Table 6-1. It was demonstrated that the exponent n was strongly affected by the addition of TEOS. It can be observed that the n value of pure CS NPs was higher than that intertwined with TEOS IPN. Pure CS NPs with n=0.831 (the non-Fickian release behavior) may suggest that the release of myoglobin was controlled by a combination of diffusion from pure CS NPs and dissolution of NPs. Further, the n value would be reduced from 0.807 to 0.418 as the TEOS increased from 9.1% to 33%. In this case, higher TEOS content enhanced the degree of cross-linking and decreased the pore size of the network, making a structurally denser IPN matrix. This compact structure is believed to restrict the diffusion of protein and result in a decrease of exponent n, indicating that protein release shifts from swelling-controlled towards diffusion-controlled mechanism. The n for the hybrid NPs with TEOS/CS weight ratio of 1:2 (33%) has the smallest value.

Table 6-1. Kinetics contants (K), and release exponents (n) following linear regression of release of myoglobin from CS and TEOS NPs.

TEOS/CS Weight ratio	Kinetics Constant K[a]	Release Exponent n[b]
0:1	16.907	0.831
1:10 (9.1%)	6.371	0.807
2:10 (15%)	5.558	0.752
3:10 (23%)	2.614	0.628
5:10 (33%)	0.93881	0.418

[a] The value of k calculated from Eq. (4).

[b] The value of n calculated from Eq. (4).

Fig. 6-5 shows the pulsatile release profile of myoglobin as an electric field was applied with an “on” and “off” operation. When a DC electric field is applied, the polyelectrolyte polymer (pure CS NPs) will undergo shrinkage. This shrinkage produced a pulsatile release of protein and the degree of the pulse was influenced by the intensity of the applied electric field. The shrinkage of the NPs is explained by the fact that an electric field gradient will produce different osmotic pressure in the NPs and it is the driving force for releasing of the protein entrapped in the matrix.

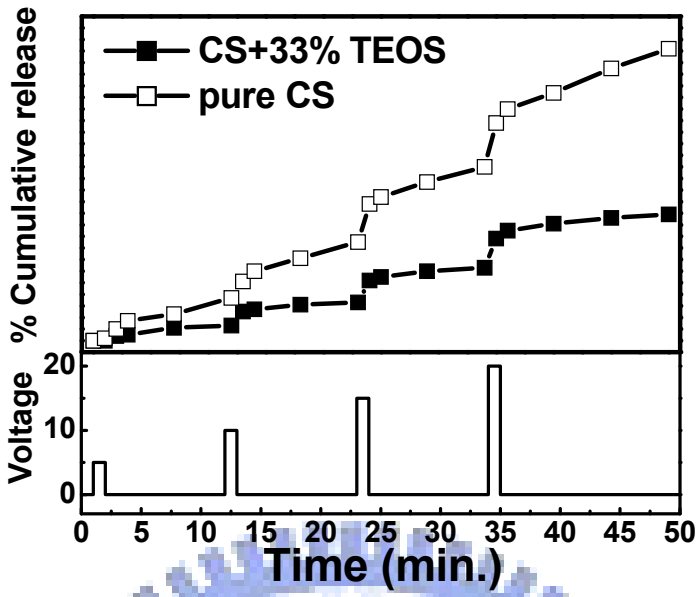

Figure 6-5 The pulsatile myoglobin release profiles with different TEOS contents when applied DC electric field was switched "on" and "off".

However, the cumulative release amount still increased continuously when the electric field was switched off. It was suggested that the pure CS NPs were eroded under an applied DC electric field. On the other hand, the hybrid NPs revealed a different release behavior. The shrinkage in the hybrid NPs equally occurred when the electric field was applied. However, when the electrical voltage was switched "off", the followed release profile displayed near-zero release. As illustrated in Fig. 6-6, CS incorporated in the TEOS network structure gives the electric-sensitivity to the CS/TEOS NPs. TEOS network structure, a rigid frame, is expected not to deswell by itself under an applied voltage. However, the incorporated CS in CS/TEOS NPs shrinks according to the external electrical field. Hence, a burst release from NPs was occurred when the electrical field was applied. On another hand, the near-zero release was observed when the electric field was switched off. It was suggested that the TEOS network structure is able to prevent the resulting

NPs from degradation up numerous shrinkage-swelling, i.e., on-off, operations and also effectively manipulate the outward diffusion of protein. These results provided a new drug delivery system to precisely and effectively control the release of protein.

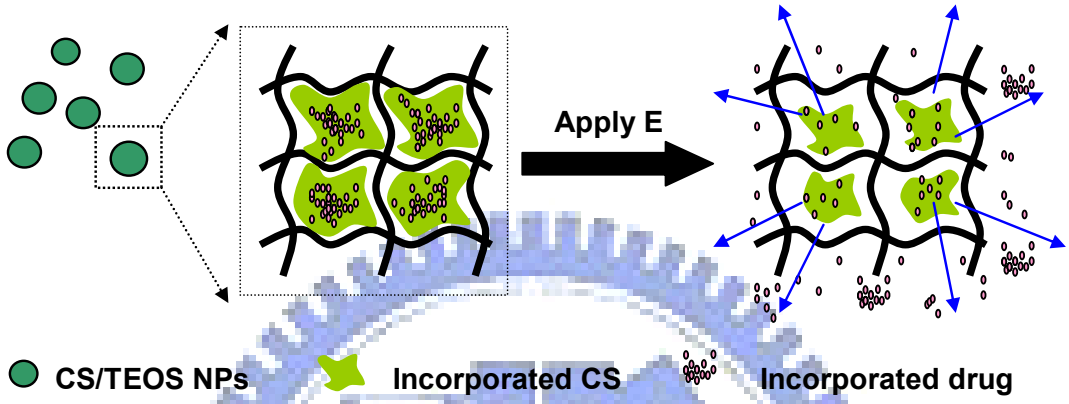

Figure 6-6 Illustration of the proposed electric-sensitive drug release mechanism of CS/TEOS NPs.

Chapter 7

Self-Assembled hollow nanocapsule from amphiphatic carboxymethyl-hexanoyl chitosan as drug carrier

7.1 Introduction

Nanotechnology has received greatest attentions because of its potential that can literally revolutionize each field in which it is being exploited. The importance of nanotechnology in drug delivery is in the concept and ability to manipulate molecules and supramolecular structures for producing devices with programmed functions. In biotechnology and medicine, by controlling the composition, structure, and function of the nanosized polymer materials, such as nanoparticles, micelles, and nanocapsules, they can serve as effective vehicles for drug delivery, drug controlled release and gene therapy. Compared to nanoparticle (monolithic-type device), hollow nanocapsules (reservoir-type device) have been attracting increasing interest because of their potential ability to encapsulate large quantities of therapeutic and diagnostic agents in their hollow inner cavities and release them at a later stage in a controlled manner. Even though several different routes, such as layer-by-layer deposition of polyelectrolytes onto a template core [103], microemulsion polymerization [104], and self-assembly of block copolymers in a selective solvent [105], have been successfully developed, these strategies require the templates to be removed to create a hollow interior, or need greater quantities of surfactants to form nanosized micelles. Furthermore, most of the hollow nanocapsules described to date are ill-suited for biomedical application, and the lack of biocompatibility and degradability is of another important

concern. Therefore, the use of natural polymer with properties desirable for many practical considerations in the field of biomedicals is of most interest.

As was well recognized, chitosan (CS), β-(1,4)-link glucosamine unit, is produced by deacetylation of chitin, which is extracted from the shells of crabs, shrimp, and krill. It exhibits several characteristics such as biocompatibility, nontoxicity, and bioadhesivity that make it as an ideal material for biomedical uses, such as drug delivery. However, its poor solubility in water and common organic solvents has so far limited its widespread utilization. The reactive amino groups in the backbone of chitosan make it possible to chemically conjugate with various biological molecules [106]. As a result, there have been many works about the methods to enhance the solubility of chitosan, one of which was derivateization. For example, the introduction of carboxylgroups to chitosan derivatives leaded to the anionic or amphotheric properties are water-soluble and are attracting much attention as metal collecting materials and biomaterials. Hence, hydrophilically, hydrophobically, and amphiphilically modified chitosan derivatives are being studied to form the monodisperse self-aggregated nanoparticles by sonication in aqueous media due to non-covalent association arising from intra- or/and intermolecular interactions among hydrophobic segments in aqueous media. However, in these studies, the formation of hollow structure is more difficult than that of particle structure.

In this study, a new type of chitosan hollow structure, i.e., carboxymethyl-hexanoyl chitosan (CHC), which was modified first by hydrophilic carboxymethylation to increase the flexibility of chitosan molecular chains in water [107] followed by hydrophobic modification with hexanoyl groups to add amphiphilic character, was employed to study its self-aggregation behavior to form nanocapsule in aqueous solution and

nanostructural evolution. The stability of nancapsules and formation mechanism of the CHC macromolecules were explored through the use of critical aggregation concentration (CAC), zeta-potential, electron microscopy, and dynamic light scatter (DLS). By taking the advantage of self-aggregation nature, the CHC was employed to encapsulate doxorubicin (DOX), an anticancer agent of broad spectrum with reasonable therapeutic index and intriguing biological and physicochemical actions [108], to further understand its loading efficiency and release behavior.

7.2 Synthesis of CHC

According to our previous report [109], CHC can be successfully prepared through following steps. Briefly, 5 g of chitosan was suspended in 2-propanol (50 mL) at room temperature while being stirred for 30 min. The resulting suspension was gently mixed with 12.5 mL NaOH solution. The mixture containing NaOH of 13.3M was mixed with 25 g of chloroacetic acid to prepare carboxymethyl chitosan (CC) sample with a high degree of carboxymethyl substitution. Obtained and dried sample (2g) was dissolved in distilled water (50 mL) while being stirred for 24 h. These resulting solutions were mixed with methanol (50 mL), followed by the addition of hexanoyl anhydride at concentration of 0.2 M, 0.3 M, 0.4M, and 0.5M for the CHC samples with different degrees of hexanoyl substitution, respectively. After the reaction time of 12 h, the resulting solutions were collected by dialysis membrane (Sigma Chemical Company, USA) after dialysis with ethanol solution (25% v/v) for 24 h. CHC samples with various degrees of hexanoyl substitution (DH) were named and shown in Table 1. The sites and degrees of substitution were confirmed by ^{1}H NMR analysis in previous work [109].

7.3 Preparation of drug-loaded and non-loaded CHC Hollow Nanocapsules

100 mg/ml CHC sample was suspended in a distill water under gentle shaking at 25°C for 24 h, followed by ultrasonication using a probe type sonifier (Automatic Ultrasonic Processor UH-500A, China) at 30W for 2 min. The sonication was repeated three times to get an optically clear solution. To inhibit the heat build-up during sonication, the pulse function was used (pulse on 5.0 s; pulse off 1.0 s).

Drug-loaded hollow nanocapsules were prepared by dissolving 20 μg/mL of DOX in 20 ml acquired nanocapsule suspension before ultrasonication. Insoluble, free DOX was removed by centrifugation at 2000 rpm and 4oC for 5 min. The drug-containing nanocapsules were then separated from the aqueous solution by centrifugation at 15000 rpm and 4°C for 15 min. Drug concentration in the supernatant was analyzed by ultraviolet absorption (UV) at wavelength of 490 nm, a strong absorption band of DOX, with reference to a calibration curve on a UV-VIS spectrometer (SP-8001, Metertech Inc.). The measurements were performed in triplicate. The amount of the drug in the hollow nanocapsules could be calculated by the total amount of DOX subtracting the residual DOX in the supernatant. Encapsulation efficiency (EE) were obtained as described below

$EE = (A-B)/A \times 100$

where A is the total amount of the DOX, B is the amount of DOX remaining in the supernatant and C is the weight of the nanocapsules.

A solution of DOX or DOX-loaded nanocapsules (approximately 20 μg/mL DOX equiv) was added to a Slid-A-Lyzer dialysis cassette (Pierce) with a molecular weight cutoff of 10000. The solution was dialyzed at 37°C against

0.1 M 100 mL buffer solution. The solution was removed periodically from the dialysis cassette and characterized using an absorbance at a wavelength of 490 nm to determine the amount of DOX in the solution, then, the solution was poured back to the dialysis cassette.

7.4 Formation of CHC Nano-aggregates

The molecular structure of CHC is given in Fig. 7-1 and CHC samples with various degrees of hexanoyl substitution (DH) were confirmed by ^{1}H NMR analysis [109] as given in Table 7-1. After dispersing in water, the CHC conjugates formed self-assembled nanometric aggregates by ultrasonication.

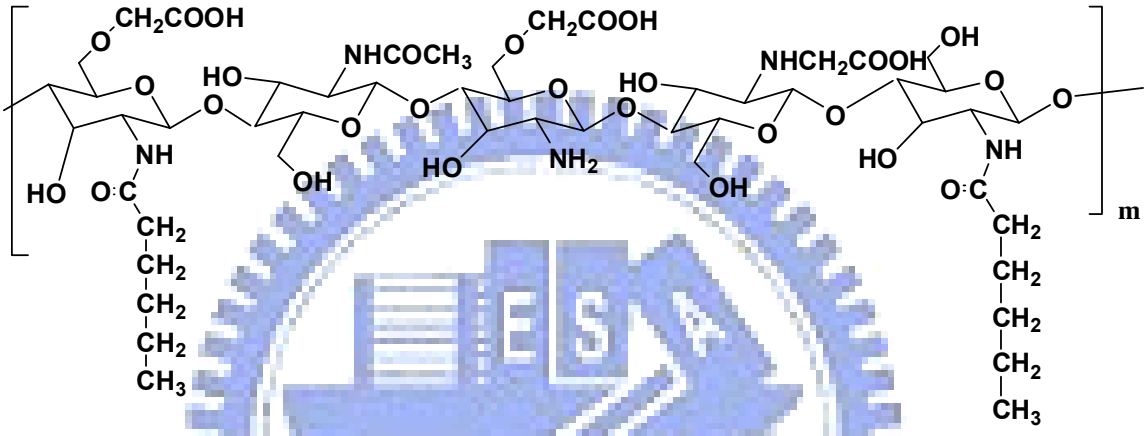

Figure 7-1 Molecular structure of carboxymethyl-hexanoyl chitosan (CHC).

Table 7-1 Sample Name and Corresponding Estimation of Substitution Degree by ^{1}H-NMR

	degree of substitution	
	carboxymethyl group	**hexanoyl group**
CC	0.5	0
CHC-1	0.5	0.13
CHC-2	0.5	0.26
CHC-3	0.5	0.33
CHC-4	0.5	0.48

The fluorescence probe technique was used to investigate the

self-aggregation behavior of the CHC at a molecular level, and pyrene was chosen as a fluorescence probe. Pyrene shows only small fluorescence intensity in a polar environment (such as water) due to its poor solubility and self-quenching, but strongly emits when the hydrophobic micro-domains are formed in an aqueous solution because the pyrene molecules show high affinity to these hydrophobic micro-domains. Therefore, pyrene is often used as a fluorescence probe to monitor the self-aggregation behavior of surfactants and/or polymers [110]. In addition, the intensity ratio of the first peak (372 nm) and the third peak (385 nm) I_{372}/I_{385} in its fluorescent spectrum is quite sensitive to the environment surrounding the pyrene molecules and has been frequently used as an indicator for a subtle change of its environment. Hence, the critical aggregation concentration (CAC), which is defined as the threshold concentration of self-aggregate formation by intra- and /or intermolecular association, can be determined from the change of the I_{372}/I_{385} value of pyrene in the presence of polymeric amphiphiles. Fig. 7-2 illustrates the changes of the I_{372}/I_{385} values as a function of the concentrations of CHC-4 and CC. For CHC-4, the I_{372}/I_{385} values were close to the value (1.72) of pyrene in water at low concentrations [111], and then followed by a linear decrease with further increasing concentration. The CAC can then be determined by the intercept of two straight lines [112]. It was found that the CHC-4 composition demonstrated the lowest CAC, i.e., 0.004 mg/ml, among the others and is lower than the critical micelle concentration of many low-molecular-weight surfactants reported, e.g. sodium dodecyl sulfate [113]. Accordingly, this finding suggests that the CHC nano-aggregates prepared in this work should be thermodynamically stable in aqueous solution and this has been further evidenced by the fact that those nanocapsules exhibited excellent colloidal

stability in PBS over a long-term storage for at least one month in refrigerator. .

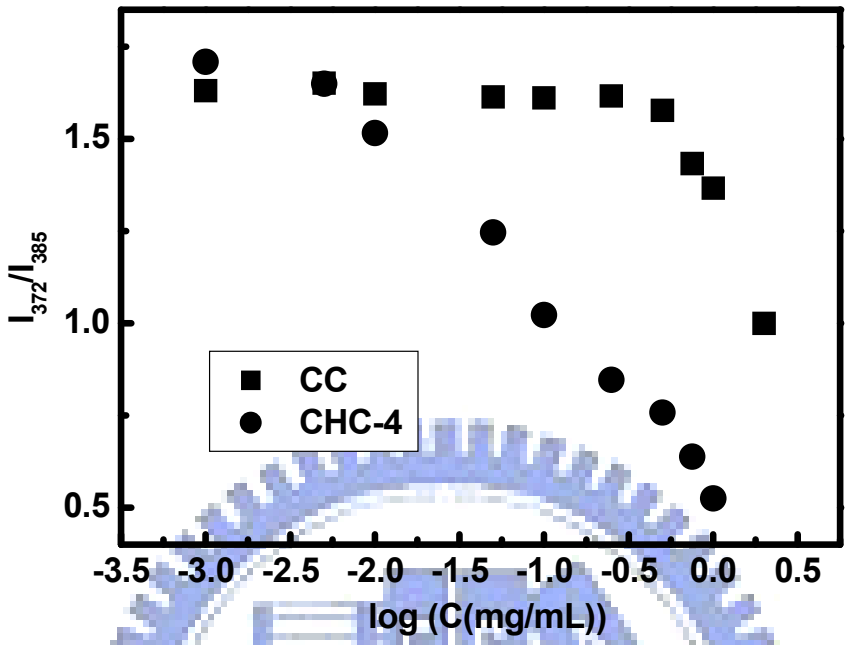

Figure 7-2 Change of the intensity ratio (I372/I385) from excitation spectra of pyrene (1.0×10-6 mol/L) with various concentrations of CC and CHC-4.

However, for CC, the I_{372}/I_{385} values decreased slightly only at high concentration (0.25 mg/ml), indicating difficulty for the CC molecules to aggregate in the studied range of concentration. Moreover, since from Table 2 the CAC values of the CHC nano-aggregates were decreased with the increase of DH, it can thus be deduced from the observation of the self-aggregate ability between CC and CHC that the aggregation of CHC in water was due to the incorporation of hydrophobic groups by increasing the degree of hexanoyl substitution. It was known that the increase of hydrophobicity in amphiphatic polymer causes the difficulty to dissolve in aqueous solution because the energy is essential to cut the H-bonding in water molecules (need to do work). Therefore, the dissolution of hydrophobic groups

in water would result in the increase of the surface free energy. In order to decrease the energy, the hydrophobic groups trend to aggregate. Hence, CHC-4, having the highest DH, is able to form nano-aggregates at a very low concentration (e.g., 0.004 mg/ml) because increase of the resulting surface energy is the greatest. On the contrary, for CC with the least hydrophobicity, the required concentration to form nano-aggregates is much higher (e.g. 0.25 mg/ml) than that of the CHC. This appears to indicate that the self-aggregate ability can be effectively enhanced with increasing hydrophobic nature of the modified chitosan in aqueous environment.

The zeta potentials of the resulting CHC self-aggregated nanoparticles in water were determined and showed to be negatively charged, Table 7-2, suggesting that the negatively charged carboxymethyl groups in the CHC molecules were mainly distributed on the outer surface of the nanoparticles contributing to hydrophilic potential. The absolute value of the zeta potential of the CHC nanoparticles decreased from 42.8 to 23.1 mV with DH increasing from 0 to 0.48, as shown in Fig. 7-3.

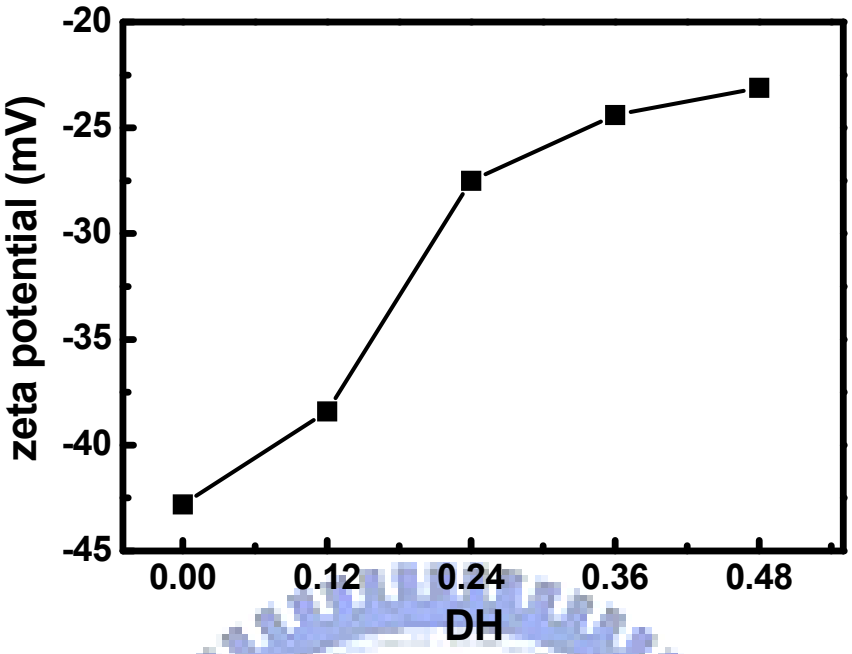

Figure 7-3 Zeta potential of carboxymethyl-hexanoyl chitosan (CHC) with different DH.

Table 7-2 Characterization of CC and CHC self-assembled hollow nanocapsules

Samples	CAC[a] ×10^{-2} (mg/mL)	Zeta Potential[b] (mV)	Mean size 1[c] (nm)	Mean size 2[c] (nm)
CC	25.0	-42.8 ± 4.26	19.8 ± 1.2	189.2 ± 2.4
CHC-1	9.21	-38.4 ± 2.27	21.5 ± 1.6	210.5 ± 1.9
CHC-2	3.17	-27.5 ± 3.49	22.3 ± 0.7	209.3 ± 1.4
CHC-3	0.91	-24.4 ± 0.48	22.9 ± 1.1	210.9 ± 0.7
CHC-4	0.40	-23.1 ± 0.86	23.5 ± 0.7	222.7 ± 2.0

a Critical aggregation concentration determined from I372/I385 data.

b The zeta potential (mean value ± standard deviation) measured by an photon correlation spectrometer with three times.

c The size and size distribution (mean value ± standard deviation) determined by the dynamic light-scattering with three times.

The change of the zeta potential (or surface charge) of the CHC nanoparticles is rapid while the substitution is below 0.26, however, it turns out to reach a plateau stage with further increase in the DH level over 0.33, suggesting the addition of the hexanoyl group may reach a level of saturation. The sharp decrease of the zeta potential from -38.4 mV to -27.5 mV when the DH is increasing from 0.13 to 0.26, suggests a reduction, albeit not significant, of the electrostatic repulsion, which, as a consequence, may cause gradual agglomeration of the CHC molecules to form larger particles while dispersing in water.

Figure 7-4 shows the transmission electron microscopy (TEM) images of the CHC nano-aggregates. The nano-aggregates show a perfect spherical geometry and have a size ranging from 20 to100 nm with increase of DH. In contrast, the self-assembled CC nano-aggregates, Fig. 7-4a, show a relatively uniform size distribution of around 20 nm in diameter. While increasing the DH to 0.48 (CHC-4), it was found that the size of nano-aggregate is increased to around 100 nm, as depicted in Fig. 7-4b. In addition, the mean size of the CHC nano-aggregates measured by dynamic light scattering (DLS) exhibits two size groups, as listed in Table 7-2: one corresponds to smaller particle size of around 40 nm (i.e., mean size 1) and the other is larger particle size of around 200 nm (mean size 2). The smaller particle size may be caused by the coil of the CHC single chain in the solution [114]**.** However, with increase of DH, the enhanced hydrophobic interaction and in the meantime, reduced intermolecular repulsive force, both facilitate self-aggregation; thus, increase the size of the aggregates.

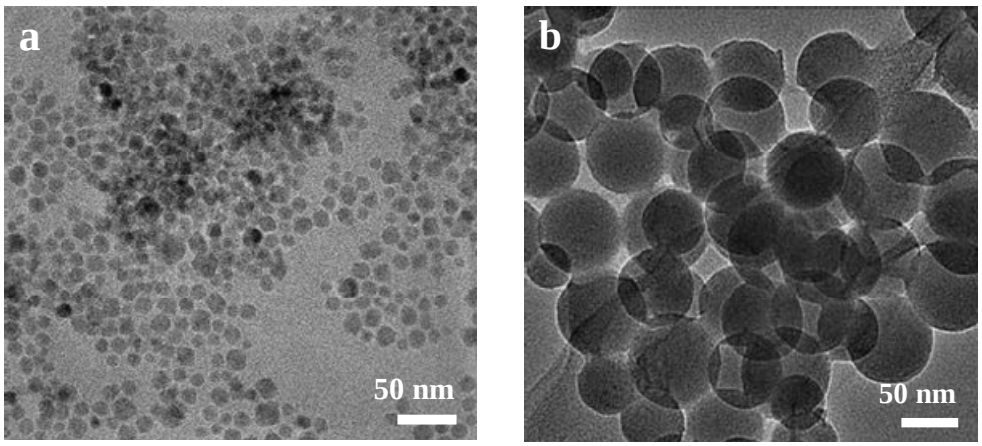

Figure 7-4 TEM images of self-aggregates prepared, respectively, from (a) CC and (b) CHC-4 by ultrasonication in water.

Such a bimodal size distribution of the CHC nanoparticle suggests that the nano-aggregates formed simultaneously by the coil of the CC single chain and/or by the hydrophobic interaction among CHC macromolecules in the solution. It was obtained from Fig. 7-5 that the CC shows a high fraction (>90%) of the nano-aggregates having a size of 40 nm, suggesting that it is difficult to form larger aggregate with lower degree of hydrophobic substitution (i.e., DH <0.13). However, as DH increased up to 0.26, the nano-aggregates show a high fraction of mean size 2 (around 200 nm), indicating that a critical concentration of hexanoyl substitution in the range between 0.13 and 0.26 dominates the self-assemble behavior of the CHC macromolecules.

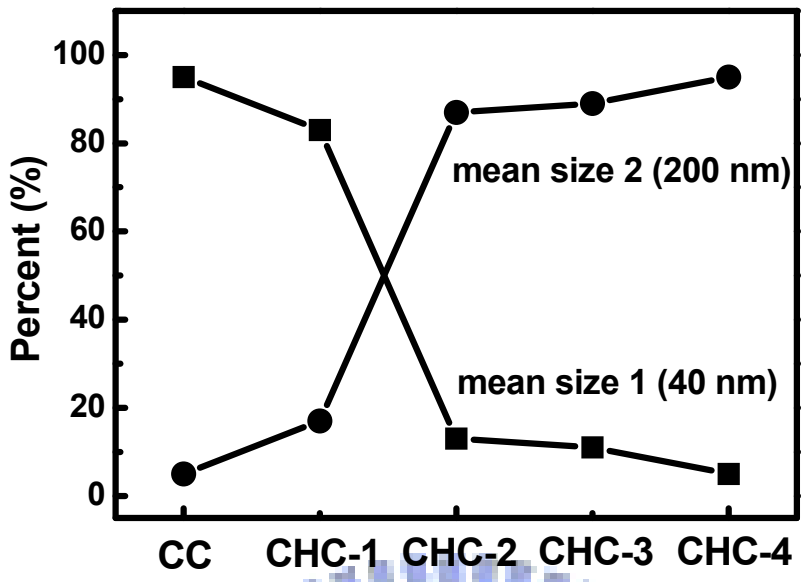

Figure 7-5 Fraction of mean size 1 and 2 of CC and CHC nano-aggregates.

7.5 Nanostructural Development of the CHC Nano-aggregates

In Fig. 7-6a, the hexanoyl-modified carboxymethyl chitosan has the amphiphilic property with hydrophile and hydrophobia. Based on the poly-core model proposed by Wang et al. [115], for hydrophobically modified polysaccharides, the hydrophobic microdomains are formed by the association of hydrophobic group, and the polysaccharide backbones coil to form the hydrophilic shells outside these hydrophobic microdomains, thus a minimal energy state is attained in aqueous media. For CC and CHC-1, the hydrophobic interaction provides the driving force for self aggregation as supported to be a combination of the effects of intermolecular H-bonding of CC (e.g. the presence of carboxylic, hydroxyl and amino groups on the CC chains); electrostatic repulsions between COO- groups on the CC chains and hydrophobic interaction among the hydrophobic moieties in CC such as acetyl groups and glucosidic rings.

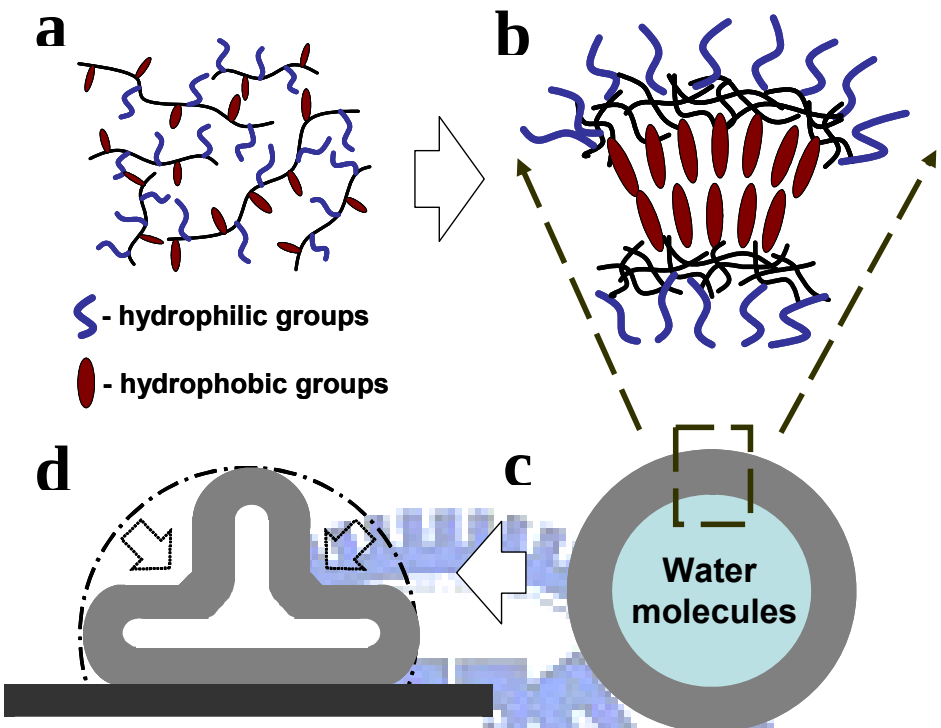

Figure 7-6 Schematic illustration of formation process of CHC hollow nanocapsules.

Hence, for the CHC with lower DH, the particle-like aggregated structure of CHC was formed. However, from a recent investigation using hydrophobic acyl group of various carbon lengths, we found that a structural change from particle to hollow capsule with increasing the DH of CHC was strongly affected by the variation of the physical state of water molecules within the aggregates (submitted in press). Accordingly, the increase of bound water within CHC matrix with increasing DH enhances difficulty in the formation of hydrophobic core and become structurally unstable. In contrast, with increase of free energy caused by increasing hydrophobicity, the CHC tends to self-aggregate to form a bilayer structure with hydrophilic-hydrophobic-hydrophilic configuration, as schematically illustrated

in Fig. 7-6b. The amphiphilic potential of the CHC with higher DH is then thermodynamically favorably to drive the resulting CHC macromolecules to self-assemble into a bilayer structure with water molecules encapsulated inside the core phase while both interior and exterior regions of the shell are stabilized by the hydrophilic groups, forming a spherical architecture with minimal surface energy, as schematically shown in Fig. 7-6c.

However, an increase in entropy change due to the formation of nano-aggregate in aqueous environment has to be compromised thermodynamically. Although there are little evidences or supports that are available in the literature in similar materials systems, an alternative mechanism proposed by Moroi [116] appears feasible. Moroi involved the peculiar properties of water by recognizing that the water molecules in the liquid state have a structure of hydrogen bonds similar to that of ice, the cavities in the structure are large enough to accommodate a hydrophobic group, such as hydrocarbon chain. Thus, occupation of a cavity by hydrophobic solute hinders the movement of free water molecules, which therefore remain stationary for longer periods, i.e., improved stability of the colloidal system. In order words, the water molecules surrounding a hydrophobic solute become more ordered than bulk water molecules and have lower entropy. Accordingly, the water molecules become more ordered around the hydrophobic solute with an increase in hydrophobicity in order to accommodate the variation of system entropy while the nano-aggregates were under developing.

Though the morphology of the nano-aggregates show spherical shape from TEM results, the scanning electron microscopy (SEM) images show entirely different morphologies of the nano-aggregates, as shown in Fig. 7-7,

where the nano-aggregates displayed collapsed structures. This variation is mainly caused by the difference of the preparation methods. For TEM sample preparation, the CHC aggregates are subjected to ambient drying, where the excellent water-absorption and water retention capability, especially the crystal water binding with the molecular structure keep the CHC nano-aggregate its structural integrity. However, when the water, i.e., both free water (i.e., unbound water) and crystal water (i.e., bound water) being removed from the CHC macromolcules using ethanol through extensive dehydration, structural integrity of the nano-aggregates can no longer preserve. It collapsed as a flatten basketball. This morphological change suggests a hollow structure evolved upon the first formation of the CHC nano-aggregates (Fig. 7-6d), indicating a capsule-like nanostructure, where a core-shell configuration developed. From the collapsed morphology, the thickness of the shell layer of the collapsed nanocapsules, from the image inserted in Fig. 7 (a combination of two shells of the nanocapsule) is about 9 nm; the layer thickness of the single shell is ca. to be 4.5 nm. Such a small scale of the shell thickness may explain the reason that the core-shell structure of the CHC nanocapsules is hard to distinctly differentiate from TEM analysis under the resolution aforementioned.

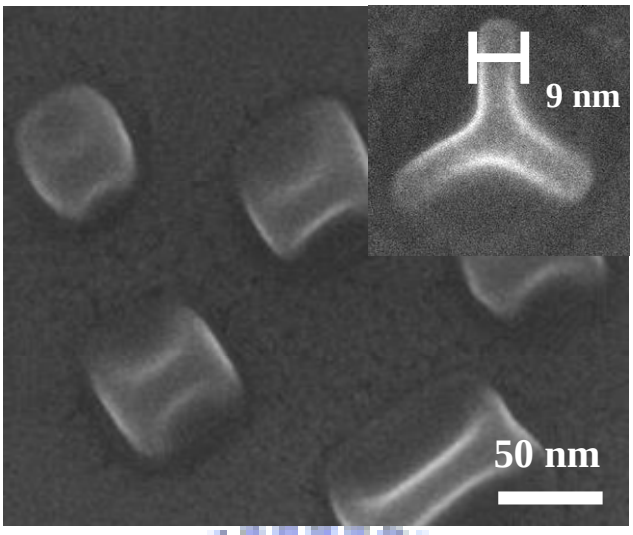

Figure 7-7 SEM images of CHC-4 nanocapsules.

7.6 DOX Loading and Release Behavior of CHC Nanocapsules

To investigate the drug-loading capacity of the CHC nanocapsules, the model drug, doxorubicin (DOX), was loaded into the CHC nanocapsules. Figure 7-8a shows the encapsulation efficiency (EE) of DOX from CHC nanocapsules with different DH. As reported by Kitaeva et al. [117], since DOX molecule contains an amino group with a pKa of 8.6, it is expected that DOX can form polyelectrolyte complex with the carboxymethyl groups of CC and CHC. Hence, for the CC (where its DH is zero), it shows a lower encapsulation efficiency of around 26.3 %. However, as increase the level of hydrophobic substitution, the DOX encapsulation efficiency increased from 26.3 to 46.8% as the DH increased form 0 to 0.48. The improved encapsulation efficiency with increase of DH of the CHC should be caused by the larger reservoir space and the increase of the hydrophobic interaction of inner shell, which restricts the outward diffusion of DOX from nanocapsules.

The release of DOX from the CHC nanocpasules was investigated using a dialysis procedure. A solution of the DOX-loaded CHC nanocapsules in a dialysis cassette was dialyzed against 100 mM buffer and the solution in the cassette was sampled at various times over a 7 day period to determine the amount of DOX remaining in the nanocapsules. Figure 7-8b shows the release profiles of DOX and DOX-loaded CHC nanocapsules with different levels of DH.

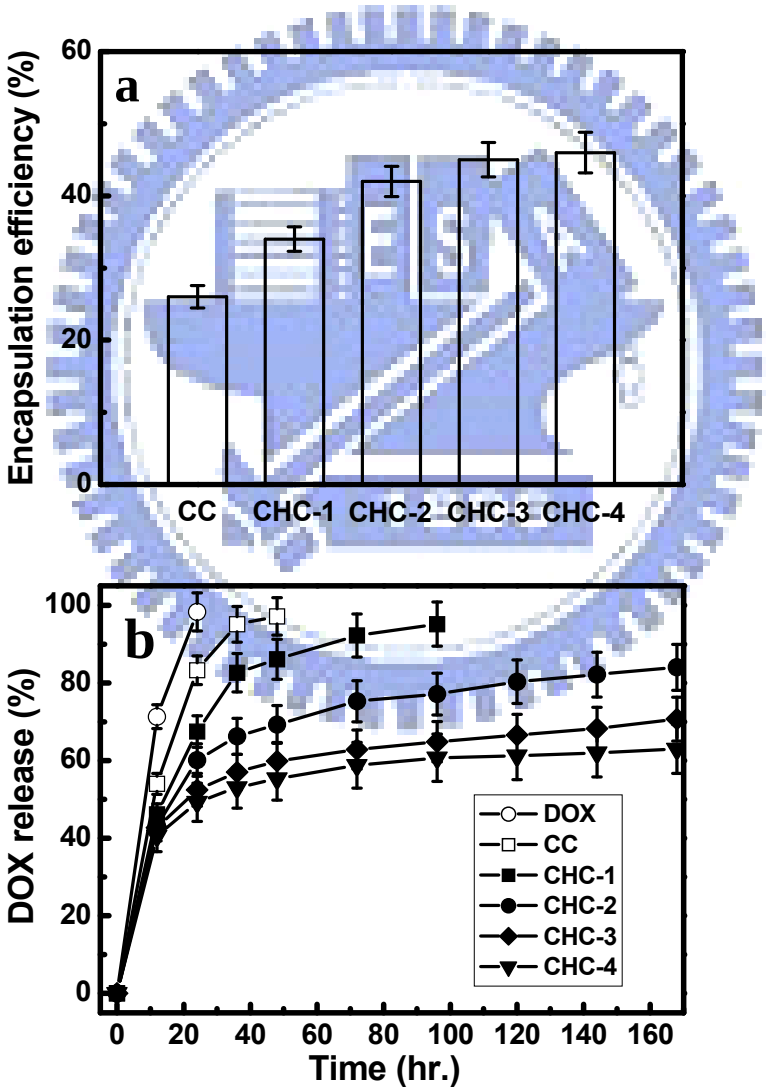

Figure 7-8 (a) DOX encapsulation efficiency and (b) DOX release profiles of CHC hollow nanocapsules

It was observed that DOX and DOX-loaded CC had a faster diffusion rate with essentially complete release after 24-36 hrs. This is consistent with the expected rate of diffusion for low molecular weight molecules across the dialysis membrane. However, DOX-loaded CHC nanocapsules show a two-step release profile. In the first step (0~12 hrs), the rapid release of DOX may caused by the diffusion of DOX on the surface of nanocapsules out of the dialysis membrane. Then, the followed a relatively slow release, which may be dominated by the DH of CHC nanocapsules. It can be found that CHC-1 showed a total release period of about 96 hrs. By contrast, with the increase of DH (i.e., CHC-2, CHC-3, and CHC-4), the entrapped DOX showed a continuous release over 7 days. It is reasonably believed that the increase of hydrophobic groups enhances encapsulation efficiency and payload of the DOX within CHC nanocapsules. These results indicate that these CHC self-assembled hollow nanocapsules can be a suitable candidate for controlled DOX delivery for anti-cancer purpose.

Chapter 8

Hydrophobic Effect on the Structural Evolution of Acylated-Carboxymethyl Chitosan and its Self-Assemble Forming of Doxorubicin-loading Nanocapsule

8.1 Introduction

The construction of supra-molecular assemblies with well-defined nanostructure is of great interest owing to their potential applications in diverse fields. Since 1995, Eisenberg et al. [118] found the multiple morphologies of crew-cut micelle-like aggregates of polystyrene-b-poly (acrylic acid) diblock copolymer in solution, the preparation and assembly of amphiphatic polymers of various architectures has become a research area of interest. Polymer amphiphiles enable the preparation of nano-aggregates with shape ranging from spheres [119] to cylinders [120], vesicles [121], donuts [122], and other geometry [123] by self-assembly. Of the various aggregates, hollow vesicles represent an important class of materials because their unique structural and surface properties may lead to a wide range of applications, especially in medicine such as capsule agents for drug delivery, encapsulation of large quantities of guest molecules, and gene therapy [124].

Recently, many efforts have been performed to prepare biodegradable and non-toxic polymeric amphiphatic on the basis of natural biomaterials such as polysaccharides. Among those natural biopolymers, hydrophilically, hydrophobically, and amphiphatically modified chitosan derivatives were

studied and realized to form monodisperse self-aggregated nano-particles by ultrasonication in aqueous solution. However, it is more technologically desirable and critical if (a) a hollow structure can be easily achieved using chitosan derivatives without the need of extensive ultrasonication, where a nanometric carrier with higher load capacity of drugs or proteins can be expected with lower operation cost, (b) a variation of the amphiphilic nature of the resulting carrier allows an enhanced affinity to different drugs or proteins, e.g., hydrophilic drugs or hydrophobic drugs, where an improved encapsulation efficiency can be designed and (c) an adjustable biocompatibility and biodegradability is clinically manageable. In chapter 7, a simple core-template-free strategy was successfully proposed and a new type of amphiphatic chitosan hollow nano-capsules was synthesized by a self-assembly mechansim. In general, polymer amphiphiles consisting of hydrophilic and hydrophobic segments can form micelles or micelle-like self-assemblies with a hydrophobic core and a hydrophilic shell due to non-covalent association arising from intra- and/or inter-molecular interactions among hydrophobic segments in aqueous media. On the other hand, among these versatile micelles, the hollow cavity enclosed by a double layer membrane is also possibly formed [125]. However, little scientific evidences can be sufficiently employed for better understanding of such a hollow cavity development for the amphiphilic chitosan.

Hence, as one of the research objectives in present study, structural evolution of the chitosan-based nano-aggregates was systematically investigated in terms of different degrees of acyl substitution (DH) and number of carbon of the acyl ligand (C_n). In addition, the doxorubicin (DOX)-encapsulated capacity of the nano-aggregates of varying degrees of

hydrophobicity, in terms of DH and C_n, was also studied.

8.2 Synthesis of carboxymethyl chitosan (CC)

Following our previous report [126], 5 g of chitosan was suspended in 2-propanol (50 mL) at room temperature while being stirred for 30 min. The resulting suspension was gently mixed with 12.5 mL NaOH solution. The mixture containing NaOH of 13.3M was mixed with 25 g of chloroacetic acid to prepare carboxymethyl chitosan (CC) sample with a high degree of carboxymethyl substitution. The resulting suspensions were stirred for 30 min and heated to 60°C for 4 h, followed by filtration, washing by methanol solution, and drying.

8.3 Synthesis of acylated carboxymethyl-chitosan (ACC)

The obtained CC sample (2g) was dissolved in distilled water (50 mL) under vigorously stirring for 24 h. These resulting solutions were then mixed with methanol (50 mL), followed by addition of acyl anhydrides, namely, acetic anhydride, hexanol anhydride, decanoic anhydride, and dodecanoic anhydride, representing acyl groups of various chain lengths (or carbon numbers). The acylated chitosan derivatives were prepared as previously described [16]. Acetyl, hexanoyl, and decanoyl carboxymethyl-chitosan were prepared at ambient temperature for 20 h. Dodecanoic carboxymethyl-chitosan was prepared at 50^{o}C for 2h, followed by standing for 18h. Different ratios of acyl anhydride to amino functionalities of CC samples were designed in order to prepare the acylated-carboxymethyl chitosan (ACC) of different degree of hydrophobic substitution (DH) until the value of DH reached up to 0.5. The DH is defined as the average number of acyl group per

repeat unit multiplied by 100, calculated according to the nitrogen content which determined by elemental analysis [127]. Finally, the resulting solutions were collected by dialysis membrane after dialysis with ethanol solution (25% v/v) for 24 h. The chemically modified chitosan was expressed using the value of n and m to define the carbon number of hydrophobic side chain (C_n) and DH, respectively, of ACC derivative in the C_n-m, where n ranges from 2, 6, 10, to 12 and m ranges from 0.125, 0.25, 0.375, to 0.5. For example, C_2-0.25 means the ACC having the approximate value of the degree of hydrophobic substitution of 0.25. The preparation conditions and the characteristics of ACC samples are given in Table 8-1.

8.4 Preparation of drug-loaded and non-loaded ACC nano-aggregates

100 mg/ml ACC samples were separately suspended in distill water under gentle shaking at 25°C for 24 h, followed by ultrasonication using a probe type sonifier (Automatic Ultrasonic Processor UH-500A, China) at 30W for 2 min till an optically clear solution was obtained. The sample solutions were filtered through a filter (1.0 μm, Millipore) to remove dust and impurity. The final solutions were then stored in stock for a subsequent sample characterization.

Drug-loaded ACC nano-aggregates were prepared by dissolving 20 μg/mL of doxorubicin (DOX) in 20 ml acquired suspension. Insoluble, free DOX was removed by centrifugation at 2000 rpm and 4°C for 5 min. The drug-containing nanoparticles were then separated from the aqueous solution by centrifugation at 15000 rpm and 4°C for 15 min. Drug concentration in the supernatant was analyzed by ultraviolet absorption (UV) at wavelength of 490 nm, a strong characteristic absorption band of DOX, with reference to a

calibration curve on a UV-VIS spectrometer (SP-8001, Metertech Inc.). The measurements were performed in triplicate. The amount of the drugs encapsulated in the nano-aggregates was then calculated by the total amount of DOX subtracting the residual DOX in the supernatant. Encapsulation efficiency (EE) were obtained as described below

$$EE= (A-B)/A\times 100$$

where A is the total amount of the DOX, B is the amount of DOX remaining in the supernatant and C is the weight of the ACC nano-aggregates.

Table 8-1 The preparation conditions and the characteristics of ACC nano-aggregates

Samples	Acyl group	DH[a]	[$(RCO)_2O$]/ [GlcN]	Temp (^oC) / Time (h)	CAC[b]$\times 10^{-2}$	$W_{nf,max}$[c] (%)
CC	-	0	-	-	25.0	10.3
C_2-0.125	Acetyl	0.11	0.2	25/20	21.0	11.8
C_2-0.25	Acetyl	0.24	0.4	25/20	12.7	14.5
C_2-0.325	Acetyl	0.31	0.5	25/20	7.20	15.9
C_2-0.5	Acetyl	0.56	1	25/20	5.00	17.9
C_6-0.125	Hexanoyl	0.13	0.2	25/20	9.20	12.4
C_6-0.25	Hexanoyl	0.26	0.4	25/20	31.7	19.8
C_6-0.325	Hexanoyl	0.33	0.5	25/20	0.91	24.8
C_6-0.5	Hexanoyl	0.48	1	25/20	0.40	29.3
C_{10}-0.125	Decanoyl	0.12	0.2	25/20	6.20	15
C_{10}-0.25	Decanoyl	0.24	0.4	25/20	1.80	24.3

C_{10}-0.325	Decanoyl	0.34	0.5	25/20	0.57	41.2
C_{10}-0.5	Decanoyl	0.45	1	25/20	0.36	57.4
C_{12}-0.125	Dodecanoyl	0.1	0.2	50/2+25/18	5.00	16.2
C_{12}-0.25	Dodecanoyl	0.22	0.4	50/2+25/18	1.20	31.4
C_{12}-0.325	Dodecanoyl	0.3	0.5	50/2+25/18	0.36	45.7
C_{12}-0.5	Dodecanoyl	0.44	1	50/2+25/18	0.32	63.9

[a] DH determined by element analysis.

[b] Critical aggregation concentration determined from I_{372}/I_{385} data..

[c] The content of bound water obtained by the DSC test.

8.5 Structural Characteristics of ACC

As shown in Scheme 8-1, ACC was synthesized using CC as the starting precursor. In previous work, it was demonstrated that a hydrogen atom on the amino group of CC can be replaced by acyl group, as confirmed by ^1H NMR analysis [126]. However, in this study, the signal intensity of the characteristic acyl protons was not in proportion to the DH of the acyl groups, which suggested that acyl groups aggregated to form hydrophobic micro-domains to minimize their interaction in D_2O (the resulting spectra were not shown here). This trend in the ^1H NMR spectra was consistent with other polymeric amphiphiles that formed aggregates in the aqueous phase [128]. Hence, the DH of ACC samples were determined by elemental analysis [127] in this study and the ACC samples with different DH and C_n were prepared through the control of various ratios of acyl anhydride to amino group of the CC, which is listed in Table 8-1.

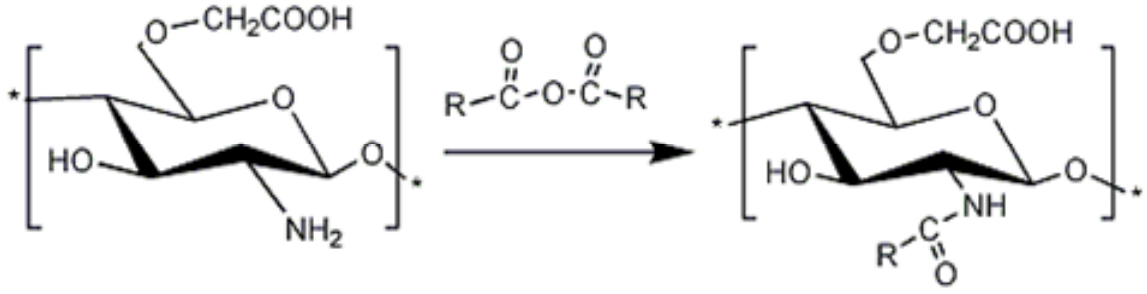

$$R=C_{n-2}H_{2(n-2)}CH_3;\ n=2,\ 6,\ 10,\ 12.$$

Scheme 8-1 Acylation Reaction of carboxymethyl chitosan

Scheme 8-1 shows the molecular structure of the amphiphilically modified chitosan with different lengths of acyl side chains (with carbon number, C_n, ranging from 2, 6, 10, to 12) attached on the amino groups of chitosan. From the FT-IR analysis, shown in Fig. 8-1, the absorption peaks of

CS at ca. 1655 cm^{-1} can be assigned to the carbonyl stretching of secondary amides (amide I band), at 1570 cm^{-1} to the N–H bending vibration of nonacylated 2-aminoglucose primary amines, and at 1555 cm^{-1} to the N–H bending vibrations of the amide II band [127]. The presence of both 2-aminoglucose and 2-acetamidoglucose repeat units was confirmed by bands at 1655, 1570, and 1555 cm^{-1}. After carboxymethylation, CC shows absorption peak at ca. 1730 cm^{-1}, which was assigned to the carboxymethyl dimer (O=COH…O=COH). Compared to CC, the vibrational band of C_{12}-0.5 corresponding to primary amino groups at 1570 cm^{-1} was disappeared, while prominent bands at 1555 cm^{-1} were observed. In addition, peaks at 2850–2950 cm^{-1} ascribed to $-CH_2$ with their absorption intensity was proportional to the acyl chain length [129]. These results clearly confirmed a successful acyl substitution on the carboxymethyl chitosan.

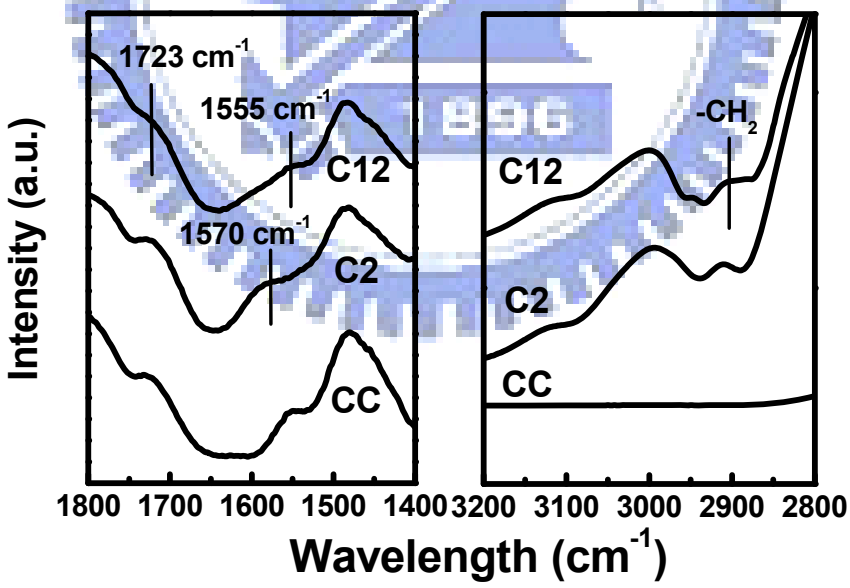

Figure 8-1 FTIR spectra of CC, C_2-0.5, and C_{12}-0.5.

8.6 Self-assemble behavior of ACC

After dispersing in water, the ACC molecules can form self-assembled nanometric aggregates with an aid of ultrasonication for better dispersion as has been demonstrated in previous work [126]. The fluorescence probe technique can be used to monitor the self-aggregation behavior of ACC at a molecular level, and pyrene was chosen as a fluorescence probe. The intensity ratio of the first peak (372 nm) and the third peak (385 nm) I_{372}/I_{385} in its fluorescent spectrum is quite sensitive to a subtle change in the environment around the pyrene molecules. Hence, the critical aggregation concentration (CAC), which is defined as the threshold concentration of self-aggregate formation by intra- and/or inter-molecular interactions, can be determined from the variation of the I_{372}/I_{385} value of pyrene in the presence of polymeric amphiphiles. Fig. 8-2a shows the change of CAC of ACC nano-aggregates with different levels of DH and hydrophobic side chain length (C_n). It was found that the CAC of ACC with DH and C_n varying from 0.125 to 0.5 and from 2 to 12, respectively, has a smaller value than that of the CC (which was 0.25mg/ml as previously reported [126]), indicating that the ACC possesses stronger self-aggregation behavior than that of CC in aqueous solutions. This stronger tendency of the self-aggregation can be deduced from the increased hydrophobicity caused by the introduction of greater DH and C_n. In addition, it is also observed that the CAC values of ACC nano-aggregates were decreased with the increase of DH and/or C_n. It has realized that the increase of hydrophobicity in amphiphatic polymer causes the difficulty to dissolve in aqueous solution because the energy is essential to dissociate the H-bonding in water molecules (need to do work). Therefore, the dissolution of hydrophobic groups in water will give rise to an increase of the surface free

energy. In order to reduce the energy, the hydrophobic groups will aggregate to form micelle-like structure with hydrophobic core and hydrophilic shell, or a bi-layer structure of hydrophilic-hydrophobic-hydrophilic configuration. Hence, with larger DH and/or C_n, the ACC is able to form nano-aggregates easily at very low concentrations because it tends to reach the largest surface energy. This demonstrates that the self-aggregation ability can be effectively enhanced with increasing hydrophobic nature, e.g., DH and/or C_n, of the ACC in aqueous environment. However, it seems to have the lowest value of CAC even if the DH or/and C_n is infinitely increased. This means that the CAC of the ACC nano-aggregates will reach a lowest value over a critical level of hydrophobicity. In addition, a linear correlation between ln(CAC) and DH was observed, except the case when C_n is 12 and DH is 0.5, as shown in Fig. 8-2b. The same linear correlation between ln(CAC) and C_n can be also obtained. Such a linear correlation proves that the CAC of the ACC nano-aggregates decreased exponentially with the increase of DH and C_n. Hence, a mathematical relationship among ln(CAC), DH and C_n can be derived as follow,

$$\ln(CAC) = a_1 X_{Cn} \cdot X_{DH} + b_1 X_{DH} + c_1 X_{Cn} + d_1 \qquad \text{at } X_{DH} < 0.5,\ X_{Cn} < 12 \qquad (8\text{-}1)$$

or

$$CAC = \exp\left[a_1 X_{cn} \cdot X_{DH} + b_1 X_{DH} + c_1 X_{cn} + d_1\right] \qquad \text{at } X_{DH} < 0.5,\ X_{Cn} < 12 \qquad (8\text{-}2)$$

where the coefficients, i.e., a_1, b_1, c_1, and d_1 having the value of 0.24, -6.87, -0.21, and -0.38, respectively, were obtained by regression analysis. From eq. (8-2), it suggests that the hydrophobic effect resulting from both the DH and

side chain length, C_n dominates the self-aggregation ability of the ACC nano-aggregates. Compared to the case of C_2, the slopes were apparently increased for the cases of C_6 and C_{12} in the semi-log plot, Fig. 8-2b, indicating that a potentially stronger hydrophobic effect can be developed through a longer-chain acyl substitution, where a much lower value of CAC, by 2-3 orders of magnitude, can be obtained.

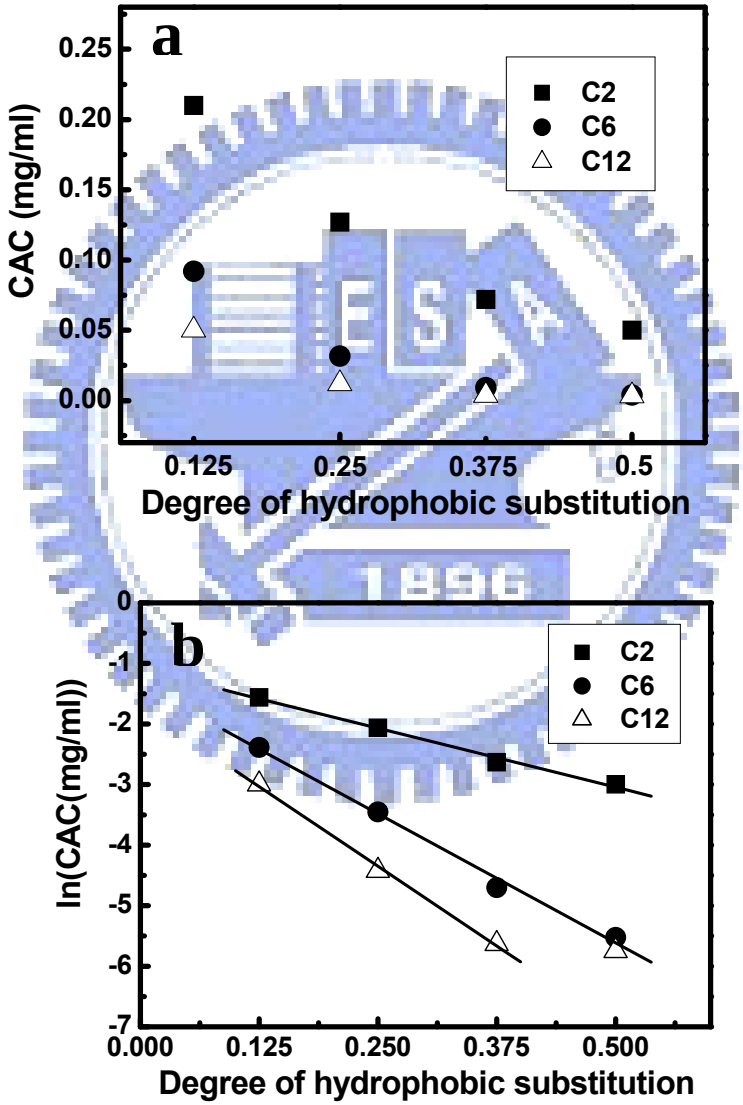

Figure 8-2 Dependence between the DH of ACC as C_n=2, 6 and 12 and (a) the critical aggregation concentration, CAC and (b) ln(CAC), respectively.

8.7 Molecular configuration of water in ACC

The hydrophobic substitution is also found to affect profoundly water uptake behavior of the resulting ACC. It was generally accepted that the hydrophobic modification of amphiphatic chitosan derivatives with various chain lengths may cause a change in the molecular configuration of water that being trapped in the matrix. In order to better understand the physical state of water molecules that being trapped in the ACC network, DSC analysis was conducted. Accordingly, the configuration of the water molecules, corresponding to the resulting DSC spectrum, can be classified into three different physical states [130]: (1) free water which can freeze at the usual freezing point (corresponding to an endothermic peak close to 4.8 ^{o}C), (2) freezable bound water which freezes at a temperature lower than the usually freezing point (corresponding to an endothermic peak much lower than 4.8 ^{o}C) and (3) non-freezable bound water which cannot freeze at the usual freezing point (which is hardly detected by the DSC).

In the initial swelling process, water molecules first disrupt the intermolecular hydrogen bonds and then bind to the hydrophilic sites, such as carboxymethyl groups in this case. These water molecules, which are isolated and uniformly distributed throughout the polymer, have greatly restricted mobility and are referred to as non-freezable bound water. Above a certain level of the bound water, the additional water is preferentially oriented around the bound water and the polymer network structure as a secondary or tertiary hydration shell, which is in a form generally called “clusters”. These cage-like structures result from the tendency of water molecules to form the maximum amount of hydrogen bonds among them in the available space. This type of water is called freezable bound water. As the water uptake further increases,

the splitting of the melting peak will becomes more apparent in the DSC curves, suggesting the existence of two states of freezing water, i.e., freezable bound water and free water, in the polymers. Figure 8-3 shows the DSC spectra of the samples with different chain length of acyl groups measured at water content of about 200%.

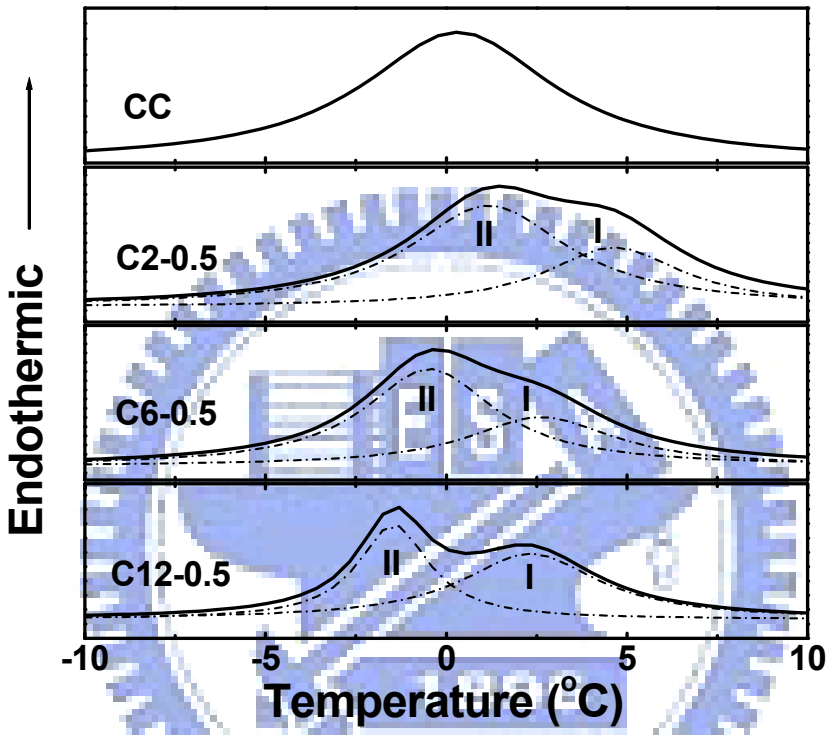

Figure 8-3 DSC curves of CC and ACC derivates (C_n-0.5) measured at water content=200%. Dash lines represent the curve fitting by Lorentzian curve-fitting procedure.

A heavily overlapped band (solid line) is observed and can be clearly differentiated as an overlap of several peaks (depicted as dash lines) using the Lorentzian curve-fitting procedure. For the CC sample, the endothermic peak of free water was not observed under fully swollen state. Instead, the endothermic peaks at 1.3 °C and below assigned to freezable bound water were detected. However, after acyl modification, the samples show different DSC spectra, suggesting the state of water in the ACC network was

significantly different from that in the CC. It can be found that the peak I which is close to 4.8 ^{o}C suggesting that the ACC contained free water when the water content $\geq$ 200%. On the other hand, the peak II was assigned to freezable bound water. With increase of the side chain length from C_n = 2 to 12, peaks I and II shifted toward lower temperature and the peak intensity was decreased, which may be caused by the decrease of the intermolecular volume for free water and freezable bound water. This implies that the chain length of acyl group plays an important role in affecting the amount of free water and freezable bound water within the network structure.

Hence, in order to understand the interaction between water molecules and hydrophobic side chain of the ACC, DSC is also used to quantitatively determine the amount of water, i.e., both freezable and non-freezable bound water in the ACC matrix. Figure 8-4 shows the $W_{nf,max}$ in ACC with different hydrophobic side chain lengths (carbon number, C_n). It was found that the CC displays the lowest $W_{nf,\,max}$ of 10.3% than other samples. This is due to the fact that the samples with high carboxymethyl substitution favored the formation of intermolecular hydrogen bonding (polymer-polymer interaction), resulting in a structure with fewer tight water-binding sites (water-polymer interactions) [24]. However, with the increase of the hydrophobic side chain length, the $W_{nf,max}$ of ACC is proportionally increased with the C_n until C_n = 12. This C_n-dependent increment can be attributed to a so-called “hydrophobic effect” under which water becomes more structured and less mobile in the vicinity of the hydrophobic group [131]. It has been known from surface-thermodynamic analyses that the attractive interactions between apolar (hydrophobic) molecules immersed in water are driven by the strong hydrogen-bonding free energy of cohesion between the surrounding water molecules [132]. Hence,

increasing C_n of side chain will cause an increase of the hydrophobizing capacity of water since it tends to increase the tendency of self-hydrogen-bonding among water molecules, rather than the interactions between water molecule and host molecule. Differing from the CC (which has a stronger water-polymer interaction), the hydrophobic interaction between acyl groups is suggesting to cause more self-hydrogen-bonding for those neighboring water molecules. The strong hydrophobic effect coming from the hydrophobic substitution will enhance the hydrophobizing capacity of water and this behavior is increased with increasing hydrophobicity of the ACC as the acyl chain length increased (i.e., larger C_n).

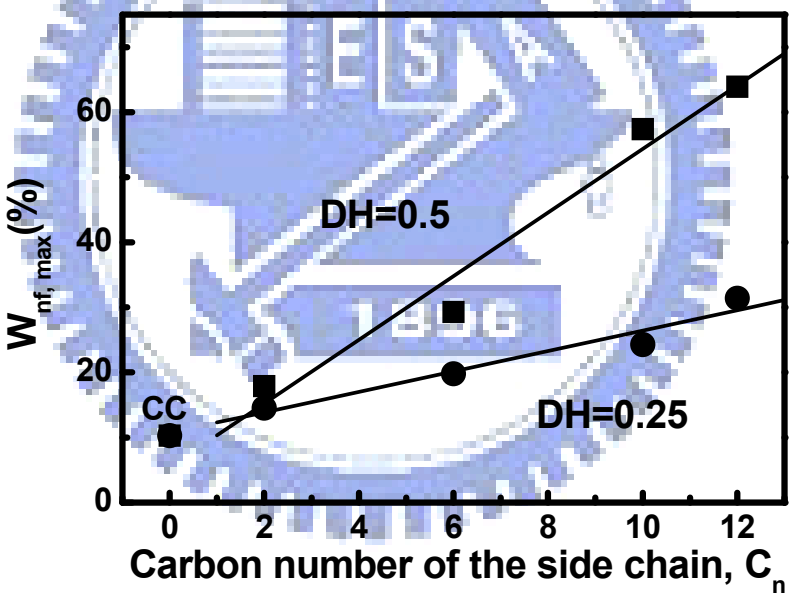

Figure 8-4 Dependence between the content of bound water, $W_{nf,\ max}$, and the hydrophobic side chain with different C_n of ACC in DH=0.25 and 0.5.

On this basis, a linear correlation between $W_{nf,\ max}$ of the ACC and the C_n with DH of 0.5 and 0.25 is then revealed as depicted in Fig. 8-4, which provides a direct evidence that the content of bound water in the ACC is profoundly dependent on the hydrophobic side chain length. Moreover, the

slope of these curve-fitting straight lines is increased linearly with the increase of DH. The linearity correlation suggests the “bound water” is affected linearly with both the DH and Cn, and accordingly, linear mathematical equations can be derived directly from the experimental data, which give as follows,

$$Y_w = (11.87 \cdot X_{DH} - 1.2) \cdot X_{Cn} + K_1 \qquad (8\text{-}3)$$

and

$$Y_w = (11.22 \cdot X_{Cn} - 3.16) \cdot X_{DH} + K_2 \qquad (8\text{-}4)$$

where Y_w is the concentration of bound water, X_{DH} is the degree of hydrophobic substitution, X_{Cn} is the carbon number, and K_1, K_2 are constant. Further integration of Eqns (8-3) and (8-4), a mathematical model can be constructed as follow,

$$Y_w = a_2 X_{Cn} \cdot X_{DH} + b_2 X_{DH} + c_2 X_{Cn} + d_2 \qquad \text{at } X_{DH} < 0.5,\ X_{Cn} < 12 \qquad (8\text{-}5)$$

The coefficients a_2, b_2, c_2, and d_2, having values of 11.9, -13.8, -1.20, and 13.1, respectively, were obtained by regression analysis. This new model, having exactly the same as Eqn. (8-1), indicates that the bound water is a complex function of, C_n and DH. To be more specific, the bound water is influenced adversely by X_{DH} and X_{Cn} alone, but more significant by the term of ($X_{DH} \times X_{Cn}$). For the later, it implies that the concentration of bound water trapped within this newly-formed ACC is profoundly influenced by a composite effect of DH and side chain length. Comparing to Eqn. (8-1) and (8-5), it is believed that the

self-aggregation behavior should be physically correlated with the content of bound water within the resulting ACC aggregates. And the composite effect as a result of both the degree of acyl substitution and chain length aforementioned should play an important role in determining the self-assembly behavior of the ACC molecules.

8.8 Self-Assembly Map

On this basis, an interesting finding can be drawn from Figure 8-5, showing the plot of CAC and $W_{nf,\,max}$ of ACC with different values of ($X_{DH} \times X_{Cn}$), where an intercept at product of ($X_{DH} \times X_{Cn}$) = 1.5 was observed. Below 1.5, assigned as Zone I, the values of CAC decreased readily with increasing ($X_{DH} \times X_{Cn}$) up to 1.5 and reached a minimum value. The content of bound water, $W_{nf,\,max}$, in the ACC was increased only slightly in region of Zone 1. However, when the value of ($X_{DH} \times X_{Cn}$) exceeded 1.5 (i.e., Zone II), $W_{nf,\,max}$ increases considerably to a level as high as 64% with increase of ($X_{DH} \times X_{Cn}$), whilst the CAC kept relatively constant. These findings strongly indicate that the hydrophobic effect was dominated by an interaction of both DH and C_n, rather than individual component alone. Further, the hydrophobicity associated with DH and C_n strongly affected the self-aggregation ability and the hydrophobizing water capacity of the ACC nano-aggregates. It is clearly demonstrated that a critical level of hydrophobicity that can effectively generate conspicuous changes in both CAC and $W_{nf,\,max}$ is evidenced in the self-assembly map constructed in Fig. 8-5, when the composite effect of the degree of acyl substitution and acyl chain length, i.e., the product of ($X_{DH} \times X_{Cn}$), is closed to 1.5.

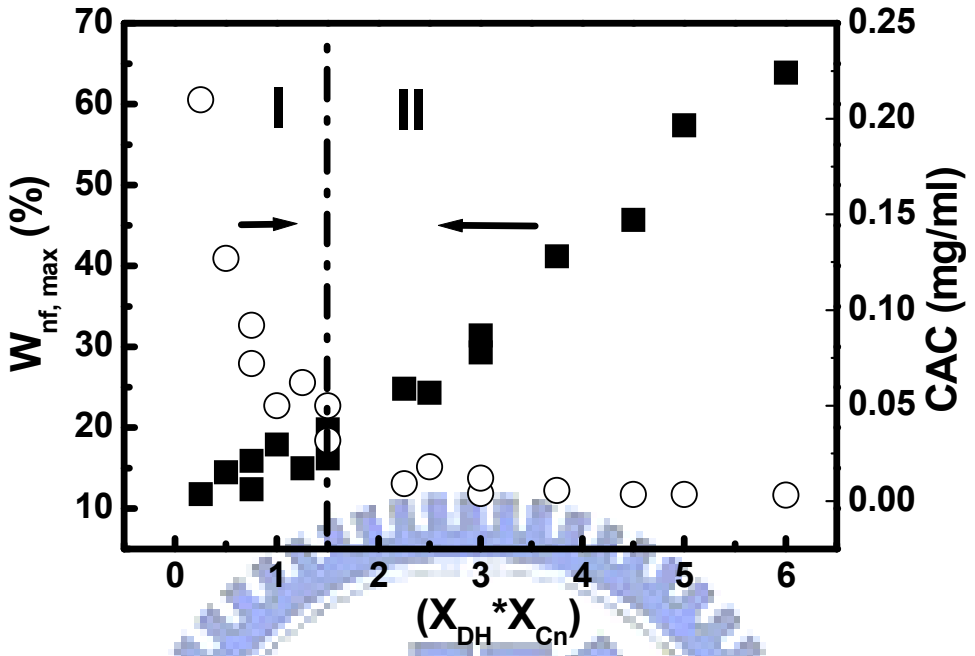

Figure 8-5 Plot of CAC (○) and $W_{nf,\ max}$ (■) of ACC derivates with different values of ($X_{DH} \times X_{Cn}$).

Upon self-assembly, the hydrophobicity of the ACC was detected to fatefully dominate the structural evolution of the nano-aggregates. Therefore, it is reasonably to believe from Eqns (8-1) and (8-5), together with Fig. 8-5, that the composite effect between the DH and C_n may play a key role in controlling the structural morphology of the resulting nano-aggregates. In Zone I of Fig. 8-5 (the region where the value of ($X_{DH} \times X_{Cn}$) is lower than 1.5), i.e., the nano-aggregates with C_n = 2 and DH = 0.5 showed a compact particle morphology with a relatively uniform size distribution of around 25 nm in diameter, as shown in Fig. 8-6a. This observation is similar to the case of the CC in previous work. However, when ($X_{DH} \times X_{Cn}$) exceeded 1.5, i.e., Zone II; the resulting nano-aggregates exhibited entirely different structural morphology. In the case of C_n = 6 and DH = 0.5, the ACC nano-aggregates shows a perfect spherical geometry with a size of about 100 nm, shown in Fig. 8-6b. After dehydration, the spherical nano-aggregates structurally collapsed (Fig. 8-6c)

and the broken nano-aggregates after electron-induced rupturing (shown in Fig. 8-6d), illustrated a hollow core, indicating such a class of nano-aggregate is virtually a capsule-like structure.

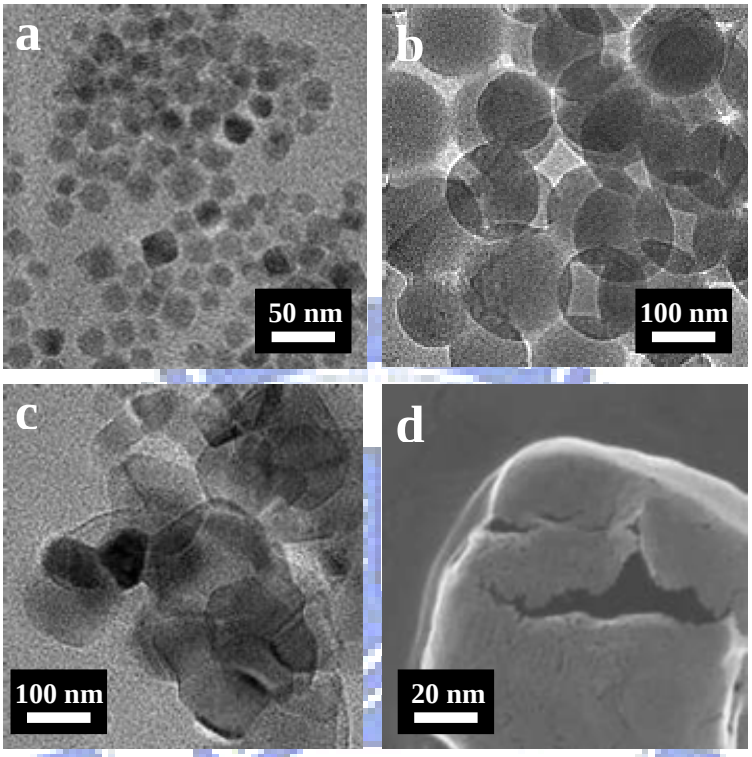

Figure 8-6 TEM images of (a) C_2-0.5, (b) C_6-0.5, and C_6-0.5 after dehydration; and (d) SEM image of the ACC nano-aggregates after electron-induced rupturing.

As revealed from the fluorescence probe test, the CAC values for the nano-aggregates with smaller ($X_{DH} \times X_{Cn}$) rapidly decreased till ($X_{DH} \times X_{Cn}$) approaching to 1.5. According to the poly-core model proposed by Wang et al., the amphiphatic potential drives the resulting ACC macromolecules to self-assemble into a micelle-like structure with hydrophobic groups turning into the core structure while the hydrophilic segments structurally turning into water environment to establish a shell structure, as schematic illustrated in the reaction scheme of A → B1 in Fig. 8-7, forming a spherical architecture with

minimal surface energy (as the drawing of B2 in Fig. 8-7). Furthermore, from experimental observation, it was discovered that the ACC with less hydrophobicity, e.g., Zone I where ($X_{DH} \times X_{Cn}$) <1.5, tends to form nano-particle dispersion.

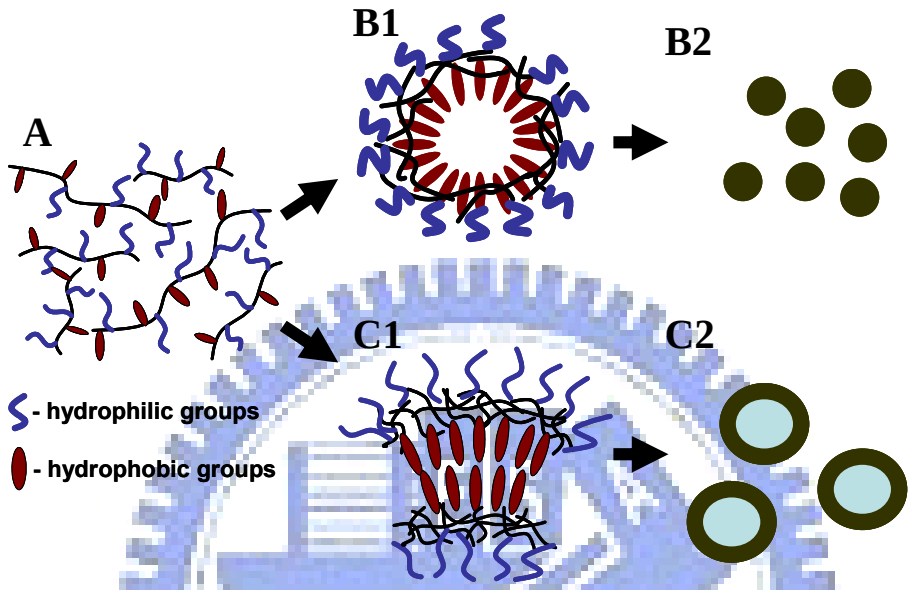

Figure 8-7 Schematic illustration of formation process of ACC nano-aggregates.

From a series of experimental observations, hollow structure exists only when the term of ($X_{DH} \times X_{Cn}$) >=1.5. As aforementioned, the hydrophobizing water capacity of the nano-aggregates increased rapidly as a result of increasing hydrophobicity in Zone II region. However, this would further cause structural in-stability when dispersed in aqueous solution due to the formation of an un-compatibilized interface between the aqueous phase and hydrophobic compartments of the ACC. Therefore, from the energy viewpoint, the ACC with higher hydrophobic nature, i.e., the compositions underlying the region of Zone II, prefers to self-aggregating into a more thermodynamically stable form as such that a sandwich structure with hydrophilic-hydrophobic-hydrophilic configuration can be expected, as

illustrated in the reaction scheme of A → C1→ C2 of Fig. 8-7 where a final capsule-like structure can be developed, which is similar to that of bi-layer liposomal structure. On this basis, the ACC nano-capsules with hydrophilic layers residing in the outermost and inner regions of the capsules ensure a thermodynamic and colloidal stability in aqueous solutions, and this is evidenced from a stability test where the nano-capsules are well suspended in an aqueous suspension for 1-month period of time.

Doxorubicin loading

To investigate the drug-loading capacity of the ACC nano-aggregates, doxorubicin (DOX), a clinically important anti-cancer drug, was employed as a model molecule, and loaded into the ACC nano-capsules. Since DOX molecule contains an amino group with a pKa of 8.6, it is expected that DOX can form polyelectrolyte complex with the carboxymethyl groups of ACC [28]. Figure 8-8 shows the plots of the DOX encapsulation efficiency (EE) in the ACC nano-aggregates with different values of ($X_{DH} \times X_{Cn}$). For CC, it showed only 26.3% encapsulation efficiency (EE) due to the physical interaction between DOX molecules and carobxymethyl groups, as demonstrated in pervious work [126]. After acyl modification (where C_n=2), DOX encapsulation efficiency of the ACC nano-aggregates was slightly reduced from 26.3% to 24.5% with increase of DH from 0 to 0.5. This decrease of EE is due to a decrease in the population of functional group, i.e., carboxymethyl groups, along the ACC chains. This is further evidenced from Fig.8-1 where the intensity of the characteristic peaks at 1730 cm^{-1} is reduced, indicating a reduction of intermolecular interaction between carboxymethyl dimers as the C_n was increased. However, the EE of the ACC nano-aggregates for the DOX

is increased considerably with the composite effect of both acyl chain length, i.e., C_n=6, 10, and 12 and the degree of acyl substitution, to a value of about 56%. This finding clearly suggests a considerable improvement in chemical and/or physical affinity between the nano-capsules and the DOX, thus, resulting in an enhancement of drug load efficiency by more than 200% compared to the CC composition.. However, it should be noted that optimal encapsulation efficiency has not yet practiced for the ACC through other processing skills in this study, instead, the current experimental outcomes of the EE are simply illustrating the power of the hydrophobic nature and a successful design of hydrophobic interactions, i.e., the effect of ($X_{DH} \times X_{Cn}$), of the ACC nano-aggregates, that can be used as an indicator for better drug loading manipulation.

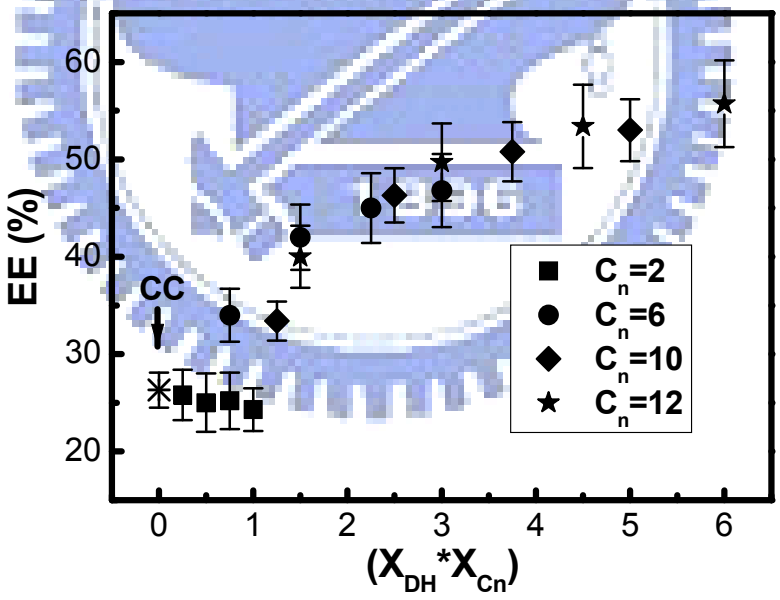

Figure 8-8 DOX encapsulation efficiency of ACC nano-aggregates with various values of ($X_{DH} \times X_{Cn}$).

Chapter 9

Conclusion

9.1 electric-sensitive of clay/chitosan hybrids

1. The increased cross-linking density with considerable increase of clay content improved the mechanical properties of hybrids, but restricted the swelling-deswelling kinetics.
2. After repeatedly on-off switch operation of a given electric field, a relatively constant deswelling-swelling behavior for over 10 times on-off operation can be reached for the hybrids with higher C_{clay} (>0.5 wt %), compared to that of the pure CS.
3. The release kinetics of vitamin B12 displays a pseudo-zero order release and the release mechanism shifted from diffusion-controlled towards swelling-controlled mode when lower MMT content (1 wt %) was added. However, as MMT contents exceed 1 wt %, both diffusion exponent n and responsiveness to electrical stimulation were decreased.
4. The resulting nanostructure of the nanohydrogels can be well manipulated to keep the pulsatile release profile relatively constant after repeated on-off switching operations.
5. The nanohydrogels with 2 wt % MMT addition was demonstrated to exhibits excellent anti-fatigue behavior and better pulsatile release compared to that of the pure CS.

9.2 electric-sensitive of TEOS/CS nanoparticles

1. The nanoparticles with particle size of 50-130 nm composed of chitosan (CS) and tetraethyl orthosilicate (TEOS) were obtained through emulsion and

sol-gel process.

2. LC and AE were effectively enhanced by increasing the TEOS content.

3. The existence of TEOS network structure significantly altered the release behavior from swelling-controlled to diffusion-controlled mechanism.

4. Burst release from nanoparticles was occurred when the electrical field was applied. This release behavior provided a new drug delivery system to precisely and effectively control the release of protein.

9.3 Acylated-carboxymethyl chitosan nanocapsule

1. A simple and direct method that amphiphilic CHC hollow nanocapsules were developed in aqueous system without the aid of surfactants, organic solvents, emulsion phases, or template cores.

2. Higher hexanoyl substitution promoted larger nanocapsules, ca. 200 nm in diameter, whilst a reduced zeta potential was correspondingly detected, and vice verse, forming smaller nanocapsules, ca. 20 nm in diameter.

3. An encapsulation efficiency of 46.8% was reached, and a corresponding drug release from the nanocapsules for a time period exceeded 7 days can be achieved in vitro.

4. Evolution of resulting self-aggregation structure of the ACC has been explored where a transformation from solid nano-particle to hollow nano-capsule of the ACC was observed as a result of hydrophobic effect, i. e., a product of ($X_{DH} \times X_{Cn}$), induced from acyl substitution (amount and chain length), exceeded a critical value of 1.5.

5. An improved affinity and capacity of doxorubicin drug encapsulation can be technically designed according to the nature of the resulting nanocapsules for controlled delivery.

References

[1] NIH Roadmap Initiatives. http://nihroadmap.nih.gov/initiatives.asp

[2] J. Kreuter, *Nanoparticles*. In: J. Kreuter, ed. Colloidal drug delivery systems. New York: Marcel Dekker Inc.; 1994, 219-342.

[3] C.Peniche, A.M. Waldo, N. Davidenko, R. Sastre, A. Gallardo, J.S. Roman, *Biomaterials* **20** (1999) 1869-1878.

[4] Y.H. Bae, *Stimuli-sensitive Drug Delivery*, In: K. Park, ed. Controlled Drug Delivery: Challenge and Strategies, American Chemical Society, Washington, DC, 1997, 147-160.

[5] Y. Ueoka, J. Gong, Y. Osada, *J. Intelligent Mater. Syst. Struct.* **8** (1997) 465-471.

[6] T. Shiroya, N. Tamura, M. Yasui, K. Fujimoto, H. Kawaguchi, *Colloids Surf. B* **4** (1995) 267-274.

[7] B.A. Firestone, R.A. Siegel, *J. Appl. Polym. Sci.* **43** ((1991) 901-914.

[8] X.Q. Wirsen, A.-C. Albertsson, *Polym.* **41** (2000) 4589-4598.

[9] M.H. Khalid, L. Ho, F. Agnely, N. Yagobi, J.L. Grossiord, G. Couarraze, *Euro. J. Pharm. Sci.* **15** (2002) 425-432.

[10] S.J. Kim, S.J. Park, S.I. Kim, *React. Func. Polym.* **55** (2003) 53-59.

[11] S.A. Dergunov, I.K. Nam, G.A. Mun, Z.S. nurkeeva, E.M. Shaikhutdinov, *Radia. Phys. Chem.* **72** (2005) 619-623.

[12] H.G. Schild, *Prog. Polym. Sci.* **17** (1992) 163-249.

[13] M.Z. Wang, Y. Fang, D.D. Hu, *React. Func. Polym.* **48** (2001) 215-221.

[14] M.F. Leung, J. Zhu, F.W. Harris, P. Li, *Macromol. Rapid Commun.* **25** (2004) 1819-1823.

[15] C.L. Lin, W.Y. Chiu, C.F. Lee, *Polym.* **46** (2005) 10092-10101.

[16] G. Sun, X.-Z. Zhang, C.-C. Chu, *J. Mater. Sci.: Mater. Med.* **18** (2007)

1563-1577.

[17] J.R. Khurma, A.V. Nand, *Polym. Bull.* **59** (2008) 805-812.

[18] B.L. Guo, J.F. Yuan, Q.Y. Gao, *Colloids Surf. B* **58** (2007) 151-156.

[19] C.J. Whiting, A.M. Voice, P.D. Olmsted, T.C.B. McLeish, *J. Phys. Condens. Matter.* **13** (2001) 1381-1393.

[20] T. Tanaka, I. Nishio, S.T. Sun, S. Ueno-Nishio, *Science* **218** (1982) 467-469.

[21] S. Ramanathan, L.H. Block, *J. Control. Release* **70** (2001) 109-123.

[22] S.H. Gehrke, *Adv. Polym. Sci.* **110** (1993) 81-144.

[23] J.P. Gong, T. Nitta, Y. Osada, *J. Phys. Chem.* **98** (1994) 9583-9587.

[24] T. Budtove, I. Suleimenov, S. Frenkel, *Polym. Gels networks* **3** (1995) 387-393.

[25] S.J. Kim, S.J. Park, M.-S. Shin, S.I. Kim, *J. Appl. Polym. Sci.* **86** (2002) 2290-2295.

[26] S.J. Kim, S.J. Park, M.-S. Shin, S.I. Kim, *J. Appl. Polym. Sci.* **86** (2002) 2285-2289.

[27] S.J. Kim, S.G. Toon, S.I. Kim, *J. Polym. Sci. B* **42** (2004) 914-921.

[28] S.J. Kim, S.G. Toon, K.B. Lee, Y.D. Park, S.I. Kim, *Solid State Ionics* **164** (2003) 199-204.

[29] S.S. Ray, K. Yamada, M. Okamoto, Y. Fujimoto, A. Ogami, K. Ueda, *Polym.* **44** (2003) 443-450.

[30] L.A. White, *J. Appl. Polym. Sci.* **92** (2004) 2125-2131.

[31] S.S. Ray, K. Okamoto, M. Okamoto, *Macromolecules* **36** (2003) 2355-2367.

[32] J. Lu, C.K. Hong, R.P. Wool, *J. Polym. Sci. B* **42** (2002) 1441-1452.

[33] M. Darder, M. Colilla, E. Ruiz-Hitzky, *Chem. Mater.* **15** (2003) 3774-3780.

[34] F. Asira, *Adv. Chitin Sci.* **46** (2000) 1-6.

[35] S.F. Wang, L. Shen, Y.J. Tong, L. Chem, I.Y. Phang, P.Q. Lim, T.X. Liu, *Polym. Degra. Stab.* **90** (2005) 123-131.

[36] C. Breen, *Appl. Clay Sci.* **15** (1999) 187-219.

[37] Y.H. Lin, H.F. Liang, C.K. Chung, M.C. Chen, H.W. Sung, *Biomaterials* **26** (2005) 2105-2113.

[38] A.P. Zhu, M. Zhang, Z. Zhang, *Polym. Int.* **53** (2004) 15-19.

[39] X.G. Chen, H.J. Park, *Carbohydr. Polym.* **53** (2003) 355-359.

[40] A. Zhu, A.B. Chan-Park, S. Dai, L. Li, *Colloids Surf. B* **43** (2005) 143-149.

[41] X. Shi, Y. Du, J. Yang, B. Zhang, L. Sun, *J. Appl. Polym. Sci.* **100** (2006) 4689-4696.

[42] E. Rotureau, C. Chassenieux, E, Dellacherie, A. *Durand, Macromol. Chem. Phys.* **206** (2005) 2038-2046.

[43] W.G. Liu, X. Zhang, S.G. Sun, G.J. Sun, D.K. Yao, *Bioconjug. Chem.* **14** (2003) 782-789.

[44] K.Y. Lee, I.C. Kwon, W.H. Jo, S.Y. Jeong, *Polym.* **46** (2005) 8107-8112.

[45] W. Wang, A.M. McConaghy, L. Tetley, I.F. Uchegbu, *Langmuir* **17** (2001) 631-636.

[46] Y.-S. Wang, L.-R. Liu, Q. jiang, Q.-Q. Zhang, *Euro. Polym. J.* **43** (2007) 43-51.

[47] C. Schatz, A. Bionaz, J.-M. Lucas, C. Pichot, C. Viton, A. Domard, T. Delair, *Biomacromol.* **6** (2005) 1642-1647.

[48] M. Lee, Y.W. Cho, J.H. Park, H. Chung, S.Y. Jeong, K. Choi, D.H. Moon, S.Y. Kim, I.-S. Kim, I.C. Kim, *Colloid. Polym. Sci.* **284** (2006) 506-512.

[49] C.-G. Liu, K.G.H. Desai, S.-G. Chen, H.-J. Park, *J. Agric. Food Chem.* **53** (2005) 437-441.

[50] G. Li, Y. Zhuang, Q. Mu, M. Wang, Y. Fang, *Carbohydr. Polym.* **72** (2008) 60-66.

[51] Y.H. Kim, S.H. Gihm, C.R. Park, *Bioconjug. Chem.* **12** (2001) 932-938.

[52] W. Yinsong, L. Lingrong, W. Juan, Q Zhang, *Carbohydr. Polym.* **69** (2007) 597-606.

[53] S. Stewart, G.J.Liu, *Chem. Mater.* **11** (1999) 1048-1054.

[54] S. General, J. Rudloff, A.F. Thunemann, *Chem. Commun.* (2002) 534-535.

[55] J. Jang, H. Ha, *Langmuir* **18** (2002) 5613-5618.

[56] Y. Hu, X. Jiang, Y. Ding, Q. Chen, C. Yang, *Adv. Mater.* **16** (2004) 933-937.

[57] Y. Hu, Y. Ding, D. Ding, M. Sun, L. Zhang, X. Jiang, C. Yang, *Biomacromol.* **8** (2007) 1069-1976.

[58] Y.H. Lin, H.F. Liang, C.K. Chung, M.C. Chen, H.W. Sung, *Biomaterials* **26** (2005) 2105-2113.

[59] K. Nakamura, R.J. Murray, J.I. Joseph, N.A. Peppas, M. Morishita, A.M. Lowman, *J. Control. Release* **95** (2004) 589-599.

[60] G.P. Carino, J.S. Jacob, E. Mathiowitz, *J. Control. Release* **65** (2000) 261-269.

[61] C. Prego, D. Torres, M.J. Alonso, *Expert. Opin. Drug. Deliv.* **2** (2005) 843-854.

[62] Y.-H. Lin, F.-L. Mi, C.-T. Chen, W.-C. Chang, S.-F. Peng, H.-F. Liang, H.-W. Sung, *Biomacromol.* **8** (2007) 146-152.

[63] F.-L. Mi, Y.-Y. Wu, Y.-H. Lin, K. Sonaje, Y.-C. Ho, C.-T. Chen, J.-H. Juang, H.-W. Sung, *Bioconjug. Chem.* **19** (2008) 1248-1255.

[64] S.Y. Kim, Y.M. Lee, *J. Appl. Polym. Sci.* **74** (1999) 1752-61.

[65] M. Wilhelm, C. Zhao, Y. Wang, R. Xu, M.A. Winnik, J. Mura, *Macromolecules* **24** (1991) 1033-1044.

[66] Y. Ueoka, J. Gong, Y. Osada, *J. Intel. Mat. Syst. Str.* **8** (1997) 465–71.

[67] H. Feil, Y.H. Bae, S.W. Kim, *J. Memb. Sci.* **64** (1991) 283–91.

[68] X.Z. Shu, K.J. Zhu, *Int. J. Pharm.* **212** (2001) 19–28.

[69] Q. Gan, T. Wang, C. Cochrane, P. McCarron, *Colloid Surface B* **44** (2005) 65–73.

[70] K. Sutani, I. Kaetsu, K. Uchida *Radiat. Phys. Chem.* **61** (2001) 49–54.

[71] T. Shiga, T. Kurauchi, *J. Appl. Polym. Sci.* **39** (1990) 2305–2320.

[72] M. Doi, M. Matsumoto, Y. Hirose, *Macromolecules* **25** (1992) 5504–5511.

[73] T.J. Pinnavaia, G.W. Beall, *Polymer–clay composites*, New York: John Wiley & Sons; 2001.

[74] R.A. Vaia, R. Krishnamoorti, *Polymer nanocomposites*, Washington, DC: American Chemical Society; 2001.

[75] P. Chen, L. Zhang, *Biomacromol.* **7** (2006) 1700–1706.

[76] K. Haraguchi, T. Takegisa, S. Fan, *Macromolcules* **35** (2002) 10162–10171.

[77] J.M. Rojo, E. Ruiz-Hitzky, J. Sanz, *Inorg. Chem.* **27** (1988) 2785–2790.

[78] F. Bueche, *Physical properties of polymers*, New York: Wiley; 1962.

[79] L.R. Ludikhuyze, I.V. Broeck, C.A. Weemaes, C.H. Herremans, J.F. van Impe, M.E. Hendricks, Biotechnol. Prog. 13 (1997) 532–538.

[80] J.C. Rodriguez-Cabello, S. Prieto, J. Reguera, F.J. Arias, A. Ribeiro, *J. Biomat. Sci. Polym. E* **18** (2007) 269–286.

[81] K.M. Gupta, S.R. Barnes, R.A. Tangaro, M.C. Roberts, D.H. Owen, D.F. Katz, *J. Pharm. Sci.* **96** (2007) 670–681.

[82] S.F Peteu, *J. Intel. Mat. Syst. Str.* **18** (2007) 147–152.

[83] C.C. Lin, A.T. Metters, *Adv. Drug Deliver. Rev.* **58** (2006) 1379–1408.

[84] S.B. Chen, J. Singh, *Pharm. Dev. Technol.* **10** (2005) 319–325.

[85] A.S. Hoffman, *Intelligent polymers*, In: Park K, editor. Controlled drug delivery: challenges and strategies. Washington, DC: American Chemical Society; 1997.

[86] Y. Yang, J.B.F.N. Engberts, Colloid. Surf. A: Physicochem. Eng. Aspects. 169 (2000) 85–94.

[87] L. Liang, J. Liu, X Gong, *Langmuir* **16** (2000) 9895–9599.

[88] W. Xu, A. Nikolov, D.T. Wasan, *J. Colloid. Interface Sci.* 197 (1998) 160–169.

[89] N.A. Peppas, Pharm. *Acta. Helv.* **60** (1985) 110–111.

[90] R. Hejazi, M. Amiji, *J. Control. Release* **89** (2003) 151-165.

[91] S. Mitra, U. Gaur, P.C. Ghosh, A.N. Maitra, *J. Control. Release* **74** (2001)

317-323.

[92] K.A. Janes, P. Calvo, M.J. Alonso, *Adv. Drug Deliver. Rev.* **47** (2001) 83-97.

[93] S.C.W. Richardson, H.V.J. Kolbe, R. Duncan, *Int. J. Pharm.* **178** (1999) 231-243.

[94] P. Galvo, C. Remuñán-López, J.L. Vila-Jato, M.J. Alonso, *J. Appl. Polym. Sci.* **63** (1997) 125-132.

[95] H. Zhang, M. Oh, C. Allen, E. Kumacheva, *Biomacromolecules* **5** (2004) 2461-2468.

[96] D. Tian, P.H. Dubois, R. Jérôme, *J. Polym. Sci. Pol. Chem.* **35** (1997) 295-301.

[97] S.-B. Park, J.-O. You, H.-Y. Park, S.J. Haam, W.-S. Kim, *Biomaterials* **22** (2001) 323-331.

[98] K. Kataoka, A. Hrada, Y. Nagasaki, *Adv. Drug Deliver. Rev.* **47** (2001) 113-131.

[99] I. Gill, A. Ballesteros, *J. Am. Chem. Soc.* **120** (1998) 8587-8598.

[100] A.D. Sezer, J. Akbuga, *Int. J. Pharm.* **121** (1995) 113-124.

[101] C. Barbé, J. Bartlett, L. Kong, K. Finnie, H.Q. Lin, M. Larkin, S. Calleja, A. Bush, G. Calleja, *Adv. Mater.* **16** (2004) 1959-1963.

[102] K.Y. Lee, W.H. Park, W.S. Ha, *J. Appl. Polym. Sci.* **63** (1997) 425-438.

[103] F. Caruso, R.A. Caruso, H. Mohwald, *Science* **282** (1998) 1111–1114.

[104] H.-P. Hentze, E.W. Kaler, *Curr. Opin. Colloid. Interf. Sci.* **8** (2003) 164-171.

[105] H. Huang, E.E. Remsen, K.L. Kowalewski, K.L. Wooley, *J. Am. Chem. Soc.* **121** (1999) 3805-3809.

[106] M. Lee, J.W. Nah,Y. Kwon, J.J. Koh, K.S. Lo, S.W. Kim, *Pharm. Res.* **18** (2001) 427–431.

[107] A.J. Zhao, X.B. Yuan, J. Chang, *Polym. Bull.* **4** (2004) 59–63.

[108] C. Young, R.F. Ozols, C.E. Myers, *New Engl. J. Med.* **305** (1981) 139–153.

[109] T.Y. Liu, S.Y. Chen, Y.L. Lin, D.M. Liu, *Langmuir* **22** (2006) 9740–9745.

[110] M.M. Amiji, *Carbohydr. Polym.* **26** (1995) 21–213.

[111] D.C. Dong, M.A. Winnik, J. Can, *J. Chem.* **62** (1984) 2560–2565.

[112] K.Y. Lee, W.H. Jo, *Langmuir* **14** (1998) 2329–2332.

[113] A. Rahman, C.W. Brown, *J. Appli. Polym. Sci.* **28** (2003) 1331–1334.

[114] X. Peng, L. Zhang, *J. Am. Chem. Soc.* **23** (2007) 10493–10498.

[115] Y. Wang, L. Liu, J. Weng, Q. Zhang, *Carbohydr. Polym.* **69** (2007) 597–606.

[116] Y. Moroi, *Micelles Theoretical and Applied Aspects*; Plenum Press: New York, 1992.

[117] M.V. Kitaeva, N.S. Melik-Nubarov, F.M. Menger, *Langmuir* **20** (2004) 6575–6579.

[118] L. Zhang, R.J. Barlow, A. Eisenberg, *Macromolecules* **28** (1995) 6055-6066.

[119] A.P. Marencic, M.W. Wu, R.A. Register, P.M. Chaikin, *Macromolecules* **40** (2007) 7299-7305.

[120] J.F. Gohy, B.G.G. Lohmeijer, A. Alexeev, X.S. Wang, I. Manners, M.A. Winnik, U.S. Schubert, U. S. Chem-Eur. J. 10 (2004) 4315-4323.

[121] J. Rodriguez-Hernandez, S. Lecommandoux, *J. Am. Chem. Soc.* **127** (2005) 2026-2027.

[122] D.J. Pochan, Z.Y. Chen, H.G. Cui, K. Hales, K. Qi, K.L. Wooley, *Science* **306** (2004) 94-97.

[123] N.S. Cameron, M.K. Corbierre, A. Eisenberg, *A. Can. J. Chem.* **77** (1999) 1311-1326.

[124] K. Mishima, *Adv. Drug Deliver Rev.* **60** (2008) 411–432.

[125] G. Li, Y. Zhuang, Q. Mu, M. Wang, Y. Fang, *Carbohydr. Polym.* **72** (2008) 60-66.

[126] K.-H. Liu, S.-Y. Chen, D.-M. Liu, *Macromolecules* 2008, accepted in press.

[127] J. Xu, S.P. McCarthy, R.A. Gross, D.L. Kaplan, *Macromolecules* **29** (1996) 3436-3440.

[128] K. Park, K. Kim, I.C. Kwon, *Langmuir* **20** (2004) 11726-11731.

[129] C.L. Tien, M. Lacroix, P. Ispas-Szabo, M.-A. Mateescu, *J. Contol. Release* **93** (2003) 1-13.

[130] Y.L. Guan, L. Shao, K.D. Yao, *J. Appl. Polym. Sci.* **61** (1996) 2325-2335.

[131] Y. Tamai, H. Tanaka, K. Nakanishi, *Macromolecules* **29** (1996) 6750-6760.

[132] C.J. van Oss, R.F. Giese, *J. Disper. Sci. Technol.* **25** (2004) 631-655.

Curriculum Vitae

K. H. Liu (Kun-Ho Liu)

Advisor: Prof. San-Yuan Chen

Department of Materials Science Engineering,

National Chiao Tung University

1001 Ta Hsueh Road, Hsinchu, TAIWAN 300

Email: bonaanob@yahoo.com.tw

I. B. S.: I-Shou University (1997-2001), Kaohsiung, Taiwan.

Major: Materials Science and Engineering

II. M. S.: National Chiao Tung University (2001-2003), Hsinchu, Taiwan

Major: Materials Science and Engineering

Prof.: San-Yuan Chen

Research Topic: Growth process and physical characteristics of Zn-ZnO nanocrystals via thermal reduction

III. Ph.D.: National Chiao Tung University (2003-2008), Hsinchu, Taiwan

Major: Materials Science and Engineering

Prof.: San-Yuan Chen

Research Topic: Study on the nanostructural evolution and controlled drug release behavior of chitosan nanocomposites.

Publications

Kun-Ho Liu

Patent:

- 雙性幾丁聚醣衍生物之空心圓球及使用其之醫藥用雙性幾丁聚醣衍生物複合物(Hollow sphere of amphiphilic chitosan derivatives and amphiphilic chitosan derivative complex using the same for medical use), Taiwan patent, Japan patent, and the United State patent, *in press*.

SCI Paper:

1. **Kun-Ho Liu**, Chin-Ching Lin, and San-Yuan Chen, Growth and Physical Characterization of Polygon Prismatic Hollow Zn-ZnO Crystals. *Cryst. Growth Des.* **5** (2005) 483-487 *(Impact Factor: 4.046)*

2. **Kun-Ho Liu**, Ting-Yu Liu, San-Yuan Chen, and Dean-Mo Liu, Effect of clay content on electrostimulus deformation and volume recovery behavior of a clay–chitosan hybrid composite. *Acta Biomater.* **3** (2007) 919–926 *(Impact Factor: 3.113)*

3. **Kun-Ho Liu**, Ting-Yu Liu, San-Yuan Chen , and Dean-Mo Liu, Drug release behavior of chitosan–montmorillonite nanocomposite hydrogels following electrostimulation. *Acta Biomater.* **4** (2008) 1038–1045 *(Impact Factor: 3.113)*

4. **Kun-Ho Liu**, Ting Yu Liu, Dean-Mo Liu, and San-Yuan Chen, Electrical-Sensitive Nanoparticle Composed of Chitosan and TEOS for Controlled Drug Release, *J. Nanosci. Nanotechno.* (2008) *in press (Impact Factor: 1.987)*

5. **Kun-Ho Liu**, San-Yuan Chen, Dean-Mo Liu, and Tse-Ying Liu, Self-Assembled Hollow Nanocapsule from Amphiphatic Carboxymethyl-hexanoyl Chitosan as Drug Carrier. *Macromolecules* 41 (2008) 6511-6516 *(Impact Factor: 4.411)*

6. **Kun-Ho Liu**, San-Yuan Chen, Dean-Mo Liu, Hydrophobic Effect on the Structural Evolution of Acylated-Carboxymethyl Chitosan and its

Self-Assemble Forming of Doxorubicin-loading Nanocapsule. *In Prepared*.

7. Chin-Ching Lin, **Kun-Ho Liu**, and San-Yuan Chen, Growth and characterization of Zn–ZnO core-shell polygon prismatic nanocrystals on Si, *Journal of Crystal Growth* **269** (2004) 425–431 *(Impact Factor: 1.950)*

8. Ting-Yu Liu**,** Shang-Hsiu Hu, **Kun-Ho Liu**, Dean-Mo Liu and San-Yuan Chen, Preparation and characterization of smart magnetic hydrogels and its use for drug release, *J. Magn. Magn. Mater.* **304** (2006) e397-e399 *(Impact Factor: 1.212)*

9. Ting-Yu Liu, Shang- Hsiu Hu, **Kun-Ho Liu**, Dean-Mo Liu and San-Yuan Chen, Study on controlled drug permeation of magnetic-sensitive ferrogels: Effect of Fe_3O_4 and PVA, *J. Control. Release* **126** (2008) 228-236 *(Impact Factor: 4.756)*

10. Ting-Yu Liu**,** Shang- Hsiu Hu, **Kun-Ho Liu**, Dean-Mo Liu and San-Yuan Chen, Instantaneous Drug Delivery of Magnetic/Thermal Sensitive Nanospheres by a High Frequency Magnetic Field, *Langmuir* (2008) *revised (Impact Factor: 4.009).*

11. Ting-Yu Liu, **Kun-Ho Liu**, Dean-Mo Liu, San-Yuan Chen and I-Wei Chen, Temperature-sensitive Nanocapsules for Controlled Drug Release Caused by Magnetically Triggered Structural Disruption. *Adv. Funct. Mater.* (2008) *in Press. (Impact Factor: 7.496)*

International Conferences:

Kun-Ho Liu, Ting-Yu Liu**,** Dean-Mo Liu and San-Yuan Chen, Ultra-fast reactive drug release system composed of electrical-sensitive chitosan and TEOS-IPN hybrid nanoparticle under applied DC electrical fields, *NIPER-NANO-2006-Nanotechnology in advanced drug delivery Conference* **(2006)** Chandigarh, India.